

STUDY OF DEVELOPING REGION FOR LAMINAR
FLOW IN CONCENTRIC ANNULI

By
A.K.M. SADRUL ISLAM

A Thesis

Submitted to the Department of Mechanical Engineering
in partial fulfilment of the requirements for the degree
of

MASTER OF SCIENCE IN MECHANICAL ENGINEERING



June, 1984



© A.K.M. Sadrul Islam, 1984

All Rights Reserved


STUDY OF DEVELOPING REGION FOR LAMINAR
FLOW IN CONCENTRIC ANNULI

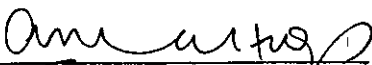
A Thesis


by


A.K.M. Sadrul Islam

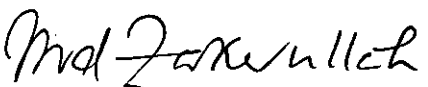
Approved as to style and content

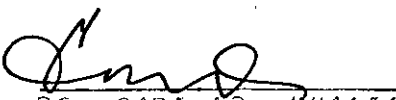

DR. S.M. NAZRUL ISLAM
Chairman & Supervisor


DR. A.M. AZIZ-UL-HUQ
Member & Head of the Dept.


DR. MUSHARRIF HUSSAIN KHAN
Member


DR. M. ABU TAHER ALI
Member


DR. MD. ZAKER ULLAH
Member (External)


DR. GAZI MD. KHALIL
Member (External)

June, 1984

ABSTRACT

Integral method together with Finite Difference method was used to study the laminar flow characteristics in the entrance region of an annulus for a flat velocity profile at the entry. A velocity profile based on the fully developed flow in the boundary layer, and a constant ratio of inner to outer boundary layer thicknesses in the entrance region were used for the Integral method. An algebraic equation for the pressure distribution in the entrance region of annuli was derived by this method, which was also used in the Finite-Difference-method. The analytical results for pressure distribution were extended for comparison with the experimental results for flow through a parallel plate channel.

From the characteristics of the results obtained from the Finite Difference method, the entrance region was divided into two zones, viz. (i) the inlet region, and (ii) the filled region. At the end of the inlet region the boundary layers met together but the velocity profile was not identical to that of the fully developed one. In the filled region, adjustment of the completely viscous profile took place until the fully developed similar profile attained at the end of it.

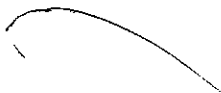
The fully developed velocity profile was not symmetrical about the centre of the hydraulic radius of the annuli. The magnitude of this asymmetric nature of the velocity profile was higher for smaller radius ratio of the annuli. But this

asymmetry of the velocity profile near the entrance was very small and gradually increased to its fully developed nature at a far downstream distance.

The magnitude of the radial velocity obtained from the Finite Difference method was small compared to that of the axial component. The radial velocity was also asymmetric about the centre of the hydraulic radius and this asymmetry was quite prominent for smaller radius ratio. The radial velocity decayed with axial distances, but such decaying was very rapid for smaller radius ratio at the inner wall.

Entrance length was calculated on the basis of the viscous term rather than the core velocity. Results of axial and radial velocity, wall shear stress, boundary layer development in the entrance region of five different radius ratio annuli were presented. The results indicated that the influence of the radius ratio on flow characteristics was very small for $0.5 \leq \alpha \leq 1.0$.

To my parents



ACKNOWLEDGEMENTS

The author expresses his deep sense of gratitude and profound indebtedness to Dr. S.M. Nazrul Islam, without whose constant and unparalleled guidance and invaluable suggestions, this work would not have been possible.

The author is highly grateful to Dr. Musharrif Hussain Khan, Dr. M. Anwar Hossain, Dr. A.M. Aziz-ul Huq, Dr. M. Abu Taher Ali, Dr. Gazi Md. Khalil and Dr. Md. Zaker Ullah for their constructive suggestions and cooperation.

The author is also grateful to his family and his colleagues for their considerate attitude and profuse inspiration without which this study could have never been materialised.

The author thanks the staff of the computer centre, BUET for the help extended while using the computer facilities.

Thanks are also due to Mr. M.A. Malek for his neat typing and to Mr. Abdus Salam for drawing the sketches of this thesis. The author wishes to thank all those who have extended their help and admits his inability to mention them by name which he ardently wishes.

TABLE OF CONTENTS

	Page
ABSTRACT	iii
DEDICATION	v
ACKNOWLEDGEMENTS	vi
TABLE OF CONTENTS	vii
LIST OF FIGURES	ix
LIST OF TABLES	xi
LIST OF APPENDICES	xii
NOMENCLATURE	xiii
CHAPTER I INTRODUCTION	
1.1 Entrance Region	1
1.2 Annulus and Its Application	2
1.3 Statement of the Problem	2
CHAPTER II LITERATURE SURVEY	
2.1 General	4
2.2 Boundary Layer Solution: Integral Approach	5
2.3 Numerical Method	17
2.4 Experimental Investigations	22
CHAPTER III THEORY	
3.1 General	24
3.2 Governing Equations	24
3.3 Equations for Fully Developed Flow	26
3.4 Integral Method	27
3.5 Differential Method	
3.5.1 Equations and Boundary Conditions	30
3.5.2 Calculation Technique.	30
CHAPTER IV THE EXPERIMENTAL SET-UP AND THE EXPERIMENT	
4.1 General	32
4.2 Experimental Facilities	32
CHAPTER V RESULTS AND DISCUSSION	
5.1 General	34
5.2 Pressure Drop	34
5.3 Velocity Distribution	37
5.4 Length of the Entrance Region	39
CHAPTER VI CONCLUSIONS	42
REFERENCES	44

	Page
FIGURES	47
APPENDICES	83

LIST OF FIGURES

Figure		Page
1	Coordinate System for Annuli	47
2	Experimental Set-up for Measuring Pressure Drop in the Entrance Region of a Parallel Plate Channel	48
3	Finite Difference Grid Size for Annuli	49
4	Fully Developed Core Velocity and Pressure Gradient for Different Radius Ratio Annuli	50
5	(dX/dB_2) vs. B_2 for Different Radius Ratio Annuli	51
6	Incremental Pressure Drop $K(X)$ vs. X for Different Radius Ratio Annuli	52
7	Pressure Drop vs. Axial Distance for Flow through Parallel Plate Channel (Aspect ratio 97)	53
8	Axial Velocity Profile at Different Axial Distances for:	
	(a) $\alpha = 0.01$	54
	(b) $\alpha = 0.05$	55
	(c) $\alpha = 0.10$	56
	(d) $\alpha = 0.25$	57
	(e) $\alpha = 0.50$	58
9	Axial Development for Core Velocity for $R_1/R_2 = 0.05, 0.25$ and 0.50	59
10	Radial Velocity at Different Axial Distance for:	
	(a) $\alpha = 0.01$	60
	(b) $\alpha = 0.05$	61
	(c) $\alpha = 0.10$	62
	(d) $\alpha = 0.25$	63
	(e) $\alpha = 0.50$	64
11	Wall Shear Stresses Variation Along Axial Distance for:	
	(a) $\alpha = 0.01$	65
	(b) $\alpha = 0.05$	66

Figure		Page
	(c) $\alpha = 0.10$	67
	(d) $\alpha = 0.25$	68
	(e) $\alpha = 0.50$	69
	(f) $\alpha = 0.01$	70
	(g) $\alpha = 0.05$	71
	(h) $\alpha = 0.10$	72
	(i) $\alpha = 0.25$	73
	(j) $\alpha = 0.50$	74
12	Boundary Layer Development Along Axial Distance for:	
	(a) $\alpha = 0.01$	75
	(b) $\alpha = 0.05$	76
	(c) $\alpha = 0.10$	77
	(d) $\alpha = 0.25$	78
	(e) $\alpha = 0.50$	79
13	Variation of Core Radius along Axial Distance	80
14	Photograph for Smoke Stream Through Parallel Plate Channel at Reynolds Number:	
	(a) $Re = 609$	81
	(b) $Re = 1066$	81
	(c) $Re = 1599$	82

LIST OF TABLES

Table	Page
2.1 Values of Incremental Pressure Drop and Entrance Length for Tube	8
2.2 Calculated Values of Incremental Pressure Drop and Entrance Length for Parallel Plate Channel	10
2.3 Calculated Values of Incremental Pressure Drop and Entrance Length for Annuli	11
2.4 Developmental Characteristics for Flow through Pipe and Parallel Plate Channel from Sparrow et al [28]	12
2.5 Results of Entrance Length and Incremental Pressure Drop for Different Reynolds Number for Pipe from Vrentas et al [35]	19
2.6 Results of Entrance Length for Different Reynolds Number for Pipe obtained from Friedmann et al [12]	21
2.7 Experimental Results obtained by Pfenninger [19]	23
5.1 Values of A & B of Pressure Drop Equation (5.1) for Different Radius Ratio Annuli	35
5.2 Skewness of the Core Radius with Respect to the Centre of the Hydraulic Radius of Different Radius Ratio Annuli	38
5.3 Results of the Lengths of the Inlet and the Entrance Region for Different Radius Ratio Annuli	41

LIST OF APPENDICES

Appendix		Page
A	Equations for Fully Developed Flow	83
B	Integral Technique	87
C	Finite Difference Technique	93
D	Stability Analysis of the Momentum Equation	99
E	Uncertainty Analysis	102
F	Computer Programme	104

NOMENCLATURE

a	half width of parallel-plate channel
A	total flow cross-sectional area, $\pi(r_2^2 - r_1^2)$; constant defined in equation (5.1)
A_1, A_2, \dots, A_{43}	defined in APPENDIX-B
B_1	$(r_1/r_{\delta_1})^2$
B_2	$(r_2/r_{\delta_2})^2$
C_1, C_2	defined in APPENDIX-B
D_h	hydraulic diameter, $2(r_2 - r_1)$
G_1, G_2	Constants defined in equation (A.2)
k	constant defined in equation (A.1)
$K(x)$	incremental pressure drop, $\Delta P = \left(\frac{dp}{dx}\right) dx$
m	constant in Ostwald de Wall power law equation
n	constant in Ostwald de Wall power law equation
p	static pressure
P	dimensionless static pressure $p/\frac{1}{2}\rho U_0^2$
r	radial distance
R	dimensionless radial distance, r/D_h
r_1	outer radius of the inner pipe
R_1	dimensionless outer radius of the inner pipe, r_1/D_h
r_2	inner radius of the outer pipe; radius of tube
R_2	dimensionless inner radius of the outer pipe, r_2/D_h
r_{δ}	radial distance of the maximum velocity
R_{δ}	dimensionless radial distance of the maximum velocity, r_{δ}/D_h
r_{δ_1}	radial distance to the edge of the inner boundary layer

R_{δ_1}	dimensionless radial distance to the edge of the inner boundary layer, r_{δ_1}/D_h
r_{δ_2}	radial distance to the edge of the outer boundary layer
R_{δ_2}	dimensionless radial distance to the edge of the outer boundary layer, r_{δ_2}/D_h
Re	Reynolds number $D_h U_o / \nu$
S	shearing rate
u	axial velocity
U	dimensionless axial velocity, u/U_o
u_1	axial velocity in the inner boundary layer
U_1	dimensionless axial velocity in the inner boundary layer, u_1/U_o
u_2	axial velocity in the outer boundary layer
U_2	dimensionless axial velocity in the outer boundary layer, u_2/U_o
U_c	core velocity
U_o	average velocity
v	radial velocity
V	dimensionless radial velocity, $v \cdot \text{Re} / U_o$
x	axial distance
X	dimensionless axial distance, $x / \text{Re} D_h$
X_k	dimensionless entrance length based on $\frac{k(x)}{k(\infty)} = 0.95$
X_v	dimensionless entrance length based on $\frac{U_c - U_o}{U_{cfd} - U_o} = 0.95$
y	distance from the wall

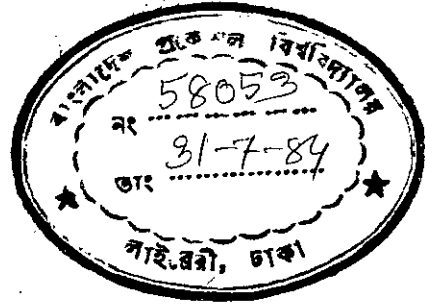
Greek symbols

α	radius ratio, r_1/r_2 or R_1/R_2
β	function defined in equation (2.3)
γ	defined in equation (3.12); specific gravity
ψ	stream function
ω	vorticity, uncertainty
δ_1	boundary layer thickness of the inner wall
δ_2	boundary layer thickness of the outer wall
δ^*	displacement thickness
τ	shearing stress
ρ	density
μ	dynamic viscosity
ν	kinematic viscosity
ϵ	function defined in equation (2.4)
Λ	function defined in equation (2.4)
Γ	defined in equation (2.5)
λ	defined in equation (2.5)
ξ	r/r_2
Δ	difference

Subscripts

c	core
e	entrance region
fd	fully developed
i	inlet region
0	entry
w	wall
w_1	inner wall
w_2	outer wall
δ	boundary layer

CHAPTER I
INTRODUCTION



1.1. Entrance Region

The hydrodynamic behaviour of a flow through a duct in the developed region is well known. But when a fluid enters a duct, the velocity profile changes along the axial direction from a definite distribution at the entrance to a particular profile far downstream. The region along the axial direction over which the velocity profile changes is known as the hydrodynamic developing region or entrance region. In this region the wall shear stress is higher than that in the developed region because of greater transverse velocity gradient near the wall. The rate of change of momentum and that of energy in the axial direction are also higher than that in the developed region because of the changing velocity profile along the axial direction. These higher wall shear stress and the higher rate of momentum transfer result in a greater axial pressure gradient in this region.

Earlier it was believed that the developing boundary layers met together at the end of the entrance region where the velocity profile attained the fully developed profile [5,13,29 etc.]*. But recent investigation in the entrance region of a pipe shows that laminar boundary layers meet at the pipe axis much before the attainment of a fully developed profile [20]. This observation motivated to subdivide the entrance region into two parts: the inlet region and the filled region. At the end of the inlet region the boundary layers meet together but the velocity profiles are not yet identical. In the filled region

* Numbers in the paranthesis indicate references

adjustment of the completely viscous velocity profile takes place until the fully developed profile is attained at the end of it.

1.2. Annulus and its Application

An annulus is formed by introducing a core through a circular tube. The ratio of the inner and outer radii (radius ratio, α) is an important parameter in addition to other variables that determines the nature of the flow in the annuli. A pipe ($\alpha = 0$) and a parallel plate channel ($\alpha = 1$) are the two limiting cases of an annulus.

In industrial heat exchangers and nuclear reactors, there are many cases where heat transfer begins immediately at the entrance of the annulus and therefore the calculation of heat transfer coefficients for these cases requires a detailed knowledge of the velocity field in the entrance region of the annular passage.

1.3. Statement of the Problem

Laminar flow characteristics in the entrance region of concentric annuli were studied theoretically. An integral method was used to determine the flow characteristics including the pressure distribution along the axial distance for the entrance region of the annuli. Experiments were also performed to compare the analytical results of pressure distribution in the entrance region of a parallel plate channel, which was one of the limiting conditions of an

annulus. Using the analytical results for pressure distribution derived from the integral method, a differential method was used to determine flow characteristics by solving the differential momentum and continuity equations for the entrance region of annuli.

CHAPTER II
LITERATURE SURVEY

2.1. General

Laminar flow of fluid can be expressed mathematically by the continuity, momentum, and energy equations. Since the conservation of energy equation in differential form and the Navier-Stokes equations are non-linear, each individual flow pattern has certain unique characteristics which are associated with its initial and boundary conditions. The basic equations have been analysed by researchers for various flow patterns; but still it is not possible to have an exact solution of differential equations for the flow in the entrance region of a duct due to the presence of the non-linear inertia terms in the equations. Yet a number of literatures are available where this problem has been analysed both theoretically and experimentally with a number of approximations for the entrance region of different types of ducts e.g. tube, parallel plate channel, annuli etc. Van Dyke [34] listed these methods in four general groups: (i) Linearisation of inertia terms, (ii) Integral method, (iii) Series expansion and (iv) Numerical finite difference solution. Most of these methods of solution have assumed:

(a) Negligible axial molecular transport of momentum with respect to that of radial transport,

$$\text{i.e. } \frac{\partial^2 u}{\partial x^2} \ll \frac{1}{r} \frac{\partial}{\partial r} \left(r \frac{\partial u}{\partial r} \right)$$

(b) Pressure to be a function of axial distance only,

$$\text{i.e. } p = p(x)$$

(c) A flat velocity profile at the entry of the duct,

$$\text{i.e. } u(0, r) = U_0$$

Besides, a few literatures are available which investigated the entrance flow experimentally. Some relevant end results of different literatures are included in Tables 2.1, 2.2 and 2.3.

In this chapter, the various methods of approximate solution for the entrance flow in connection with tube, parallel plate channel (semi-infinite) and annuli along with some experimental investigations are presented.

2.2. Boundary Layer Solution: Integral Approach

Boussinesq [2] was the first person who dealt with the entrance flow through a tube. Boussinesq represented the axial velocity, u , in the entrance region by the Poiseuille expression plus a perturbation term to obtain an approximation for the velocity profiles far from the entrance. Later, Schiller [29] applied the integral representation of the equations of motion and continuity to the boundary layers which develop along the tube wall using a parabolic velocity profile in the boundary layer and to the frictionless core. The velocity profile chosen in the entrance region of the tube was a modification of the Poiseuille solution in the sense that the tube radius was replaced by the boundary layer thickness. When the boundary layer thickness became equal to the tube radius, the analysis predicted the establishment of fully developed flow, i.e. the end of the entrance region and its length calculated by Shiller was $X = 0.02875$.

Schiller's [29] procedure was repeated by Siegel [31] for modified cubic and quartic boundary-layer velocity profiles and by Bogue [3] for cubic velocity profiles using the power law flow. The equation of power law flow:

$$\tau = m(S)^n$$

represents Newtonian flow when $n = 1.0$. Bogue included $v\partial u/\partial r$ as the radial momentum in the von Karman integral method.

Campbell and Slattery [5] reported that Schiller's solution was not applicable for $X > 0.02$. Atkinson and Goldstien [14] suggested that pressure is to be considered as a function of both axial and radial distance and thus an average value at each cross-section is to be calculated rather than assuming $p = p(x)$ in the boundary layer. Campbell and Slattery assumed the velocity distribution in the entrance region of a tube as:

$$\frac{u}{U_c} = 1 \text{ for } y > \delta, \quad x > 0 \quad (2.1)$$

$$\text{and } \frac{u}{U_c} = \left(\frac{y^2 - r^2}{\delta^2} \right) + 2 \left(\frac{r^2 - R^2}{\delta^2} \right) \text{ for } y \leq \delta, \quad x > 0 \quad (2.2)$$

and using energy balance, they derived expressions for boundary layer thickness as a function of axial distance. The velocity and the pressure drop were also obtained in terms of boundary layer thickness.

Another important integral method of solution was found by Langhaar [18] for tube, and later by Han [16] for parallel plate channel. Langhaar obtained a velocity profile over the entrance region of tubes by linearising the inertia term in the equation of motion and writing the equation in the following form:

$$\mu\beta^2 u = \frac{1}{\rho} \frac{\partial p}{\partial x} + \mu (\nabla^2 u) \tag{2.3}$$

where β was a function of x alone. The eqn. (2.3) was solved analytically and the result was satisfactory except in the regions very near the entrance and close to the wall, since v_x was not negligible in these regions and hence there β was not a function of x alone.

Trag [27] linearised the momentum equation for tube by replacing the inertia terms by $U_0 \frac{\partial u}{\partial x}$ and the pressure term by $(2v/r_2)(\partial u/\partial r)_{r=r_2}$. This assumption ignored the contribution of the momentum change to the pressure drop, and the incremental pressure drop $K(\infty)$ found by this method was 1.3.

Sparrow et al [28] modified Trag's linearisation method in order to provide information relating to the flow development and the pressure drop in tube and parallel plate channel. Sparrow et al assumed the following linearised Navier-Stokes equation:

$$\epsilon(x) U_0 \frac{\partial u}{\partial x} = \Lambda(x) + \nu \nabla^2 u \tag{2.4}$$

TABLE 2.1. Values of Incremental Pressure Drop and Entrance Length for Tube

Reference	Experimental Theoretical	$K(\infty)$	X_e	Remarks
Dorsey [8]	Experimental	1.08, 1.00	-	
Knibbs [17]	-do-	1.27 \pm 8%	-	
Nikuradse [25]	-do-	1.32	0.0625	
Rieman [26]	-do-	1.248 \pm 1%	-	
Schiller [29]	-do-	1.32 \pm 10%	-	
-do-	Theoretical	1.16	0.0288	Assuming a parabolic velocity profile within the boundary layer.
Weltman and Keller [38]	Experimental	1.2 \pm 10%	-	
Atkinson and Goldstien [14]	Theoretical	1.41	0.065	
Christiansen and Lemon [6]	-do-	1.274	0.0555	Numerical solution.
-do-	-do-	1.015	-	Numerical solution with negligible radial flow.
Bogue [3]	-do-	1.16	0.0288	Assuming cubic velocity profile within the boundary layer.

TABLE 2.1 (Contd...)

Reference	Experimental/ Theoretical	$K(\infty)$	X_e	Remarks
Boussinesq [2]	Theoretical	1.24	0.065	Perturbation method.
Collins and Schowalter [7]	-do-	1.33	0.061	Assuming power law flow.
Campbell and Sletten [5]	-do-	1.18	0.0675	Integral method assuming a parabolic velocity profile.
Langhaar [18]	-do-	1.28	0.0575	Linearising the Navier- Stokes equation.
Sigel [31]	-do-	1.08	0.03	Assuming a cubic velocity profile.
-do-	-do-	1.106	0.0296	Assuming a quartic velocity profile.
Sparrow et al [28]	-do-	1.24	0.05	Using linearised Navier-Stokes equation.
Tomita [33]	-do-	1.22	0.0505	-
Mohanty and Asthana [20]	-do-	1.152	0.075	Pahlhausen Integral method using a fourth-degree velocity profile.

TABLE 2.2. Calculated Values of Incremental Pressure Drop and Entrance Length for Parallel Plate Channel

Reference	$K(\infty)$	X_e	Remarks
Schlichting [30]	0.602	0.01	Perturbation method.
Sparrow et al [28]	0.65	0.009	Linearising the Navier-Stokes equation.
Gupta [13]	0.646	0.033	Integral method using a parabolic velocity profile.
Wang and Longwell [37]	0.7874	0.008375	Numerical solution assuming flat velocity profile at entry.
-do-	0.7512	0.0085	Numerical solution assuming a flat velocity profile at a section far upstream from entry.

TABLE 2.3. Calculated Values of Incremental Pressure Drop and Entrance Length for Annuli

Reference	$\alpha = r_1/r_2$	$K(\infty)$	X_e	Remarks
Murakawa [22]	0.636	0.64	0.052	
-do-	0.833	-	0.05176	
Heaton et al [15]	0.5	-	0.01	} Using the Linearised Navier-Stokes equation.
	0.25	-	0.012	
	0.10	-	0.015	
	0.05	-	0.019	
	0.02	-	0.0205	

- where $\epsilon(x)$ and $\Lambda(x)$ were functions of x only. $\epsilon(x)$ weighs the mean velocity U_0 and $\Lambda(x)$ includes the pressure gradient as well as the residual of the inertia terms. To facilitate the solution of equation (2.4) a stretched axial coordinate was assumed when $x^* = \int \frac{dx}{\epsilon(x)}$ in addition to the assumptions of no-slip boundary conditions at the duct wall and flat velocity profile at the entrance. $\epsilon(x)$ was derived by equating the pressure gradient from momentum and mechanical energy considerations. Trag's [27] velocity solution was equivalent to that of Sparrow et al when $\epsilon(x) = 1.0$.

Fleming and Sparrow [10] introduced a more general method of analysis with the equation (2.4) for entrance flow through ducts of arbitrary cross-section and then applied it to the rectangular and triangular ducts with the assumptions made by Sparrow et al [28]. Results for the developmental characteristics for flow through parallel plate channel and circular ducts are listed in Table 2.4.

TABLE 2.4. Developmental Characteristics for Flow through Pipe and Parallel Plate Channel from Sparrow et al [28]

Duct	Entrance length		$K(\infty)$	U_c/U_0 f_d
	X_k	X_v		
Parallel plate channel	0.0083	0.009	0.65	1.50
Circular Tube	0.038	0.044	1.24	2.00

Some interesting findings were reported by Mohanty and Asthana [20] for the entrance region of a smooth pipe. The entrance region was divided into two parts, the inlet region and the filled region. At the end of the inlet region, the boundary layers met at the pipe axis but the velocity profile was not found to be identical to that of Poiseuille. In the filled region, adjustment of the completely viscous profile took place until the Poiseuille profile was attained. The boundary layer equations in the inlet region and the Navier-Stokes equations in the Pahlhausen integral form in the filled region were solved using a fourth degree velocity profile:

$$u = \sum_{i=0}^4 A_i (\lambda, \Gamma) \xi^i \quad (2.5)$$

with the following boundary conditions:

I. Inlet region:-----

II. Filled region:

$$u = v = 0, \text{ at } \xi = \frac{r}{\delta} = 0$$

$$u = v = 0 \text{ at } \xi = r/r_2 = 0$$

$$\left. \begin{array}{l} u = U_c(x) \\ \frac{\partial u}{\partial \xi} = 0 \\ \frac{\partial^2 u}{\partial \xi^2} = 0 \end{array} \right\} \text{ at } \xi = 1.0$$

$$\left. \begin{array}{l} u = U_c(x) \\ \frac{\partial u}{\partial \xi} = 0 \\ \frac{\partial^2 u}{\partial \xi^2} = 0 \end{array} \right\} \text{ at } \xi = 1.0$$

$$\left[\frac{\partial^2 u}{\partial \xi^2} \right]_{\xi=0} - (\delta/r_2) \left[\frac{\partial u}{\partial \xi} \right]_{\xi=0} = \lambda$$

$$\left[\frac{\partial^2 u}{\partial \xi^2} \right]_{\xi=0} - \left[\frac{\partial u}{\partial \xi} \right]_{\xi=0} = 2 \Gamma - \lambda$$

Mohanty and Asthana calculated the total length of the entrance region $x_e = 0.075$ while the boundary layers met at $x_i = 0.018$ from the entry.

Schlichting [30] introduced another technique for solving the entrance flow with perturbation series and then applied it to the entrance region of a parallel plate channel. The entrance region was divided into two zones. In the zone near the entrance a boundary layer model was proposed which was analogous to that of a flat plate at zero incidence in unaccelerated flow: $\delta/a = 1.72 \sqrt{\frac{v x}{a^2 U_0}}$, where 'a' was the half width of the channel. The boundary layer development does not yield similarity type velocity profiles and an approximation was obtained in terms of perturbation series. In the zone far from the entrance, solutions were obtained as perturbations of the fully developed velocity profile as used by Boussinesq [2]. The flow development throughout the entire entrance region was described by patching together the boundary layer solution and Boussinesq type of solution at some intermediate location.

Tatsumi [32] simplified the equation of motion by assuming:

(i) $P = p(x)$

(ii) $u(0, y) = U_0$

(iii) $-\frac{1}{\rho} \frac{\partial P}{\partial x} = U_c \frac{\partial U_c}{\partial x}$

(iv) an undeformed central core

and (v) a stream function such that velocity profiles are almost similar.

The velocity profile results obtained by this method were in good agreement with those of Pfenninger [19] and Christiansen and Lemon [6] in the region very near the tube entrance.

Atkinson and Goldstien [14] modified the Schlichting's [30] method for tubes. They assumed a stream function,

$$\Psi = - r_2^2 U_0 \sum_{i=1}^n \left[\left\{ 4(x/ReD_h) \right\}^{\frac{1}{2}i} \right] f_i(\xi) \quad (2.6)$$

where $\xi = (1 - r^2/r_2^2)/4(4x/ReD_h)^{\frac{1}{2}}$

to obtain a boundary layer model solution which was believed to be accurate upto $X \leq 0.0006$ (cf. [14] p. 306). Like Schlichting, this solution was then patched at $X = 0.0006$ with a Boussinesq [2] type of solution which was valid for the region far from the entrance. Their patched relationship yielded velocity profile data which agreed with Nikuradse's [25] centre-line data. Similarly, Punnis [24] patched a downstream boundary layer solution to a Boussinesq type of solution at $X = 0.0004$ to obtain a solution for tube entrance region.

Gupta [13] obtained a solution for the entrance region of a parallel plate channel by macroscopic energy balance to all the fluid in the duct. Like Campbell and Slattery [5] he used a boundary layer velocity profile:

$$\frac{u}{U_c} = 1 - \left(1 - \frac{y}{\delta}\right)^2.$$

Van Dyke [34] and Wilson [36] studied two models of entry conditions for flow through parallel plate channel: (i) uniform parallel flow at entry, (ii) uniform parallel flow at a section far upstream, with the channel walls extended upstream as streamlines, which corresponds to an infinite cascade of equally spaced plates in a uniform oncoming stream. Using the

Blasius flat plate boundary layer solution, Van Dyke obtained a solution at $Re = 300$ for both the cases. It was found by Van Dyke that the velocity profile for the second case was convex at the entry and became concave at the centreline at a distance $X = 0.00029$ from the entrance.

Murakawa [22] obtained the velocity distribution, the pressure drop and the entrance length of an annulus after solving the Navier-Stokes equations in x-and r-directions and the continuity equation with the following boundary conditions:

$$u = v = 0 \text{ at the walls}$$

$$u = U(r) \text{ at } x = 0$$

$$u = u(r)_{fd} \text{ at } x = \infty$$

Murakawa eliminated the pressure term by equating the Navier-Stokes equations in x-and r-coordinates and derived a complex series of equations for the velocity distribution, the pressure drop and the entrance length. Murakawa showed that within the radius ratio $0.625 \leq \alpha \leq 0.99$, the influence of radius ratio on the entrance length was smaller than that of the Reynolds number.

Heaton et al [15] analyzed the flow in the entrance region of annuli ^{by} the integral method used by Langhaar [18] with the following boundary conditions:

$$u = v = 0 \text{ at the wall}$$

$$u = U_0 \text{ at } x = 0$$

$$\text{and } \left(\frac{\partial u}{\partial r} \right)_{r_c} = 0, \quad r_1 < c < r_2$$

- Heaton et al reported solutions for annuli of radius ratio of 0.001, 0.02, 0.05, 0.10, 0.25 and 0.50.

Mattai [21] formulated an ordinary differential equation by macroscopic mechanical energy balance with the following boundary conditions:

$$u = v = 0 \text{ at the wall}$$

$$u = U_0 \text{ at } x = 0$$

and assuming the fully developed velocity profile within the boundary layer and a constant ratio of the boundary layers of the inner and the outer walls for the fully developed flow in the entrance region. But Mattai's ordinary differential equation could not be solved at a region very near to the entrance.

2.3. Numerical Method

Considering the axial molecular transport of momentum and pressure gradient normal to the flow, Wang and Longwell [37] solved the entrance flow characteristics for parallel plate channel for two different entry conditions: (i) uniform parallel flow at the entrance and (ii) uniform parallel flow at a section far upstream of the entrance with the following boundary conditions:

Case I

$$u = v = 0 \text{ at wall}$$

$$\left. \begin{array}{l} \partial u / \partial y = 0 \\ v = 0 \end{array} \right\} \text{ at } y = a$$

$$\left. \begin{array}{l} u / U_0 = 1.0 \\ v = 0 \end{array} \right\} \text{ at } x = 0$$

$$\left. \begin{array}{l} u / U_0 = 3/2 \left(1 - \frac{(a-y)^2}{a^2} \right) \\ v = 0 \end{array} \right\} \text{ at } x = \infty$$

Case II

$$u = v = 0 \text{ at wall}$$

$$\left. \begin{array}{l} \partial u / \partial y = 0 \\ v = 0 \end{array} \right\} \text{ at } y = a \text{ and } y = 0.0 \quad x < 0$$

$$\left. \begin{array}{l} u / U_0 = 1.0 \\ v = 0 \end{array} \right\} \text{ at } x = -\infty$$

After eliminating the pressure gradient terms from the momentum equation in x and y direction, and introducing the stream function Ψ the equation became:

$$\frac{\partial \Psi}{\partial y} \frac{\partial}{\partial x} (\nabla^2 \Psi) - \frac{\partial \Psi}{\partial x} \frac{\partial}{\partial y} (\nabla^2 \Psi) = \frac{4}{Re} \nabla^4 \Psi \quad (2.7)$$

where $Re = \frac{4 a U_0}{\nu}$ and 'a' was the half width of the channel.

To ensure a finite boundaries they transformed x into a new independent variable x' :

$$x' = 1 - 1/(1+c),$$

where c was a constant with a positive value for $x > 0$ and a negative value for $x < 0$. This transformation compressed the scale of x at large distances from the entrance for this solution. Then both the upstream and downstream regions were transformed into squares $0 \leq y \leq 1$ and $0 \leq x' \leq 1$.

Wang and Longwell introduced the term vorticity,

$$\omega = - \nabla^2 \Psi,$$

in the equation (2.7) and solved by relaxation technique. They used a 10x10 grids in terms of x' and y with $c = 1.2$. The solution for the first case showed a definite concavity in the velocity profile near the entrance (upto $X = 0.001$).

The effect of axial diffusion of vorticity on flow development in the tube was studied by Vrentas et al [35]. A vorticity transport equation was used with no-slip boundary conditions for tube. To ensure a finite boundary, Vrentas et al

assumed a transformation of $x' = \tanh Tx$, like Wang and Longwell [37] where T is a parameter, which transformed the infinite length scale, $-\infty \leq x \leq \infty$ to a finite one, $-1 \leq x' \leq 1$. They obtained solution for a parabolic partial differential equation at high Reynolds number where axial diffusion of vorticity was assumed to be negligible compared with the other terms. The solution of this parabolic-partial differential equation was initiated at the entrance for a uniform velocity profile with $\Delta r/r_2 = 0.05$, and $\Delta x' = \frac{2 \Delta x}{r_2 Re} = 5 \times 10^{-4}$ for the first 25 steps and $\Delta x' = 5 \times 10^{-3}$ for the subsequent steps. The total axial pressure drop was calculated by integrating the momentum equation over the entire entrance region of the tube. The tube radius was divided into $(N - 1)$ equal divisions, which gave $(N - 1)$ equations of stream function and same number of equations of vorticity for each axial location, and then they were solved by tridiagonal matrix. Solutions for the entrance length and the incremental pressure drop $K(\infty)$ at different Reynolds number are given in Table 2.5.

TABLE 2.5. Results of Entrance Length and Incremental Pressure Drop for Different Reynolds Number for Pipe obtained from Vrentas et al [35]

Re	X_e	$K(\infty)$	U_c/U_{cfd}
250	0.0503	1.28	0.99
150	0.048	1.36	0.99
50	0.047	1.40	0.99
1	0.330	7.76	0.99

For $Re \geq 250$ the boundary layer equations adequately described the flow field. The concavity in the velocity profile was absent at $Re \leq 50$. For $Re > 50$ it increased with Reynolds number but existed only in the region very close to the tube entrance. According to Vrentas et al, for low Reynolds number the axial vorticity term in the vorticity transport equation should not be neglected, since it led to an elliptic finite difference equation. For solution of this elliptic equation, rectangular grids were taken within the region $0 \leq r \leq r_2$ and $-1 \leq x' \leq 1$. Applying the standard central difference approximation to the first and second derivatives, the elliptic equations were solved with the help of implicit iterative method. The solution was obtained for 10×10 grids in terms of $0 \leq r \leq r_2$ and $-1 \leq x' \leq 1$.

Christiansen and Lemon [6] assumed radial component of equation of motion to be negligible and a uniform flow at the entrance to predict the flow development in the entrance region of a tube. The entrance region of the tube was considered to comprise N concentric annuli. The momentum equation in a finite difference form was written for $(N + 1)$ cylindrical boundaries and the $(N + 1)$ velocities at the entrance were known and the corresponding values at the end of the segments were determined by solving the $(N + 1)$ equations by an iterative process (modified Gauss-Siedel method) for 200×200 matrix. They derived a pressure drop model for the entrance flow through the tube as:

$$\frac{P - P_0}{\frac{1}{2} \rho U_0^2} = \frac{13.74}{x / Re D_h} \quad (2.8)$$

Friedmann et al [12] solved the vorticity transport equation by the relaxation technique over the range $0 \leq r \leq r_2$ and $0 \leq x \leq x_e$ for low Reynolds number (upto 500) with a flat velocity profile at the tube entry. The entrance length x_e found by them is listed in Table 2.6.

TABLE 2.6. Results of Entrance Length for Different Reynolds Number for Tube Obtained from Friedmann et al [12]

Re	x_e	U_c/U_{cfd}
10	0.0880	0.99
20	0.0675	0.99
40	0.0610	0.89
100-200	0.0565	0.99
300-500	0.0560	0.99

Like Wang and Longwell [37], Friedmann et al [12] found concavity in the velocity profiles near the entrance. For very large values of Re the initially flat velocity profile was maintained over a large axial length of the tube. The maxima in the velocity profile was then pushed near to the tube wall. In the boundary layer solution, the flat velocity profile in the core could be reasonably approximated for higher values of Re because, the axial range over which the kinked velocity profile existed became vanishingly small. But for small Re, the flat velocity profile at the entry could not be maintained. Thus the results deviate from the solutions of boundary layer approximation.

2.4. Experimental Investigations:

A few literatures are available which describe the experimental results on the entrance flow of ducts. The experimental results for incremental pressure drop by various authors are listed in Tables 2.1, 2.2, 2.3.

During 1950-53 Pfenninger [19] conducted laminar flow experiments in the entrance region of a tube, at high Reynolds number and at low Mach number. Extruded aluminium alloy straight tubes of diameters 2.56 cm and 5.08 cm for five different lengths ranging from 12.5 m to 22.8 m were used as test tubes. Air was sucked from the atmosphere through 12 damping screens (0.12 mm wire dia. & 65% opening) of stainless steel and through a nozzle (contraction ratio 16) into the test tube by a compressor. All necessary precautions were taken to maintain the test section free from any sort of disturbances. The mean velocity, U_0 and the Reynolds number were calculated from the pressure difference across the inlet nozzle and the boundary layer measurements at a distance thrice the tube-diameter downstream of the entry section of the tube. The results obtained by this experiment are listed in Table 2.7.

Atkinson et al [1] used an optical technique for the quantitative determination of velocity profiles in the entrance region of a tube for Reynolds number ranging from 500 to 1500. For flow at $Re = 500$, the entrance length was found to be $X_e = 0.0177$.

The two portions of the entrance region (viz. the inlet and the filled region) were experimentally established by

TABLE 2.7. Experimental Results Obtained by Pfenninger [19]

	I	II	III	IV	V
$x(m)$	12.5	14.6	18.0	15.2	22.8
$r_2(m)$	0.0254	0.0254	0.0254	0.0128	0.0254
$U_0(m/s)$	30.50	26.66	25.04	51.3	30.0
$Re/2$	50,050	44,200	41,470	44,000	49,600
$2x/r_2 Re$	0.00972	0.0129	0.0172	0.0270	0.0181
U_c/U_0	1.304	1.348	1.397	1.504	1.41

Mohanty and Asthana [20]. Experiments were carried out by passing air through a 30 mm ID smooth aluminium tube at $Re = 1875, 2500$ and 3250 . The uniform velocity at the entry was generated by preceding the tube with a short bellmouth at the end of a large settling chamber, the area of which was 100 times larger than the tube cross-section. The velocity was measured by a 2 mm microprobe flattened at the tip, in conjunction with an Askania micromanometer of sensitivity 0.01 mm Hg.

CHAPTER III

THEORY

3.1. General

Laminar flow for Newtonian fluid is governed by the Navier-Stokes differential equations. The general solution of the non-linear Navier-Stokes equations is not yet available. However, in many practical cases where the non-linear inertia terms do not exist, it is possible to obtain exact solutions of the Navier-Stokes equations. But for the flow in the entrance region of any duct, the presence of the inertia terms, makes it difficult to obtain an exact solution of the Navier-Stokes equations. To overcome these difficulties many researchers made different empirical approximations.

3.2. Governing Equations: _____

By restricting the application of the equations of motion in cylindrical coordinates [4] to the conditions such that:

- (i) the flow is independent of time,
- (ii) the radial component of the equation of motion is negligible,
- (iii) any angular motion is negligible,
- (iv) the fluid density and viscosity are constant, and
- (v) the flow is independent of any existing body force field,

the equations of motion in cylindrical coordinates are reduced to:

$$\rho(u \frac{\partial u}{\partial x} + v \frac{\partial u}{\partial r}) = - \frac{\partial p}{\partial x} + \mu \left[\frac{1}{r} \frac{\partial}{\partial r} (r \frac{\partial u}{\partial r}) + \frac{\partial^2 u}{\partial x^2} \right] \quad (3.1)$$

In cylindrical coordinates the equation of continuity is

$$\frac{\partial(ur)}{\partial x} + \frac{\partial(vr)}{\partial r} = 0 \quad (3.2)$$

In obtaining the solutions of equations (3.1) and (3.2) for flow in an annulus entrance region:

(a) the following assumptions are made:

I. Axial molecular transport of momentum is negligible

$$\text{i.e. } \frac{\partial^2 u}{\partial x^2} \ll \frac{1}{r} \frac{\partial}{\partial r} (r \frac{\partial u}{\partial r})$$

II. The pressure is a function of x and is independent of r

$$\text{i.e. } p = p(x)$$

(b) the following boundary conditions are taken:

I. The velocity at the annulus entrance is uniform,

$$\text{i.e. } u(0, r) = U_0, \quad v(0, r) = 0.0$$

II. No slip condition at the wall

$$\text{i.e. } u = v = 0, \text{ at } r = r_1 \\ \text{and } r = r_2$$

3.3. Equations for Fully Developed Flow:

Far downstream from the entrance where the inertia term vanishes, the momentum equation (3.1) becomes,

$$\partial^2 u / \partial r^2 + \frac{1}{r} \frac{\partial u}{\partial r} = \frac{1}{\mu} \frac{\partial p}{\partial x} = \text{constant} \quad (3.3)$$

The solution of this equation for annulus boundary conditions e.g. $u = 0$ at $r = r_j$ ($j = 1, 2$) and $u = U_c$ at $r = r_\delta$ yields Lamb's fully developed velocity profile for annulus, expressed in nondimensional parameters as:

$$\frac{u}{U_c} = \frac{R^2 - R_j^2 - 2R_\delta^2 \ln R/R_j}{R_\delta^2 - R_j^2 - 2R_\delta^2 \ln R_\delta/R_j} \quad (3.4)$$

The radius for maximum velocity computed from this equation (3.4) is:

$$R_\delta = \left[\frac{R_1^2 - R_2^2}{2 \ln \alpha} \right]^{\frac{1}{2}} \quad (3.5)$$

The maximum velocity is:

$$\frac{U_c}{U_0} = \frac{(\alpha^2 - 1) \left(1 - \ln \frac{\alpha^2 - 1}{\ln \alpha^2} \right)}{(\alpha^2 - 1) - (1 + \alpha^2) \ln \alpha} \quad (3.6)$$

where $\alpha = R_1/R_2$

The pressure drop caused by the fluid friction is:

$$\frac{p - p_0}{\frac{1}{2} \rho U_0^2} = \frac{64 (1 - \alpha)^2 X}{\frac{\alpha^2 - 1}{\ln \alpha} - (1 + \alpha^2)} \quad (3.7)$$

All these equations are derived in APPENDIX-A.

3.4. Integral Method:

The fully developed velocity profile was assumed to be valid within the boundary layer in the entrance region of the annulus and it was expressed as:

$$u_{j,x}/U_c = \frac{R^2 - R_j^2 - 2 R_{\delta_{j,x}}^2 \ln R/R_j}{R_{\delta_{j,x}}^2 - R_j^2 - 2 R_{\delta_{j,x}}^2 \ln R_{\delta_{j,x}}/R_j} \quad (3.8)$$

where $j = 1, 2$ refers to parameters associated with the inner and outer wall boundary layers respectively, by replacing the radius of the maximum velocity with the radius of the boundary layer thicknesses. Equation (3.8) becomes fully developed velocity profile equation when $R_{\delta_{j,x}} = R_{\delta_{j,fd}}$. In addition, it satisfies the physical condition of no-slip at the wall and zero shear at the edge of the boundary layer. Considering the control volume ABCD in Fig. 3,

(a) the conservation of mass equation is :

$$AU_0 = 2\pi \left\{ \int_{r_1}^{r_{\delta_1}} u_1 r dr + \int_{r_{\delta_1}}^{r_{\delta_2}} U_c r dr + \int_{r_{\delta_2}}^{r_2} u_2 r dr \right\}$$

(b) the momentum equation is :

$$2\pi \{ -\tau_{w1} r_1 + \tau_{w2} r_2 \} dx - dp A = 2\pi \rho d \left\{ \int_{r_1}^{r_{\delta_1}} r u_1^2 dr + \int_{r_{\delta_1}}^{r_{\delta_2}} r U_c^2 dr + \int_{r_{\delta_2}}^{r_2} r u_2^2 dr \right\} \quad (3.9)$$

where, $\tau_{wj} = \mu \left[\frac{\partial u_j}{\partial r} \right]_{r=r_j}$; $j = 1, 2$

and (c) the energy equation is:

$$\begin{aligned}
 -AU_0 dp = 2\pi \mu \left\{ \int_{r_1}^{r_{\delta_1}} \left(\frac{\partial u_1}{\partial r} \right)^2 r dr + \int_{r_{\delta_1}}^{r_{\delta_2}} \left(\frac{\partial u_2}{\partial r} \right)^2 r dr \right\} dx \\
 + \pi \rho d \left\{ \int_{r_1}^{r_{\delta_1}} (u_1^3 - U_0^3) r dr + \int_{r_{\delta_1}}^{r_{\delta_2}} (U_C^3 - U_0^3) r dr + \int_{r_{\delta_2}}^{r_2} (u_2^3 - U_0^3) r dr \right\} \quad (3.10)
 \end{aligned}$$

Eliminating 'dp' from eqns. (3.9) and (3.10), and on rearranging equation (3.11) given below was obtained:

$$\begin{aligned}
 2\pi U_0 \{ \tau_{w1} r_1 - \tau_{w2} r_2 \} dx = 2\pi \mu \left\{ \int_{r_1}^{r_{\delta_1}} \left(\frac{\partial u_1}{\partial r} \right)^2 r dr + \int_{r_{\delta_2}}^{r_2} \left(\frac{\partial u_2}{\partial r} \right)^2 r dr \right\} dx + \pi \rho d \left\{ \int_{r_1}^{r_{\delta_1}} (u_1^3 - U_0^3) r dr + \int_{r_{\delta_1}}^{r_{\delta_2}} (U_C^3 - U_0^3) r dr + \int_{r_{\delta_2}}^{r_2} (u_2^3 - U_0^3) r dr - U_0 \int_{r_1}^{r_{\delta_1}} 2ru_1^2 dr - U_0 \int_{r_{\delta_1}}^{r_{\delta_2}} 2r U_C^2 dr - U_0 \int_{r_{\delta_2}}^{r_2} 2ru_2^2 dr \right\} \quad (3.11)
 \end{aligned}$$

Assuming,

$$\left. \frac{\delta_1}{\delta_2} \right|_{\text{at any } x} = \left. \frac{\delta_1}{\delta_2} \right|_{fd}$$

and introducing $B_j = r_j^2/r_0^2$ where $j = 1, 2$. Mattai [21] derived the following first order non-linear differential equation:

$$\frac{dX}{dB_2} = \frac{8(1 - \alpha^2)}{C_2 - C_1 \left(\frac{\gamma}{\alpha \{ \sqrt{B_2} + \frac{\gamma}{\alpha} (\sqrt{B_2} - 1) \}^3} \right)} \quad (3.12)$$

where,

$$\gamma = \left(\left\{ \frac{1 - \alpha^2}{-2 \ln \alpha} \right\}^{\frac{1}{2}} - \alpha \right) / \left(1 - \left\{ \frac{1 - \alpha^2}{-2 \ln \alpha} \right\}^{\frac{1}{2}} \right)$$

and C_1, C_2 are functions of $A_1, A_2 \dots A_{43}$ as defined in the APPENDIX-B. But this first order differential equation cannot be solved just from the entrance because (a) a singularity exists at the entrance i.e. $X = 0$ and (b) instability exists for some distance $X = X'$ from the entrance, whose value is different for different radius-ratio annuli. These two points are explained in Fig. 5. To find out the distance X' equation (3.12) was modified with the assumptions that near the entrance in the core region the Bernoulli's equation applies, i.e. $U_c \frac{dU_c}{dx} = - \frac{1}{\rho} \frac{dp}{dx}$. Then the differential equation (3.12) takes the form:

$$\frac{dX}{dB_2} \equiv \frac{MF - PF}{SF} \quad (3.13)$$

where SF, PF & MF are functions of B_1 and B_2 . Equation (3.13) was solved within the region of $0 < X \leq X'$ and then patched with the solution of equation (3.12).

Equations (3.12) and (3.13) were solved by Simpson's Integration formula with an initial value of $B_2 = 1.0001$ at

$X = 0.0$ and with an increment $\Delta B_2 = 0.01$ till $R_{\delta_1} = R_{\delta_2}$. This computation required 3-5 minutes of CPU time (depending upon the radius ratio) on the IBM 370/115 machine.

3.5. Differential Method:

3.5.1. Equations and Boundary Conditions.

Equations (3.1) and (3.2) were solved numerically with the assumptions I and II and the boundary conditions I and II (given on page 25). A model for pressure gradient was developed from the Integral method and was used for this calculation.

3.5.2. Calculation Technique

An explicit finite difference technique of the DuFort-Frankel-[9] type was applied here to the momentum equation (3.1) and the continuity equation (3.2) along with the assumptions I & II and the boundary conditions I & II to calculate the velocity development and the radial velocity decay in the entrance region. The approximations used for the derivatives in this method with the truncation errors are given in APPENDIX-C. The Finite Difference grid used for the computation is shown in Fig. 3. A FORTRAN-IV computer program was developed to solve these equations for uniform grid spacings in the x- and r- directions. The programme documentation and the list are furnished in APPENDIX-F.

von Neumann's [23] method of stability analysis with first order error was applied to the momentum equation

and found to generate a stability constraint as given in APPENDIX-D.

The DuFort-Frankel [9] technique requires information from two previous stations for the calculation to proceed in the stream-wise direction. Since the initial condition $u/U_0 = 1.0$ at $X = 0$, gives information only at the first station, a direct explicit method was used to start the solution, which requires information only at the previous station. Then the solution was proceeded by the DuFort-Frankel method from the third station.

The grid spacings in the x- and r- directions were chosen to be uniform, dividing the hydraulic radius into 50 equal divisions to attain the convergence of the solution. For a stable calculation a ratio of grid spacings $\Delta R/\Delta X = 1000$ was used.

The finite difference equations for the continuity and the momentum are given in APPENDIX-C for both the DuFort-Frankel scheme and the direct explicit scheme.

The computation reported here for one station did not require more than one second of CPU time on the IBM 370/115 computer.

CHAPTER IV

THE EXPERIMENTAL SET-UP AND THE EXPERIMENT4.1. General

Most of the experimental investigations for laminar entrance flow which appeared in the literature are for the circular tube. It is shown that the tube and the parallel plate channel are the two limiting conditions of an annulus. There are a few papers published with the experimental results for laminar entrance flow through the tube. One of the aims of the present investigation was to find out the pressure drop experimentally in the entrance region of a parallel plate channel.

4.2. Experimental Facilities

Laminar flow was produced by inducting air through a parallel plate channel from an infinite surrounding. A blower of capacity 12.5 cfm at 80 mm H₂O head was used to induct air. The inlet side of the blower was connected with a wooden diverging channel made of 6 mm thick perspex sheet. Six aluminium angles were glued (using Araldite) to the upper plate of the channel to keep it straight. The sketch of the experimental set-up is shown in Fig. 2. To avoid side effects on the flow an aspect ratio (= breadth/depth) of 97 was chosen, and this was considered to be two dimensional. The sides of the channel were made leak proof by using scotch tape over the joints. A number of 1/16 inch diameter holes were drilled at the mid-section of the upper plate at different axial locations.

The pressure was measured by using a Micromanometer of Flow Corp, USA, having a sensitivity of 0.0001 inch of manometric liquid. Measurements were taken at different Reynolds number, e.g. 610, 1067, 1234 and 1600 obtained by regulating the delivery side of the blower. In order to verify the parallelism of the flow a smoke jet was generated in the channel and the stream-lines were observed. The stream-lines were found to be reasonably straight and parallel confirming the parallelism of the flow as shown in Figs.14(a)-14(c).

The uncertainty of the measurements are functions of variations of the ambient temperature and pressure, the specific gravity of the manometric liquid and the accuracy of the manometric readings. It was found to be less than $\pm 2.5\%$. The uncertainty of the measurements for non-dimensional pressure drop is discussed in APPENDIX-E.

CHAPTER V
RESULTS AND DISCUSSION

5.1. General

Laminar flow properties in the entrance region of an annulus were calculated both by the Integral method and the Finite Difference method. The pressure gradient used in the second method was obtained from the result of the Integral method. The solution by the Integral method was obtained by assuming fully developed velocity profile within the boundary layer and a constant ratio of the inner to the outer boundary layer thicknesses. Pressure drop in the entrance region of a parallel plate channel was found experimentally. The analytical results for pressure drop obtained from the Integral method were extended to compare with the experimental ones. All calculations for both the Integral and the Finite Difference technique were carried out by assuming a flat velocity profile at the entry.

This chapter presents the results of entrance flow characteristics for five different radius ratio annuli ($\alpha = 0.01, 0.05, 0.10, 0.25$ and 0.50) along with their comparisons.

5.2. Pressure drop

A pressure drop model:

$$\begin{aligned}
 P_0 - P &= \left(\frac{dP}{dX}\right)_{fd} X + K(X) = 4X \coth(AX^{B+X}); \quad 0 \leq X \leq X_1 \quad (5.1) \\
 &= \left(\frac{dP}{dX}\right)_{fd} X + K(\infty); \quad X > X_1
 \end{aligned}$$

was proposed and the values of the constants were found by fitting the equation (5.1) with the results obtained from the Integral method. X_1 is the distance, X , where $(\frac{dP}{dX})_{X_1} = (\frac{dP}{dX})_{fd}$. The values of A and B for different radius ratio annuli are presented in Table 5.1.

TABLE 5.1. Values of A & B of Pressure Drop Equation (5.1) for Different Radius Ratio Annuli

α	A	B	RMS error %
0.01	0.18581	0.42928	1.042
0.05	0.18746	0.43155	1.155
0.10	0.18693	0.43108	1.305
0.15	0.18548	0.42944	1.497
0.20	0.18357	0.42729	1.718
0.25	0.18081	0.42434	1.999
0.30	0.17809	0.42126	2.307
0.35	0.17704	0.41928	2.563
0.40	0.17616	0.41728	2.838
0.45	0.17613	0.41579	3.098
0.50	0.17714	0.41491	3.339

The development of incremental pressure drop $K(X)$ for different radius ratio annuli was shown in Fig. 6. As may be seen from Fig. 6, the incremental pressure drop developments for $\alpha = 0.50$ and $\alpha = 1$ are approximately the same. But the curves for $\alpha = 0.01$ and $\alpha = 0.0$ are not close to each other.

This significant difference between the incremental pressure drops for very small α and $\alpha = 0$ may be attributed to the different physical boundary conditions prevailing near the centre for the two cases. For very small values of α the velocity is zero near the centre whereas for $\alpha = 0$ it is near the maximum. In the case of higher radius-ratio ($\alpha \geq 0.50$) the effect of the curvature of the inner and the outer pipes of an annulus on the flow becomes negligible and hence leads to a single pressure drop curve for $0.5 \leq \alpha \leq 1.0$.

The experimental results for pressure drop in the entrance region for flow through a parallel plate channel at Reynolds number, $Re = 609, 1066, 1234$ and 1599 are shown in Fig. 7. Very close to the entrance and at low Reynolds number, the results deviated from the curve of equation (5.1) for $\alpha = 0.5$ because of the fact that in the region very close to the entrance the derivative $(\frac{\partial^2 u}{\partial x^2})$ is not negligible relative to $\frac{1}{r} \frac{\partial}{\partial r}(r \frac{\partial u}{\partial r})$ and the pressure gradients in the radial direction were not small [37]. For small Reynolds number a concave velocity distribution ($\frac{\partial^2 u}{\partial r^2} > 0$) in the central portion existed very near ($X \approx 0.001$) for $Re = 300$ the entrance [12,37]. These deviations may be attributed to the assumptions of negligible axial momentum transport with respect to radial momentum transport and a constant velocity in the central portion near the entrance. However, at a distance far from the entrance the experimental points are close to the present theoretical curve.

5.3. Velocity Distribution:

The results from the Finite Difference method for the axial and radial velocity profiles for different radius ratio annuli ($\alpha = 0.01, 0.05, 0.10, 0.25$ & 0.50) are presented in Figs. 8(a)-8(e) and 10(a)-10(e) respectively. The velocity profiles based on the fully developed flow, which were used in the Integral method are also presented in Figs. 8(a)-8(e) for comparison. As may be seen from Figs. 8(a)-8(e), there exists a difference between the velocity profiles obtained from the Finite Difference technique and that from the Integral solution. This difference is prominent near the entrance and near to the walls.

The finite difference results predicted that the velocity profile in the entrance region was parabolic within the boundary layer but not of the same degree as that of the fully developed profile. The velocity profile was not symmetrical with respect to the centre of the hydraulic radius ($\frac{R_2 - R_1}{R_2 + R_1} = 0.5$) of the annulus. The velocity close to the inner pipe was higher than that close to the outer pipe for the same distance from the wall. But this skewness of the velocity profile towards the inner wall decreased as the radius ratio of annulus increased. The skewness of the radius of the maximum velocity with respect to the centre of the hydraulic radius is given in Table 5.2. The variation of core radius along the axial distance is shown in Fig. 13.

The results for axial variation of core velocity obtained by the Finite Difference method and that of Heaton et al [15]

TABLE 5.2. Skewness of the Core Radius with respect to the Centre of the Hydraulic Radius of Different Radius Ratio Annuli

α	$1 - \frac{R_\delta}{(R_1 + (R_2 - R_1)/2)}$	
	At far downstream	At end of Inlet region
0.01	44.63%	15.68%
0.05	22.28%	10.86%
0.10	15.7%	6.55%
0.25	6.96%	2.4%
0.50	1.93%	1.33%

are shown in Fig. 9. It can be seen from Fig. 9 that the results of Heaton et al deviate from that of the Finite Difference solution in the region near to the entrance because of the assumption of negligible radial velocity made by them.

The variation of the outer and inner wall shear stresses for the five radius ratio annuli considered are plotted in Figs. 11(a)-11(j). In Figs. 11(a)-11(e), the stresses were nondimensionalised by the shear stress at the outer wall of the fully developed flow and in Figs. 11(f)-11(j), by the respective stresses of the fully developed flow. The relative difference of the shear stress at the inner wall with that at the outer wall can be observed in Figs. 11(a)-11(e). The

stresses obtained from the Integral method are shown in Figs. 11(f)-11(j) and they deviate significantly from those obtained by the Finite Difference method. This deviation is due to the assumed velocity profile for the Integral method.

The results for radial velocity at different axial locations for different radius ratio annuli are plotted in Figs. 10(a)-10(e). The radial velocity caused by the acceleration of the fluid in the entrance region decayed along the downstream gradually. The magnitude of the radial velocity was small compared to the axial component. The radial velocity was also influenced by the radius ratio. For small radius ratio annuli ($\alpha < 0.01$) the radial velocity decayed more quickly near the inner wall than the outer wall. And at higher radius ratio annuli ($\alpha \geq 0.50$) the radial velocities originating from the two walls are almost similar.

5.4. Length of the Entrance Region

After the development of the boundary layer under the accelerating core, the final adjustment of the completely viscous velocity profile to the fully developed solution marks the end of the entrance region. Shingo (cf. [20]) identified the boundary layer region as the 'inlet region' and the fully viscous region as the 'filled region'.

Figs. 12(a)-12(e) show the growth of the boundary layers with the axial distance for five radius ratio annuli ($\alpha = 0.01, 0.05, 0.10, 0.25, \& 0.50$). The boundary layers obtained from the Integral method met at the core radius of the annulus

at the end of the entrance region. The assumptions of the velocity profile based on the fully developed profile and the constant ratio of the inner and the outer wall layer growth for the Integral solution failed to predict the two distinct regions (viz. the inlet and the filled region) which were experimentally found by Mohanty and Asthana [20] for flow through a smooth pipe. The existence of these two regions for flow through an annulus was established by the Finite Difference method. In the inlet region, at the edge of the boundary layer $(\partial U/\partial R) = 0$ and $(\partial^2 U/\partial R^2)_c = 0$. For numerical computation of the boundary layer thickness it was assumed that at the edge of the boundary layer $|\partial U/\partial R| \approx 0.01$, and the length of the inlet region was defined as the distance from the entrance where $(\partial^2 U/\partial R^2)_c \approx -2.0$, based on the assumption $U/U_c = 0.9999$. Also the length of the entrance region was defined as the distance from the entrance where the average value of the viscous term (i.e. $\nabla^2 u$) of the Navier-Stokes equation reaches 101% of that of the fully developed value. Since in the entrance region, the core velocity develops to its fully developed value asymptotically, most of the researchers [5,6,13,20,28,37 etc.] assumed the entrance length as the distance from the entrance to the point where the core velocity reaches 99% of its fully developed value. Murakawa [22] defined this entrance length for annular passage as the distance where the developing velocity profile matched with that of the fully developed one. In the present investigation, calculation of the length of the entrance region was done by

considering an average viscous property change to its fully developed value instead of the development of the axial velocity at a particular radius. The computed values of the lengths of the Inlet region and the Entrance region are listed in Table 5.3.

TABLE 5.3. Results of the Lengths of the Inlet and the Entrance Region for Different Radius Ratio Annuli

α	X_i	X_e	U_c/U_o at X_e	RMS of $(U-U_{fd})$ at X_e
0.01	0.00285	0.10	0.995	0.00075
0.05	0.00255	0.030	0.986	0.00213
0.10	0.0024	0.0165	0.982	0.00253
0.25	0.0023	0.0125	0.99	0.00147
0.40	0.00225	0.0120	0.992	0.00108
0.50	0.0022	0.0115	0.9865	0.00155

In the Finite Difference calculations, the cumulative RMS error of the U_o at each station of calculation did not exceed 0.00025.

CHAPTER VI
CONCLUSIONS

Laminar flow characteristics in the entrance region of annuli were obtained both by the Integral method and the DuFort-Frankel type of Finite Difference method for a flat velocity profile at the entry. The solution by the Integral method was obtained by assuming fully developed velocity profile within the boundary layer, and a constant ratio of the inner to the outer boundary layer thicknesses at any axial distance in the entrance region. The results for the pressure drop by this method were compared with the existing analytical results for flow through pipe and parallel plate channel. The result for the pressure drop for $\alpha = 0.5$ obtained by this method was in good agreement with that of the existing results for parallel plate channel ($\alpha = 1$).

The pressure gradient obtained by the Integral method was used in the Finite Difference method. The results obtained by the Finite Difference method for velocity profile within the boundary layer and the ratio of the inner to the outer wall layers did not agree with the assumptions for velocity profile and the boundary layer thickness made for the Integral method. The axial velocity profile in the entrance region changed with axial distance to its fully developed profile at a distance far into the downstream. The radial velocity component was calculated to be small compared with the axial velocity, and it decayed with the axial distance. Such decay of radial velocity was expected and the nature of decaying was found to be a function of radius ratio.

The growth of the boundary layers obtained by the Finite Difference method yielded two distinct zones of the entrance region viz. (i) the Inlet region and (ii) the Filled region, which were also reported earlier by Mohanty and Asthana [20] for flow through a smooth pipe. Boundary layers met together at the end of the Inlet region but the velocity profile changed with axial distance and achieved a fully developed profile at the end of the Filled region.

The asymmetry of the velocity profile near the entry was small but gradually increased along the axial distance to its fully developed nature. For annuli with radius ratio, $\alpha = 0.5$, this asymmetry was found to be small.

The length of the entrance region was calculated on the basis of the viscous term of the momentum equation rather than the development of the core velocity.

Considering the flow characteristics in the entrance region obtained in this work and the existing fully developed flow parameters, it can be inferred that the effect of the radius ratio on the flow is very small for $0.5 \leq \alpha \leq 1.0$.

The pressure distribution in the entrance region of a parallel plate channel (aspect ratio of 97) was investigated experimentally at four different Reynolds numbers, $Re = 609, 1066, 1234$ and 1599 . The analytical results for pressure drop from the Integral method were extended to compare with the experimental ones and they were found to be in good agreement at higher Reynolds number except in the region near to the entrance.

REFERENCES

REFERENCES

1. Atkinson, B., Kemblowski, Z. and Smith, J.M., "Measurements of Velocity Profile in Developing Liquid Flows", A.I.Ch.E. Journal, Vol. 13, No. 1, 1967, pp. 17-20.
2. Boussinesq, J., "Sur la maniere dont les vitesses, dans un tube cylindrique de section circularie, evase a son entree, se distribuent depuis cette entree jusqu'aux endroits on se trouve etabli un regime uniforme," Comptes Rendus, Vol. 113, 1891, pp. 9-15, 49-51.
3. Bogue, D.C., Industrial Engineering Chem., Vol. 51, 1959, p. 894.
4. Bird, R.B., Stewart, W.E. and Lightfoot, E.N., Transport Phenomena, Wiley, New York, 1960.
5. Campbell, W.D. and Slattery, J.C., "Flow in the Entrance of a Tube" Journal of Basic Engineering, Trans. ASME, 1963, pp. 41-46.
6. Christiansen, E.B. and Lemon, H.E., "Entrance Region Flow", A.I.Ch.E. Journal, Vol. 11, No.6, 1965, pp.995-999.
7. Collins, and Schowalter, W.R, A.I.Ch.E. Journal, Vol. 9, 1963, pp. 804-809.
8. Dorsey, N.E., Phys. Rev., Part 2, Vol. 83, 1926, p. 833.
9. DuFort, E.C. and Frankel, S.P., "Stability Conditions in the Numerical Treatment of Parabolic Differential Equations", Mathematical Tables Aids Computation, Vol. 7, 1953, pp. 135-152.
10. Fleming, D.P. and Sparrow, E.M., "Flow in the Hydrodynamic Entrance Region of Ducts of Arbitrary Cross-section", Journal of Heat Transfer, Trans. ASME, 1969, pp. 345 - 354.
11. Forsythe, G.E. and Wasow, W.R., Finite Difference Methods for Partial Differential Equations, Wiley, New York, 1960, pp. 88-139.
12. Friedmann, M., Gillis, J. and Liron, N., "Laminar Flow in a Pipe at Low and Moderate Reynolds Number", Appli. Sci. Res., Vol. 19, 1968, pp. 427-438.
13. Gupta, R.C., "Flow Development in the Hydrodynamic Entrance Region of a Flat Duct", A.I.Ch.E. Journal, Vol. 11, No. 6, 1965, pp. 1149-1151.
14. Goldstien, S., Modern Developments in Fluid Dynamics, Vol. 1, Clarendon Press, Oxford, 1938.

15. Heaton, H.S., Reynolds, W.C. and Kays, W.M., "Heat Transfer in Annular Passages, Simultaneous Development of Velocity and Temperature Fields in Laminar Flow", Int. Journal of Heat & Mass Transfer, Vol. 7, 1964, pp. 763-781.
16. Han, L.S., Journal of Applied Mechanics, Vol. 27, 1960, p.403.
17. Knibbs, G.H., Proc. Roy. Soc. N.S. Wales, Vol. 29, 1895, p.77.
18. Langhaar, H.L., "Steady Flow in the Transition Length of a Straight Tube", Journal of Applied Mechanics, Vol. 9, Trans. ASME, Vol. 64, 1942, pp. A-55-A-58.
19. Lachmann, G.V., Boundary Layer and Flow Control , Vol. 2, Pergamon Press., 1961, pp. 970-980.
20. Mohanty, A.K. and Asthana, S.B.L., "Laminar Flow in the Entrance Region of a Smooth Pipe", Journal of Fluid Mechanics, Vol. 90, Part 3, 1978, pp.433-447.
21. Mattai, S., "Prediction of Wall Layer Growth in Developing Laminar Flow Through Concentric Annuli", Ph.D. Thesis, University of Windsor, 1980.
22. Murakawa, K., "Heat Transfer in Entry Length of Double Pipes", Int. Journal of Heat and Mass Transfer, Vol. 2, 1961, pp. 240-251.
23. O'Brien, G.G. Hyman, M.A. and Kaplan, S., "A Study of Numerical Solution of Partial Differential Equations", Journal of Mathematical Physics, Vol.29, 1951, p. 223.
24. Punnis, B., Thesis, Gottingen, 1947.
25. Prandtl, Ludwig and Tietjens, O.J., Applied Hydro-and Aeromechanics , McGraw-Hill, New York, 1934.
26. Rieman, W.J., Journal of American Chem. Soc. Vol. 50, 1928. pp. 46-55.
27. Slezkin, N.A., Dynamics of Viscous Incompressible Fluids (in Russian), Gostekhizdat; Moscow, 1955.
28. Sparrow, E.M., Lin, S.H. and Lundgren, T.S., "Flow Developments in the Hydrodynamic Entrance Region of Tubes and Ducts", The Physics of Fluids, Vol.7, No. 3, 1964, pp. 338-347.
29. Shiller, L., Z. Angew. Math. Mech., Vol. 2, 1922, pp.96-106.
30. Schlichting, H., Boundary Layer Theory , McGraw-Hill, 6th ed., 1968, p. 176.

31. Siegel, R., "The effect of Heating on Boundary Layer Transition for Liquid Flow in a Tube", D.Sc. Thesis, MIT, 1953.
32. Tatsumi, T., "Stability of the Laminar Inlet Flow Prior to the Formation of Poiseuille Regime", Journal of Physical Society of Japan, Vol. 7, No. 5, 1952, pp. 489-495.
33. Tomita, Y., Bulletin of Society of Mechanical Engineers, Vol. 4, No. 13, 1961, pp. 77-86.
34. Van Dyke, M., "Entry Flow in a Channel", Journal of Fluid Mechanics, Vol. 44, 1970, pp. 813-823.
35. Vrentas, J.S., Duda, J.L. and Barger, K.G., "Effect of Axial Diffusion of Vorticity on Flow Development in Circular Conduits, Part 1. Numerical Solution", A.I.Ch.E. Journal, Vol. 12, No.5, 1966, pp.837-844.
36. Wilson, S.D.R., "Entry Flow in Channel, Part 2", Journal of Fluid Mechanics, Vol. 46, 1971, pp. 787-799.
37. Wang, Y. L. and Longwell, P.A., "Laminar Flow in the Inlet Section of Parallel Plates", A.I.Ch.E. Journal, Vol. 10, No. 3, 1964, pp. 323-329.
38. Weltmann, R.N. and Keller, T.A., Natl. Advisory Comm. Aeronaut. Tech. Note 3889, 1957.

FIGURES

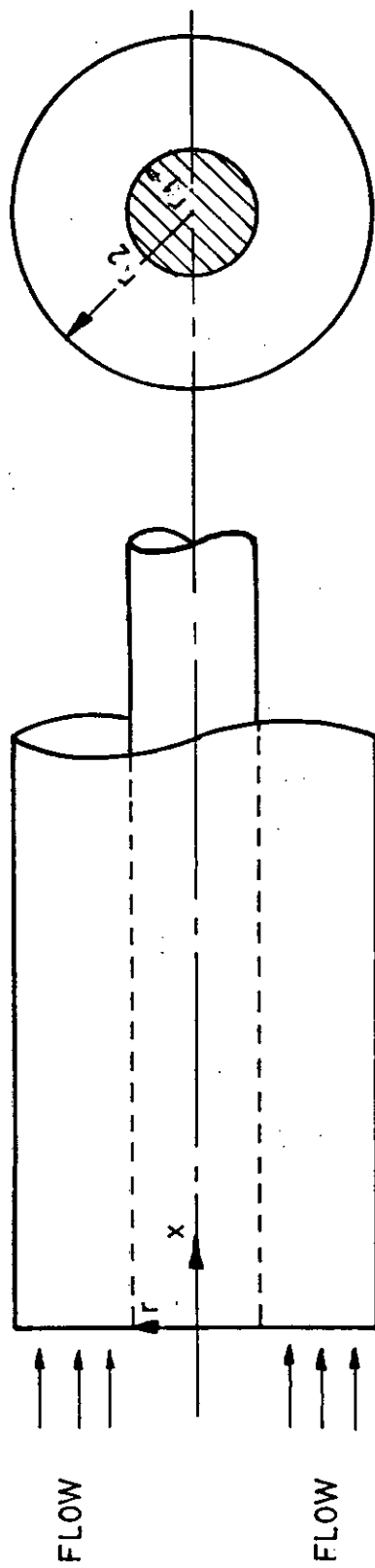


FIG. 1 COORDINATE SYSTEM FOR ANNULI

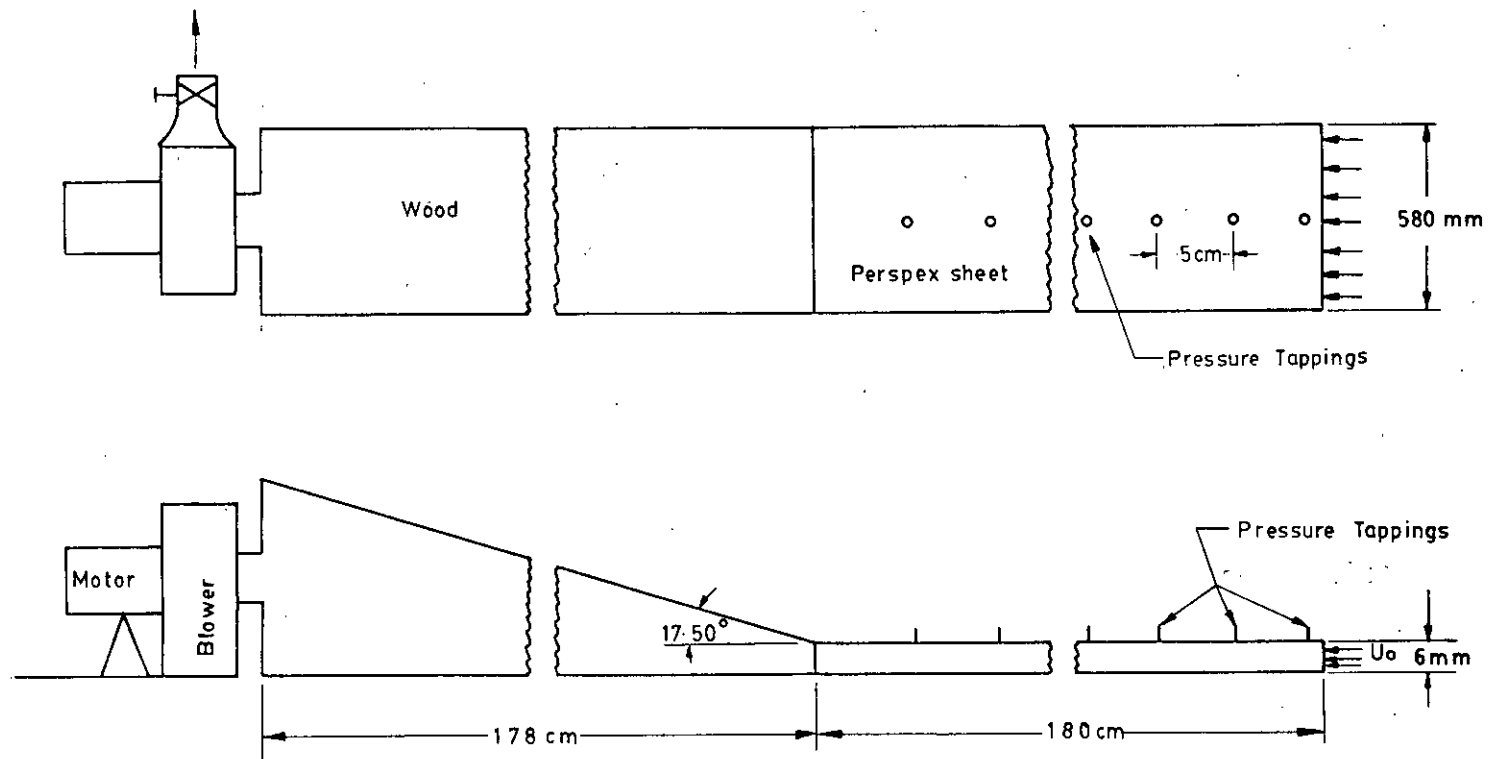


FIG.2 EXPERIMENTAL SET-UP FOR MEASURING THE PRESSURE DROP IN THE ENTRANCE REGION OF A PARALLEL PLATE CHANNEL.

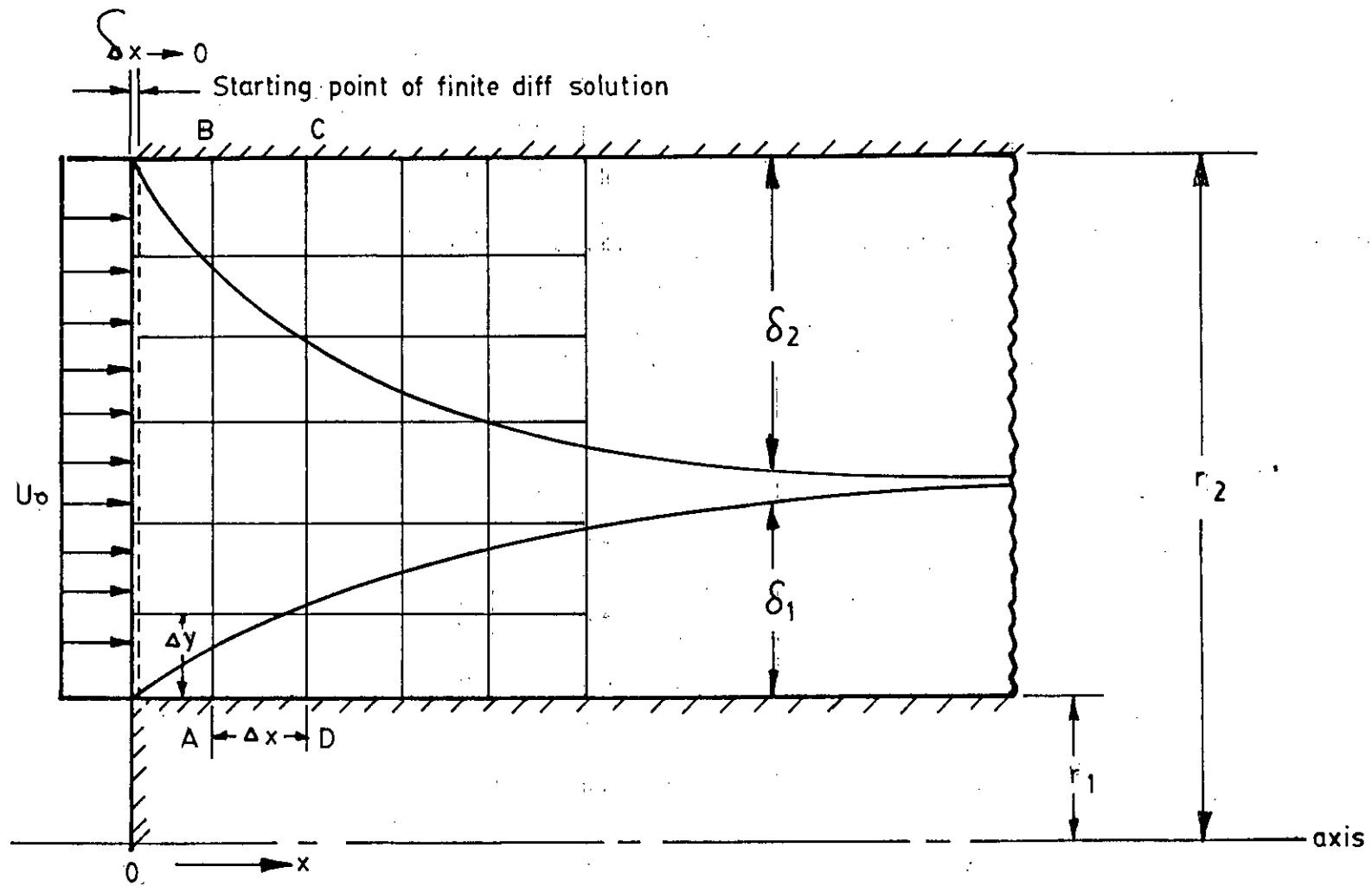


FIG-3 FINITE DIFFERENCE GRID SIZE FOR ANNULI

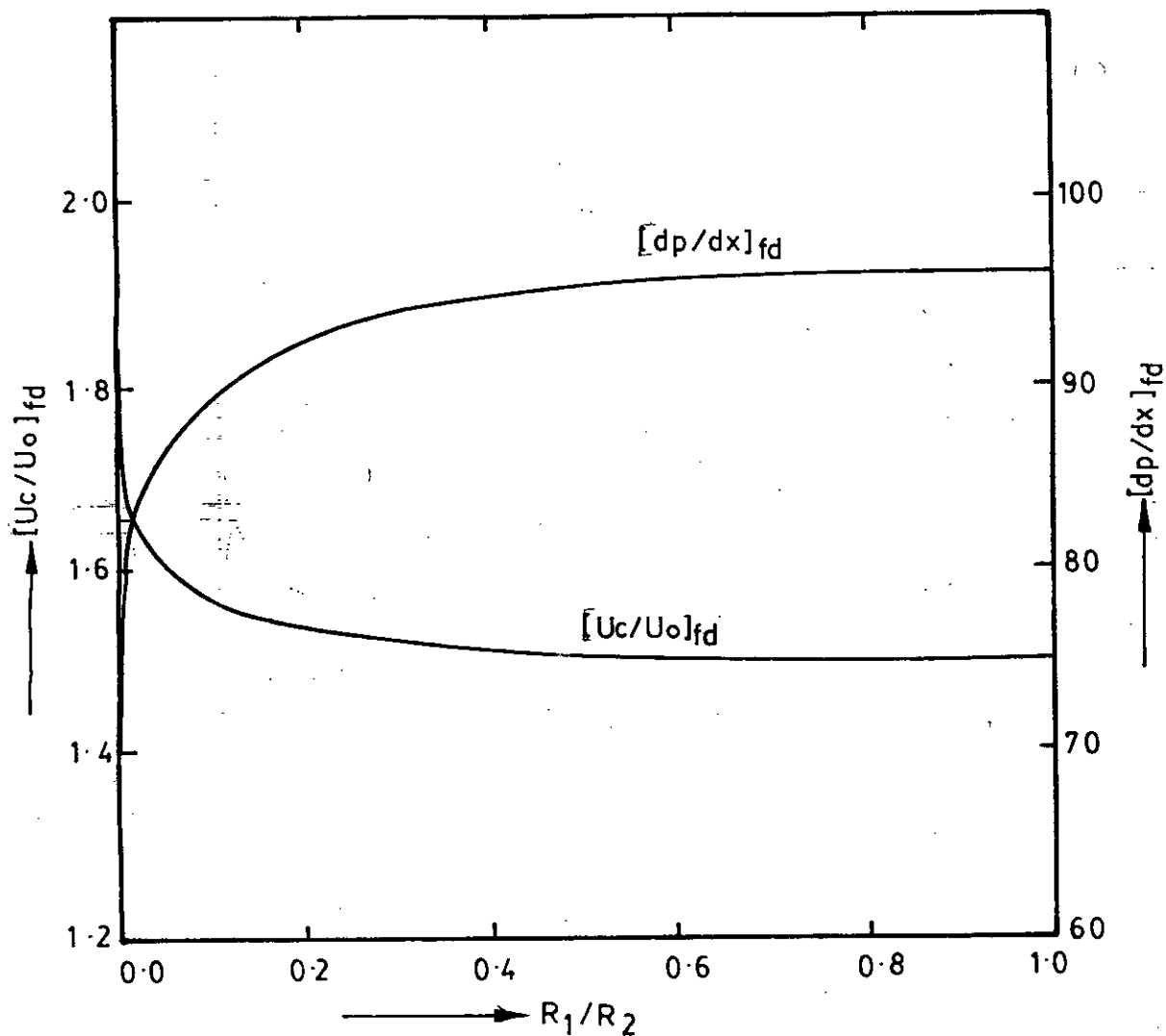


FIG. 4 FULLY DEVELOPED CORE VELOCITY AND PRESSURE GRADIENT FOR DIFFERENT RADIUS-RATIO ANNULI

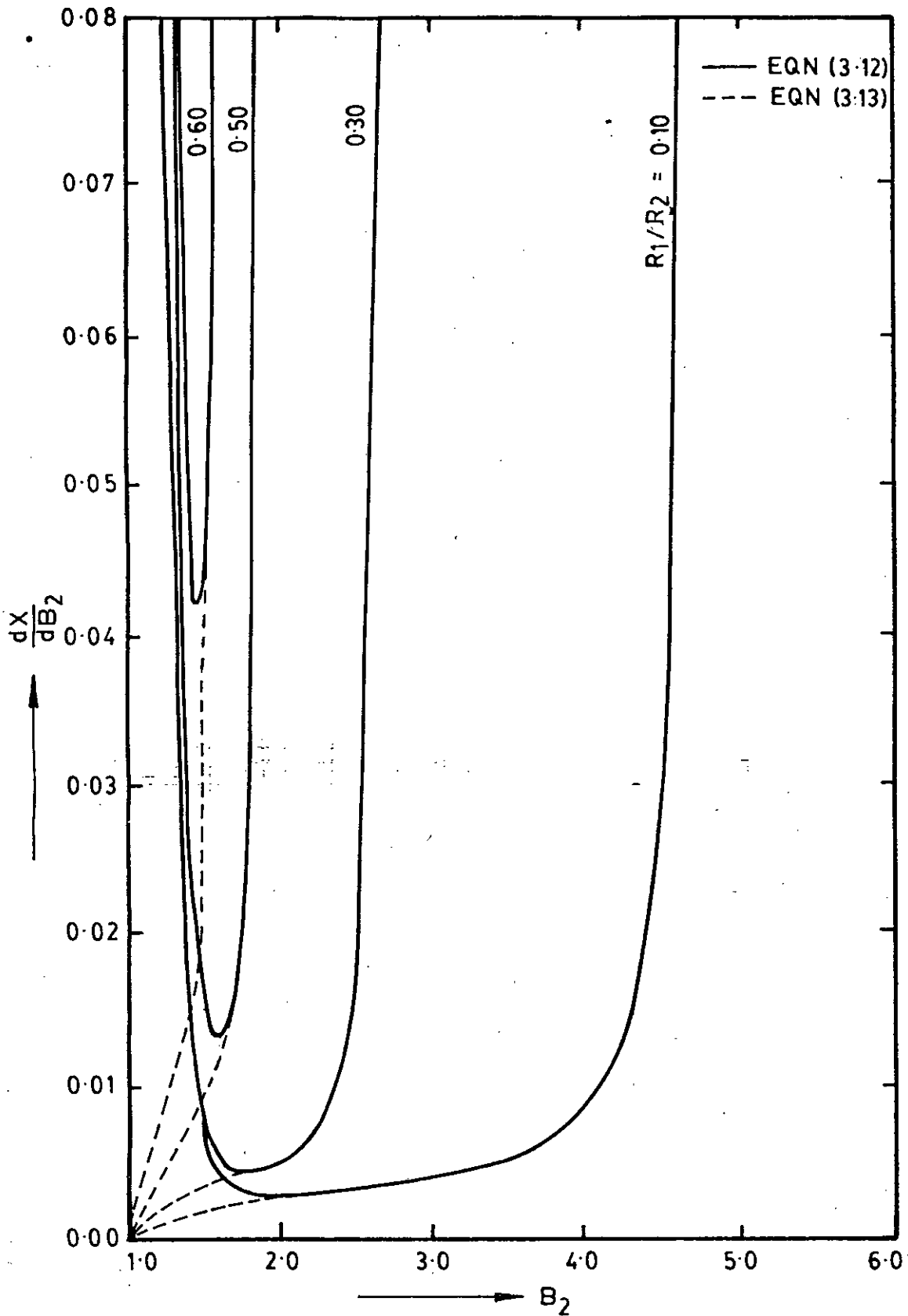


FIG-5 (dX/dB_2) VS B_2 FOR DIFFERENT RADIUS RATIO ANNULI

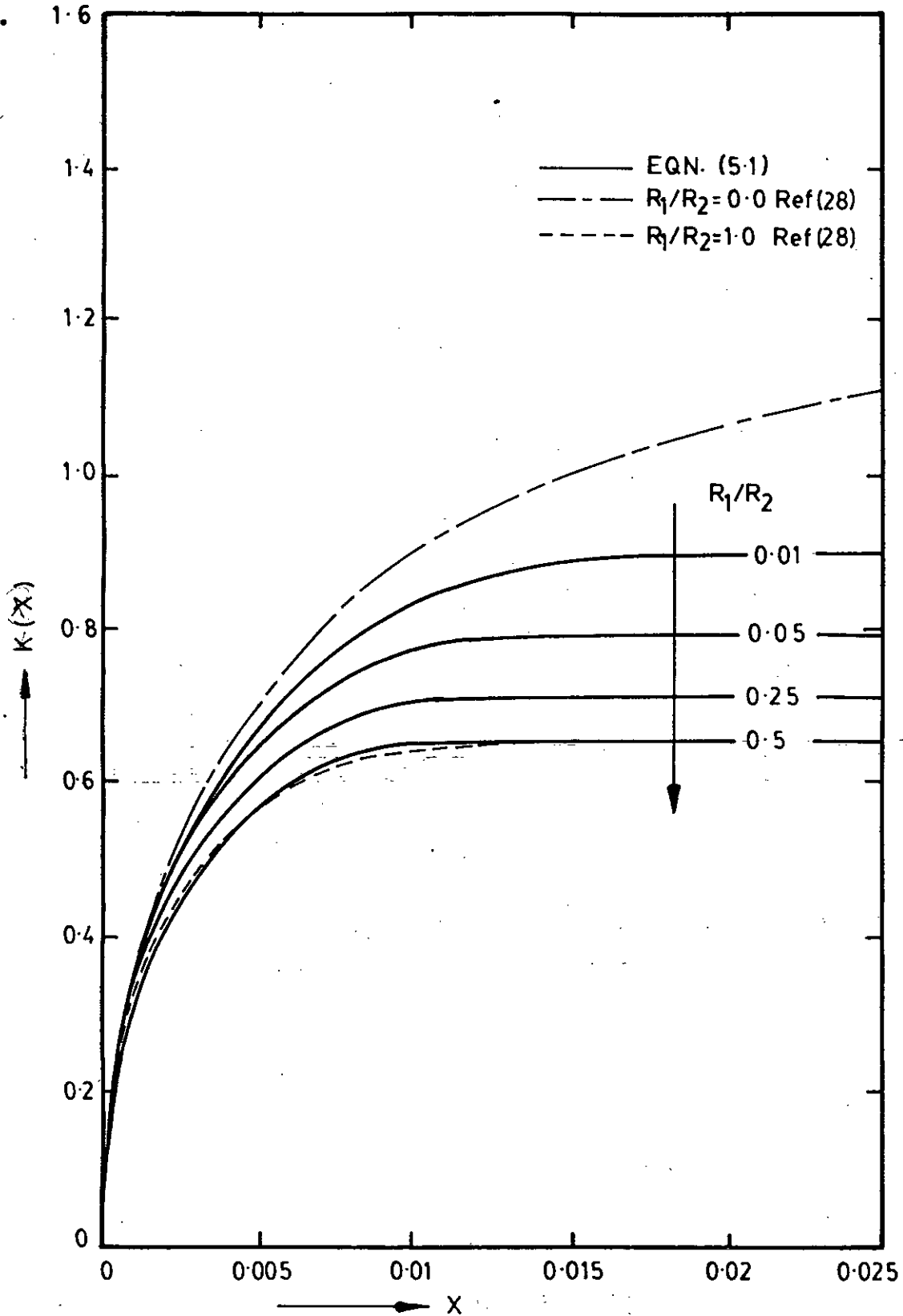


FIG. 6 INCREMENTAL PRESSURE DROP $K(X)$ FOR $R_1/R_2 = 0.01, 0.05, 0.25, 0.5$

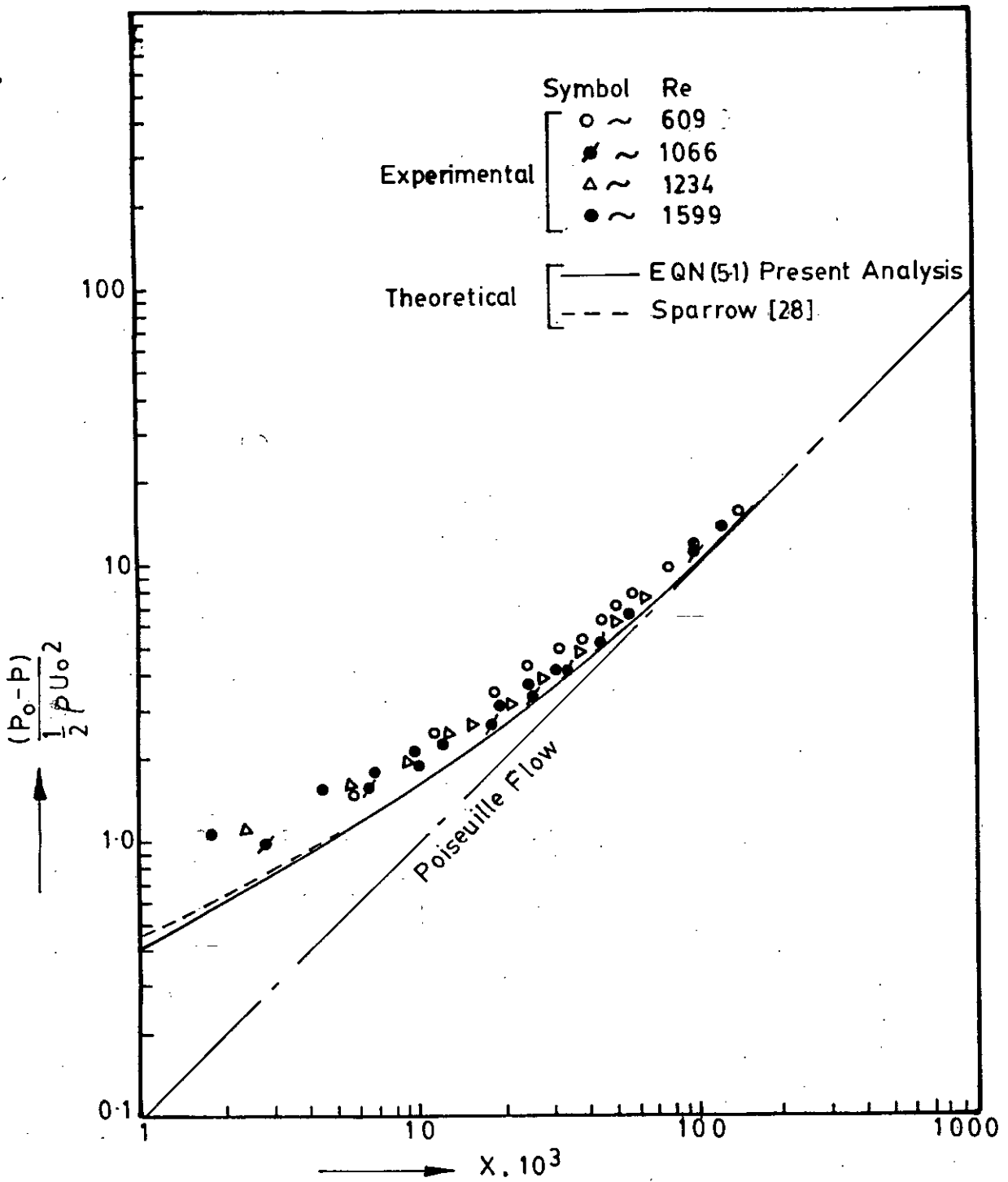
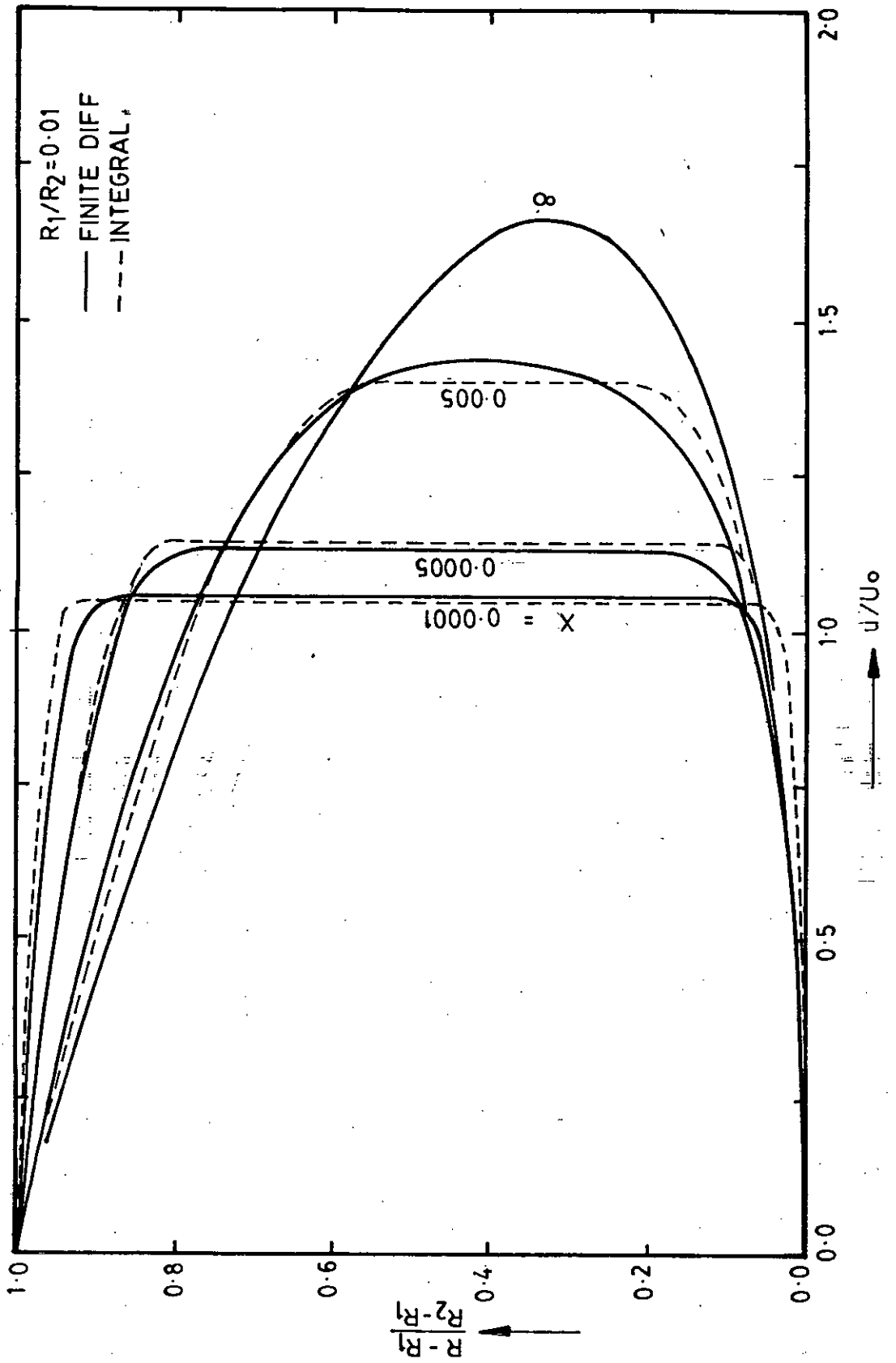


FIG. 7 Pressure Drop Vs Axial distance for Flow through Parallel Plate channel. (Aspect ratio 97)


 FIG. 8 (a) AXIAL VELOCITY PROFILE AT DIFFERENT AXIAL DISTANCES FOR $R_1/R_2 = 0.01$

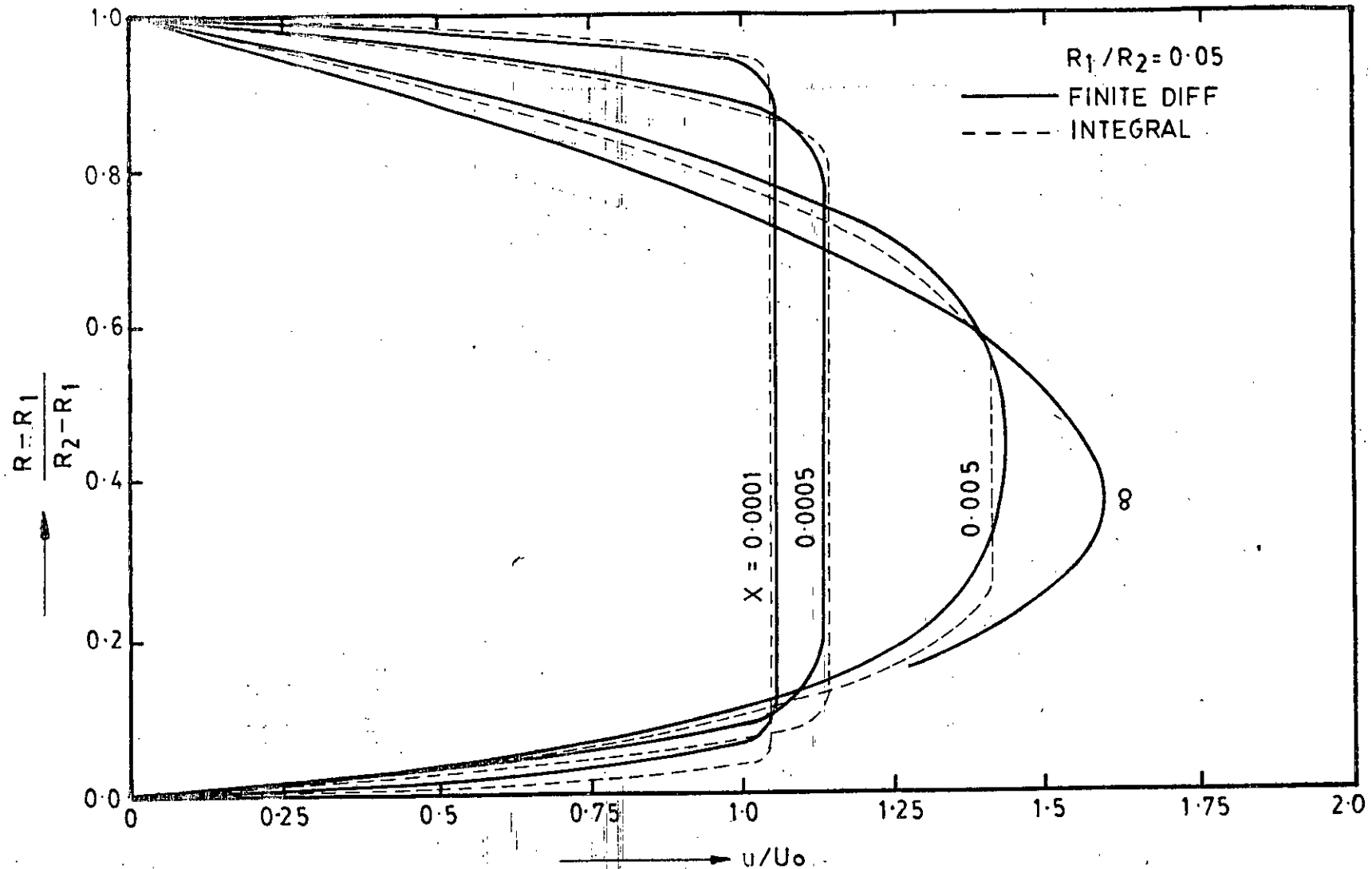


FIG. 8 (b) AXIAL VELOCITY PROFILE AT DIFFERENT AXIAL DISTANCES FOR $R_1/R_2 = 0.05$

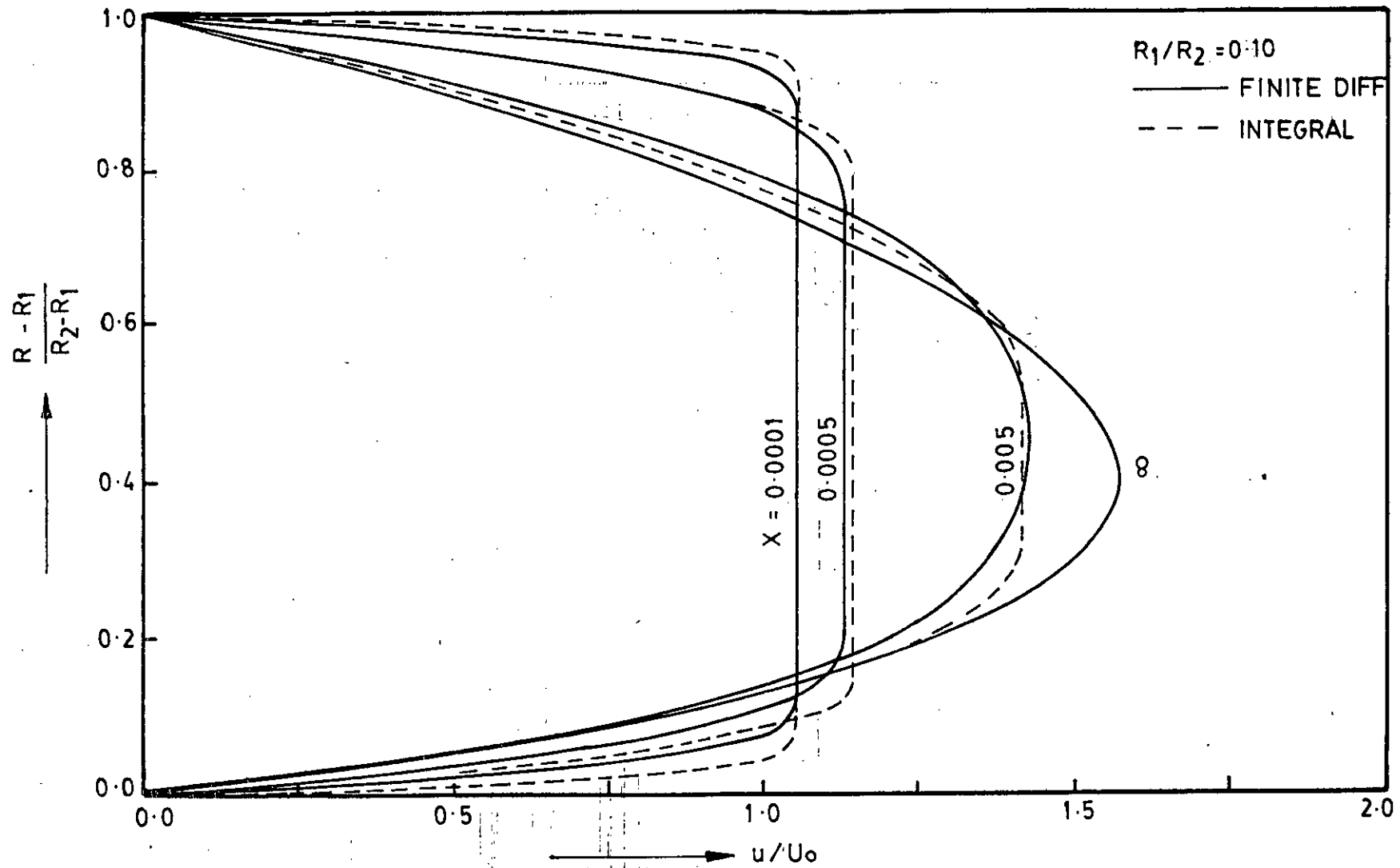


FIG. 8 (c) AXIAL VELOCITY PROFILE AT DIFFERENT AXIAL DISTANCES FOR $R_1/R_2 = 0.10$

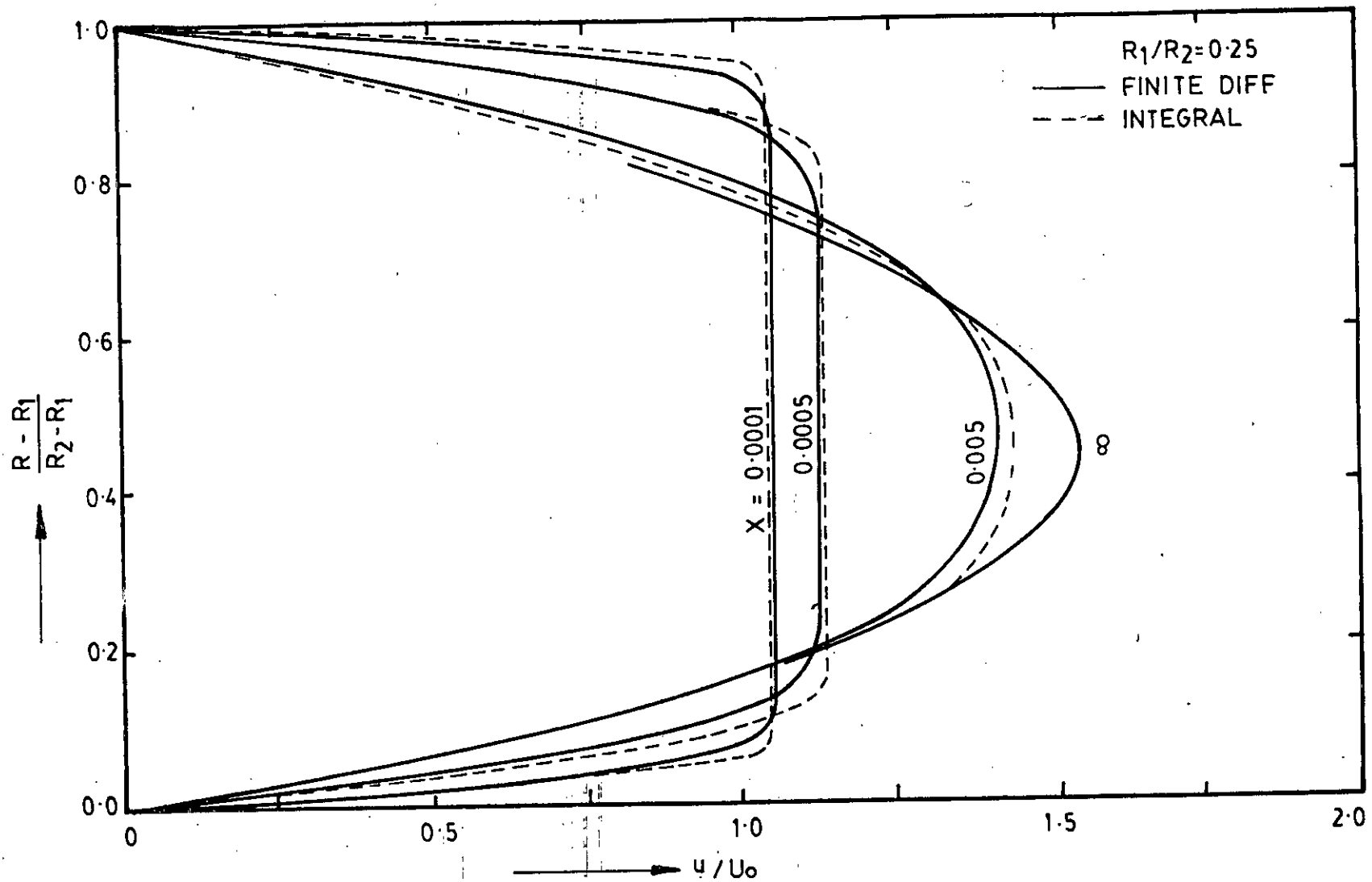


FIG. 8 (d) AXIAL VELOCITY PROFILE AT DIFFERENT AXIAL DISTANCES FOR $R_1/R_2=0.25$

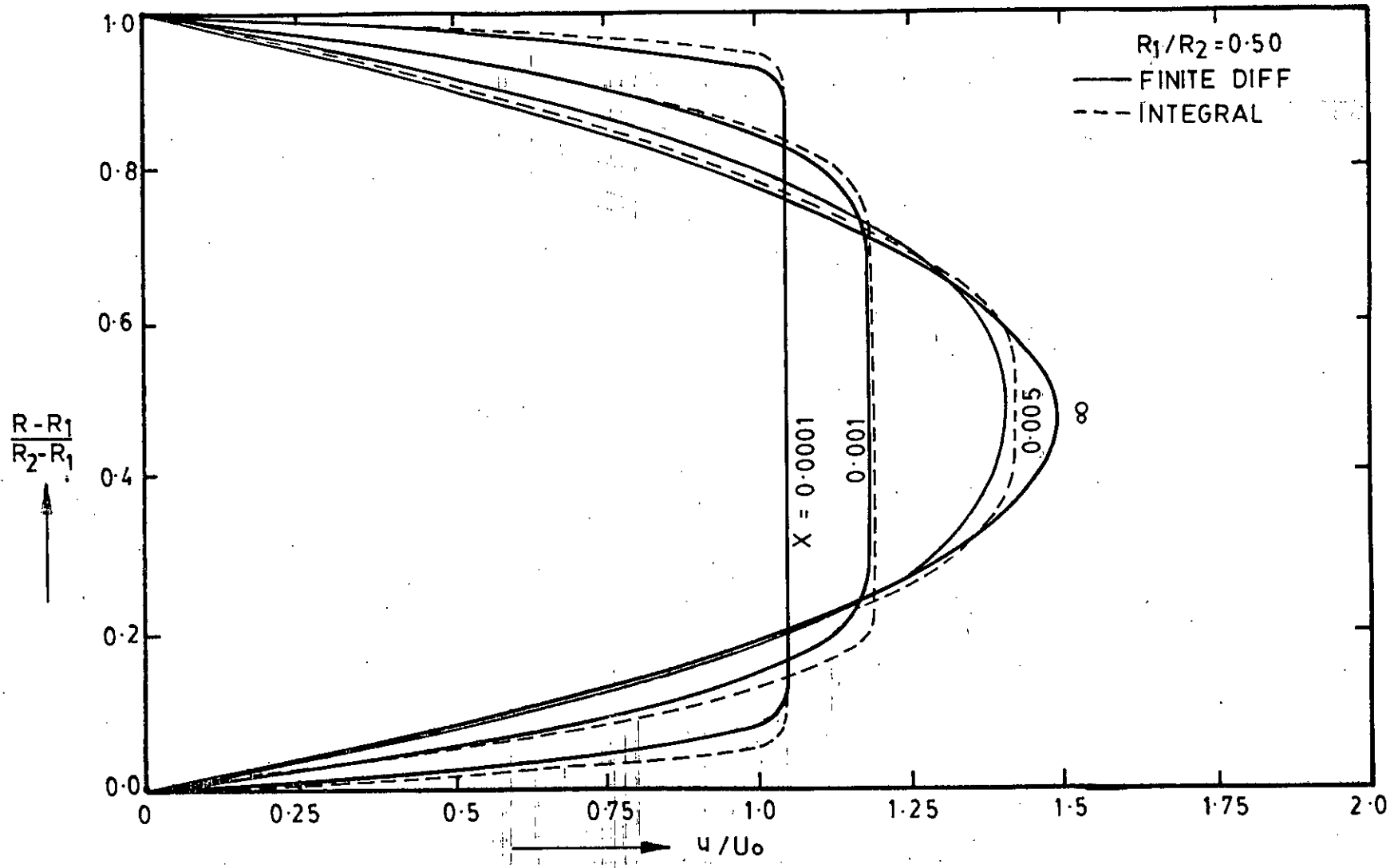


FIG. 8 (e) AXIAL VELOCITY PROFILE AT DIFFERENT AXIAL DISTANCES FOR $R_1/R_2=0.50$

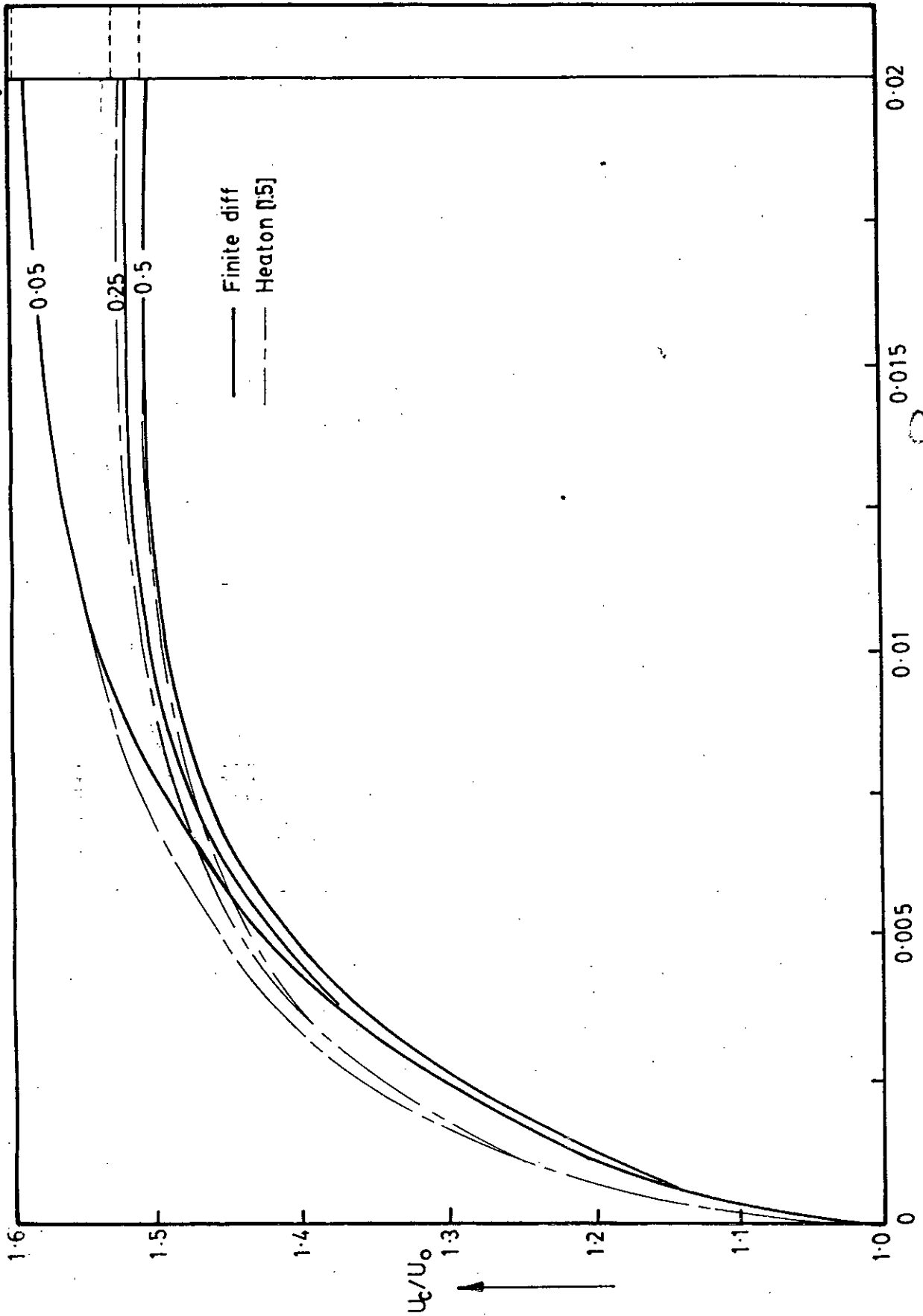


FIG. 9 Axial development of core velocity for $R_1/R_2 = 0.05, 0.25$ & 0.5

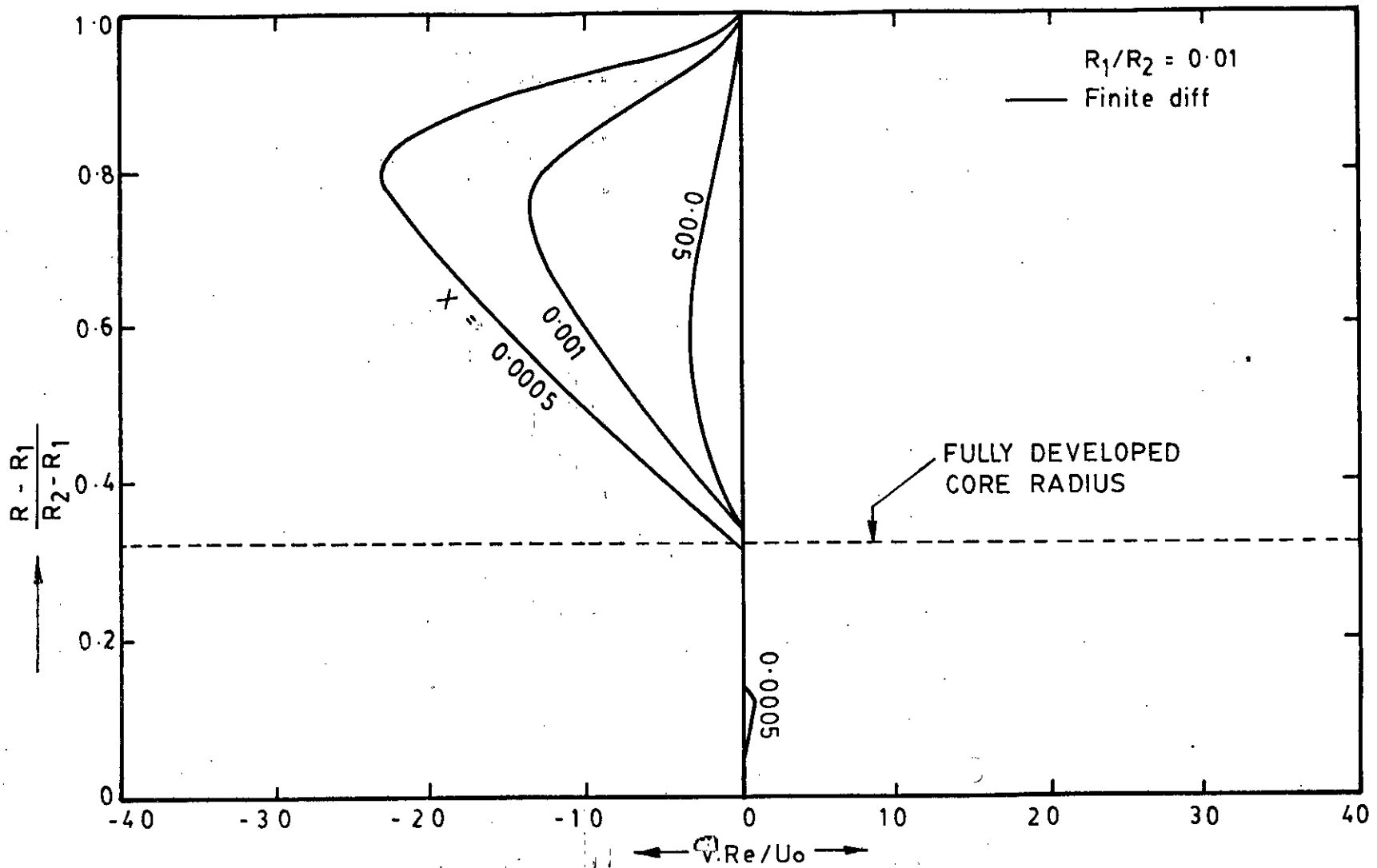


FIG. 10 (a) RADIAL VELOCITY AT DIFFERENT AXIAL DISTANCES FOR $R_1/R_2=0.01$

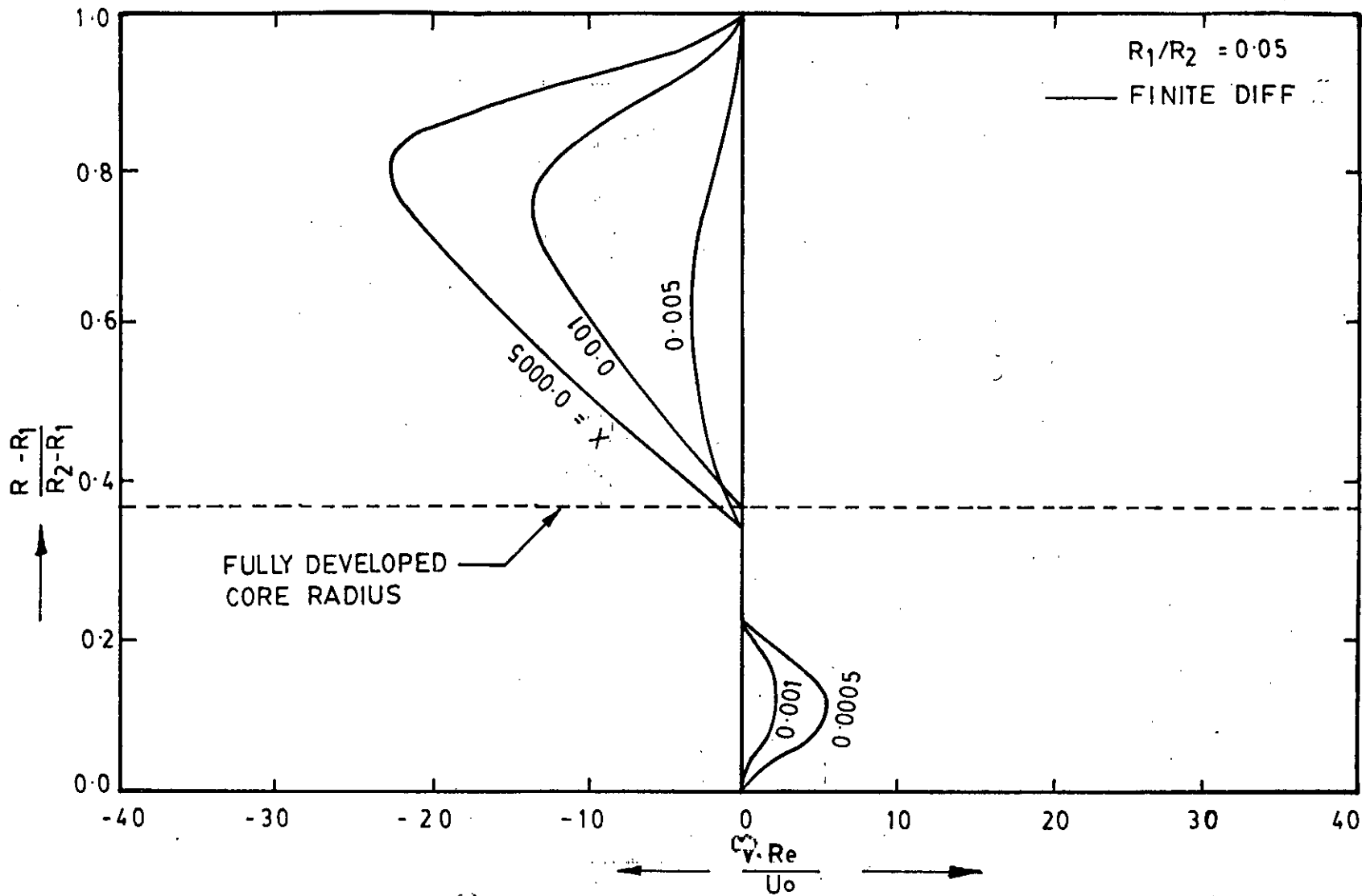


FIG. 10 (b) RADIAL VELOCITY AT DIFFERENT AXIAL DISTANCES FOR $R_1/R_2 = 0.05$

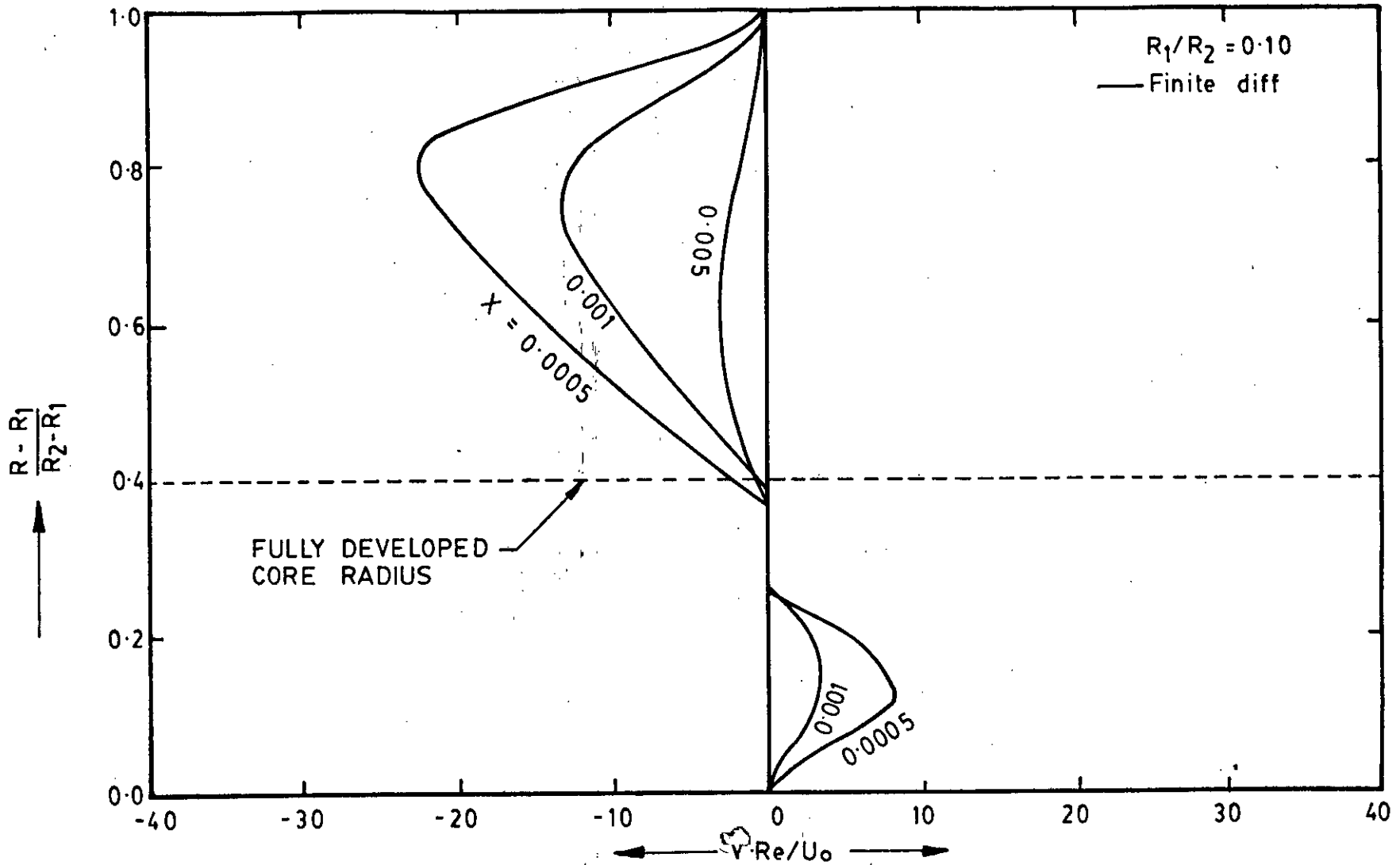


FIG. 10 (c). RADIAL VELOCITY AT DIFFERENT AXIAL DISTANCES FOR $R_1/R_2 = 0.10$

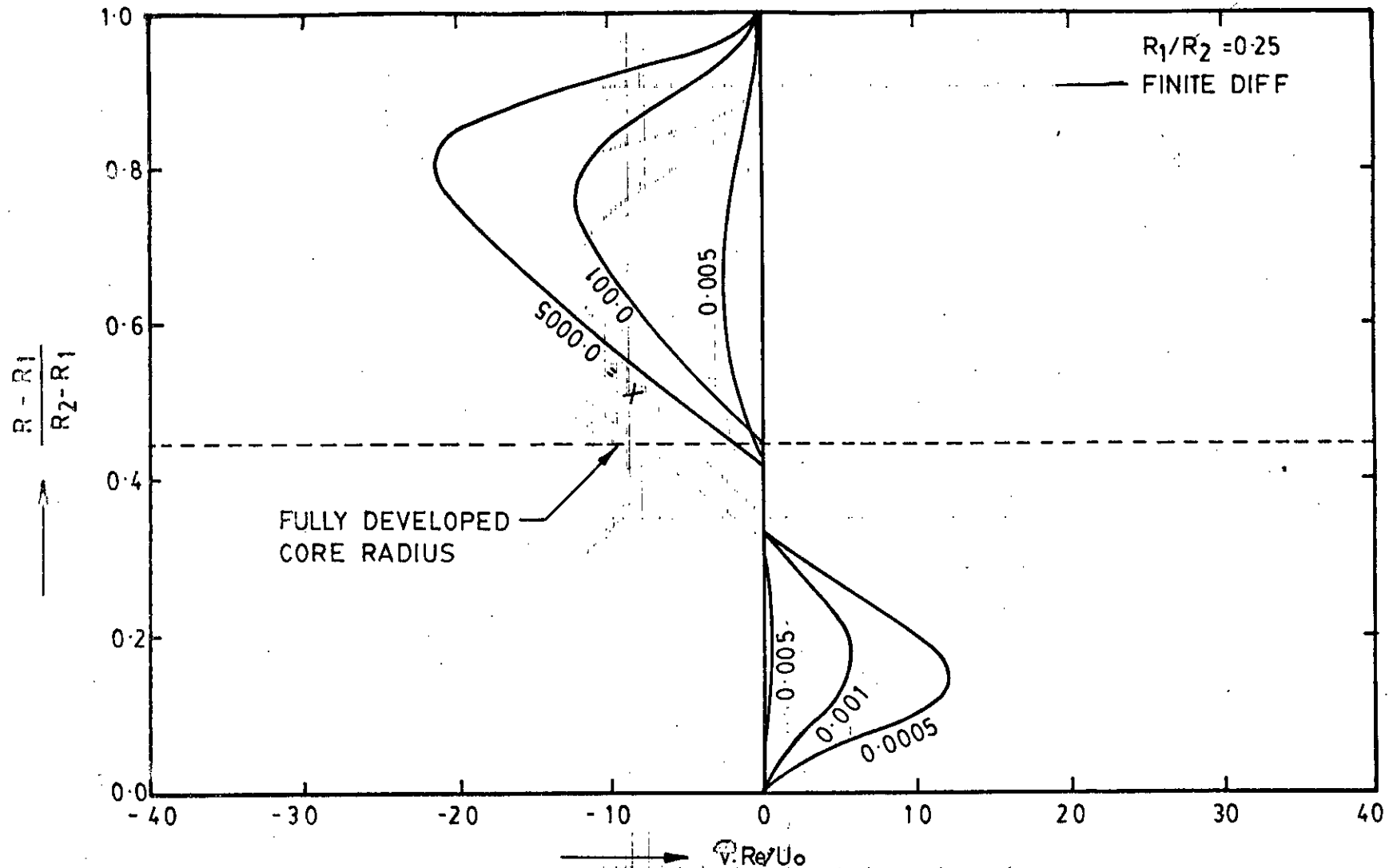


FIG. 10 (d) RADIAL VELOCITY AT DIFFERENT AXIAL DISTANCES FOR $R_1/R_2 = 0.25$

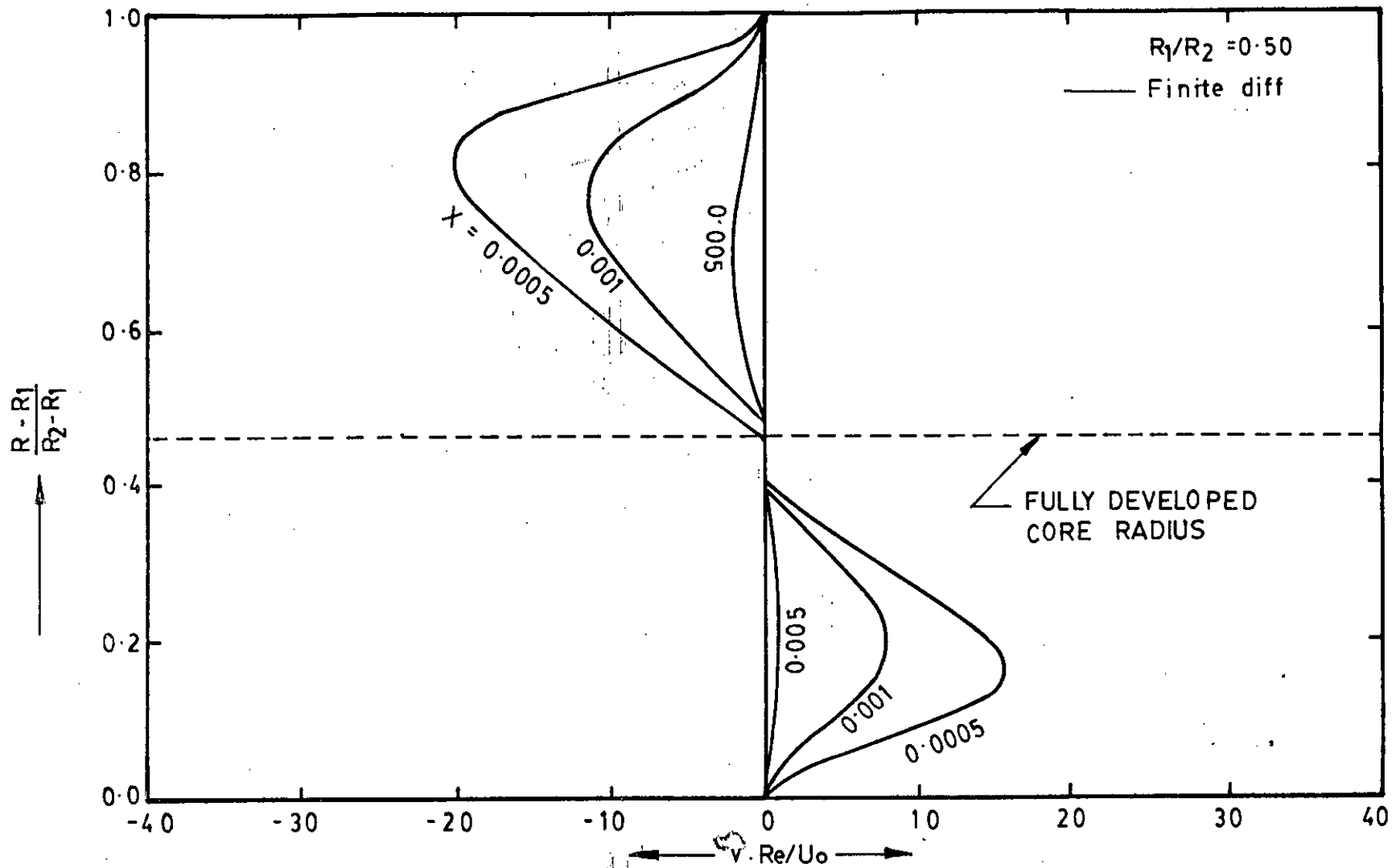


FIG. 10 (e) RADIAL VELOCITY AT DIFFERENT AXIAL DISTANCES FOR $R_1/R_2=0.5$

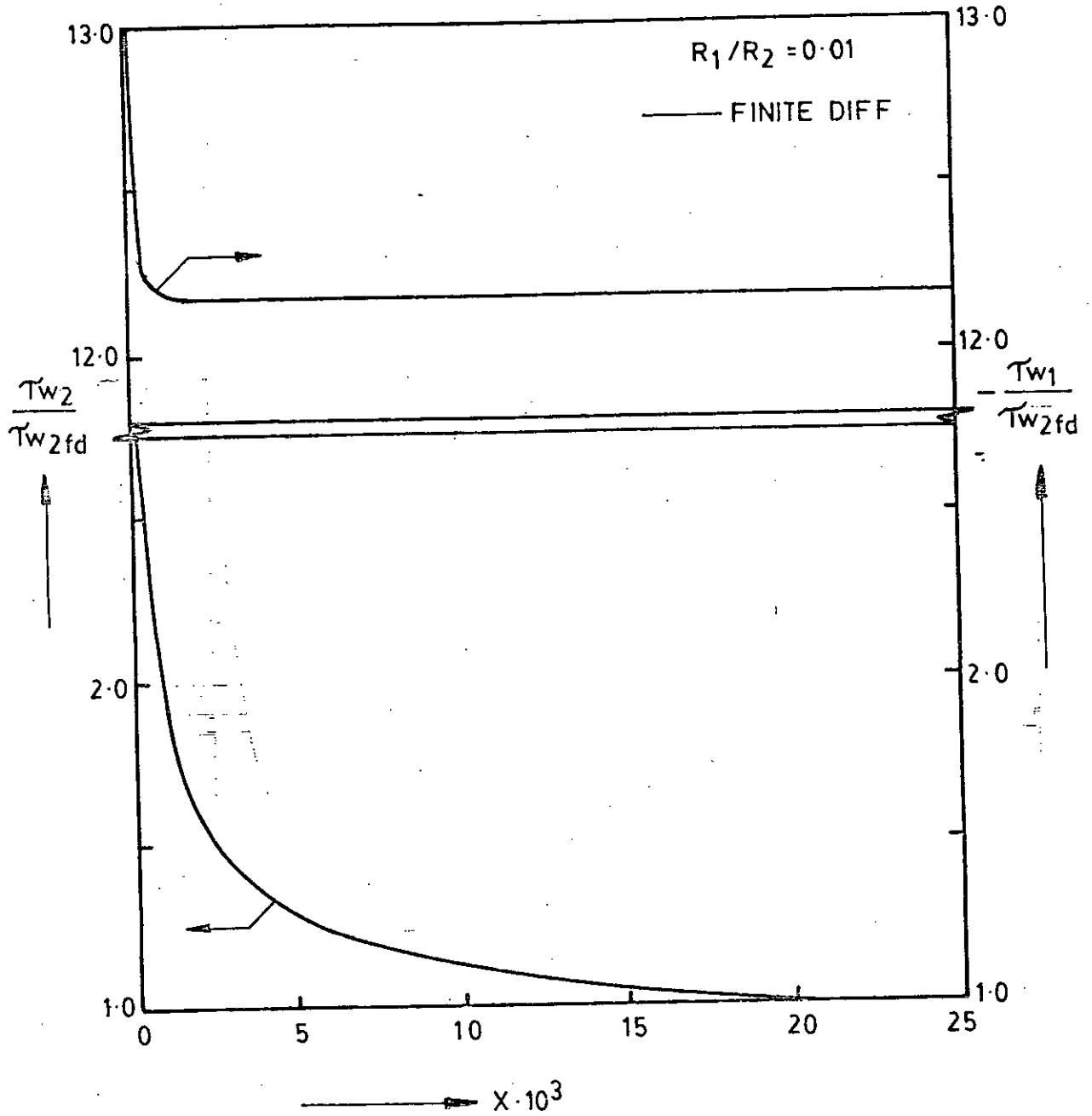


FIG. 11 (r) WALL SHEAR STRESSES VARIATION ALONG AXIAL DISTANCE FOR $R_1/R_2 = 0.01$

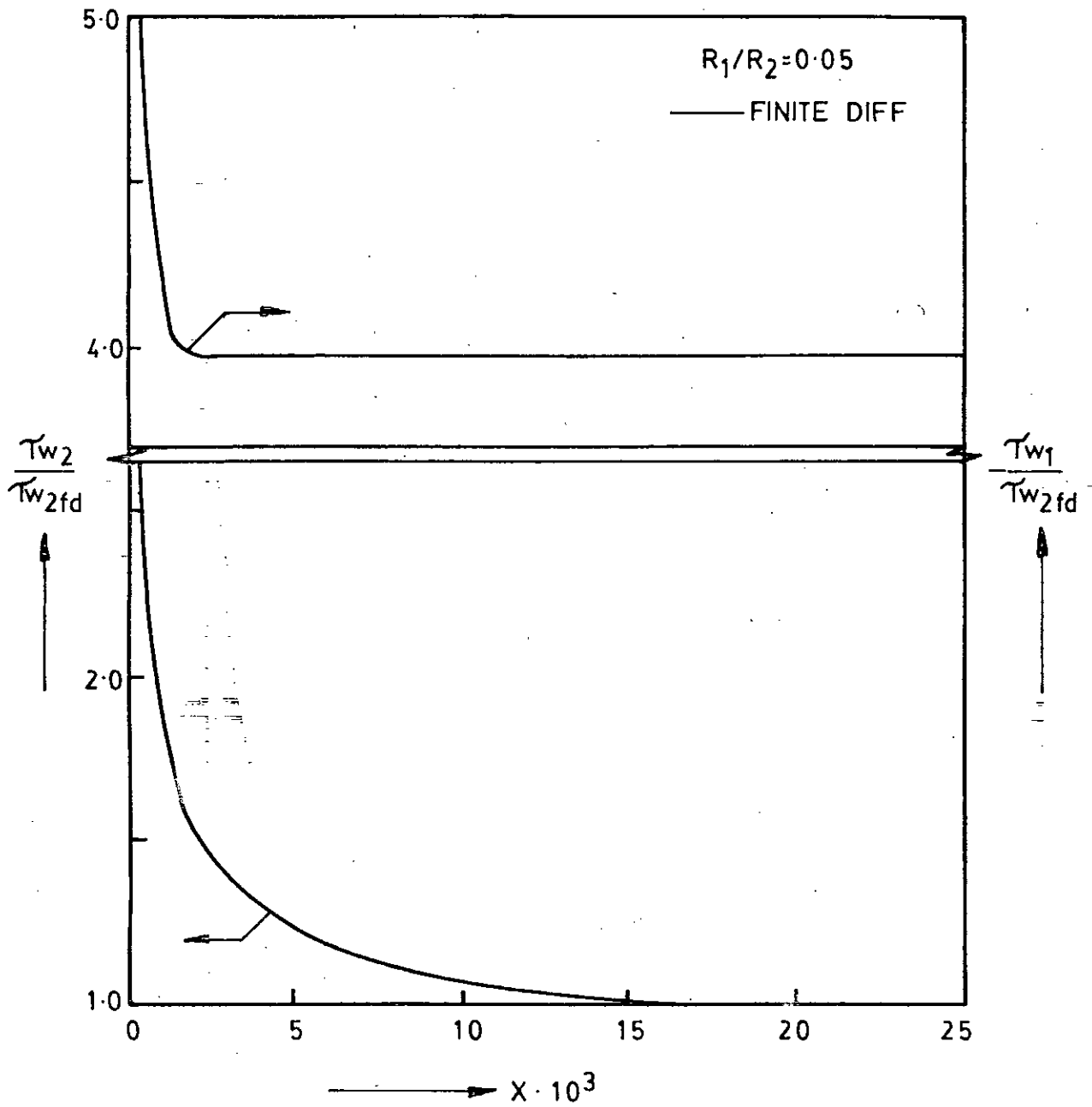


FIG. 11 (b) WALL SHEAR STRESSES VARIATION ALONG AXIAL DISTANCE FOR $R_1/R_2=0.05$

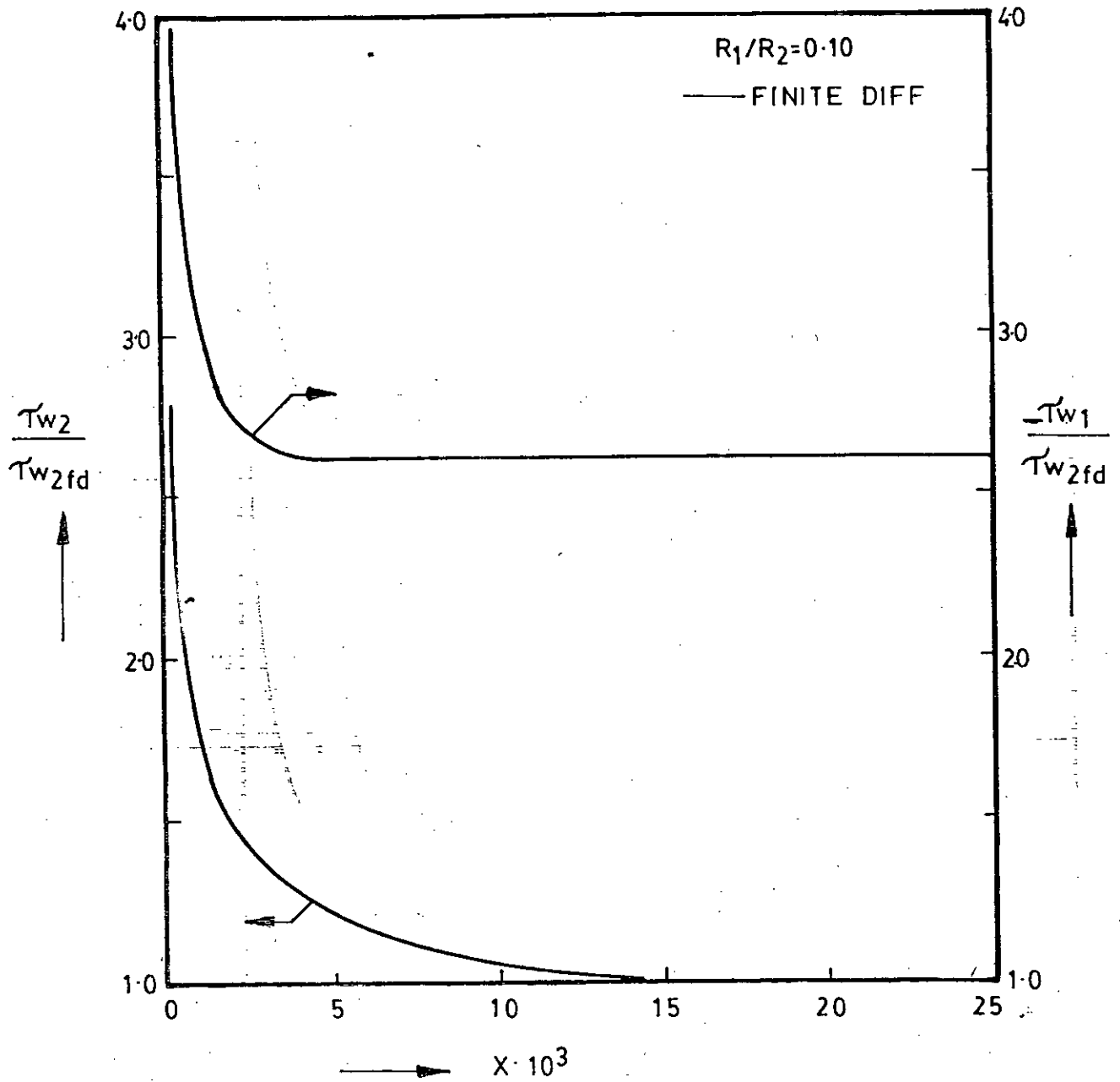


FIG.11 (c) WALL SHEAR STRESSES VARIATION ALONG AXIAL DISTANCE FOR $R_1/R_2=0.10$

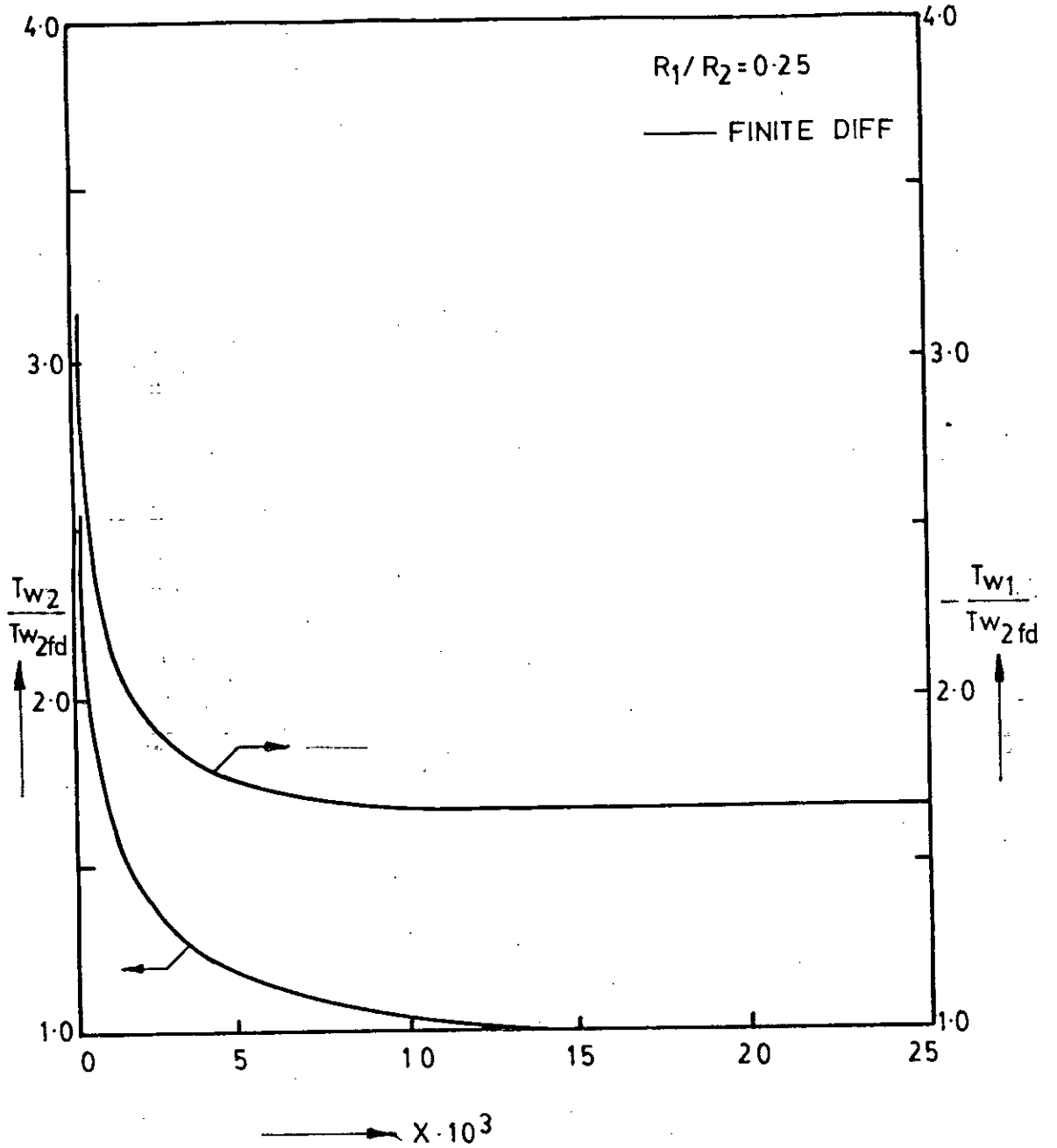


FIG. 11(d) WALL SHEAR STRESSES VARIATION ALONG AXIAL DISTANCE FOR $R_1/R_2=0.25$

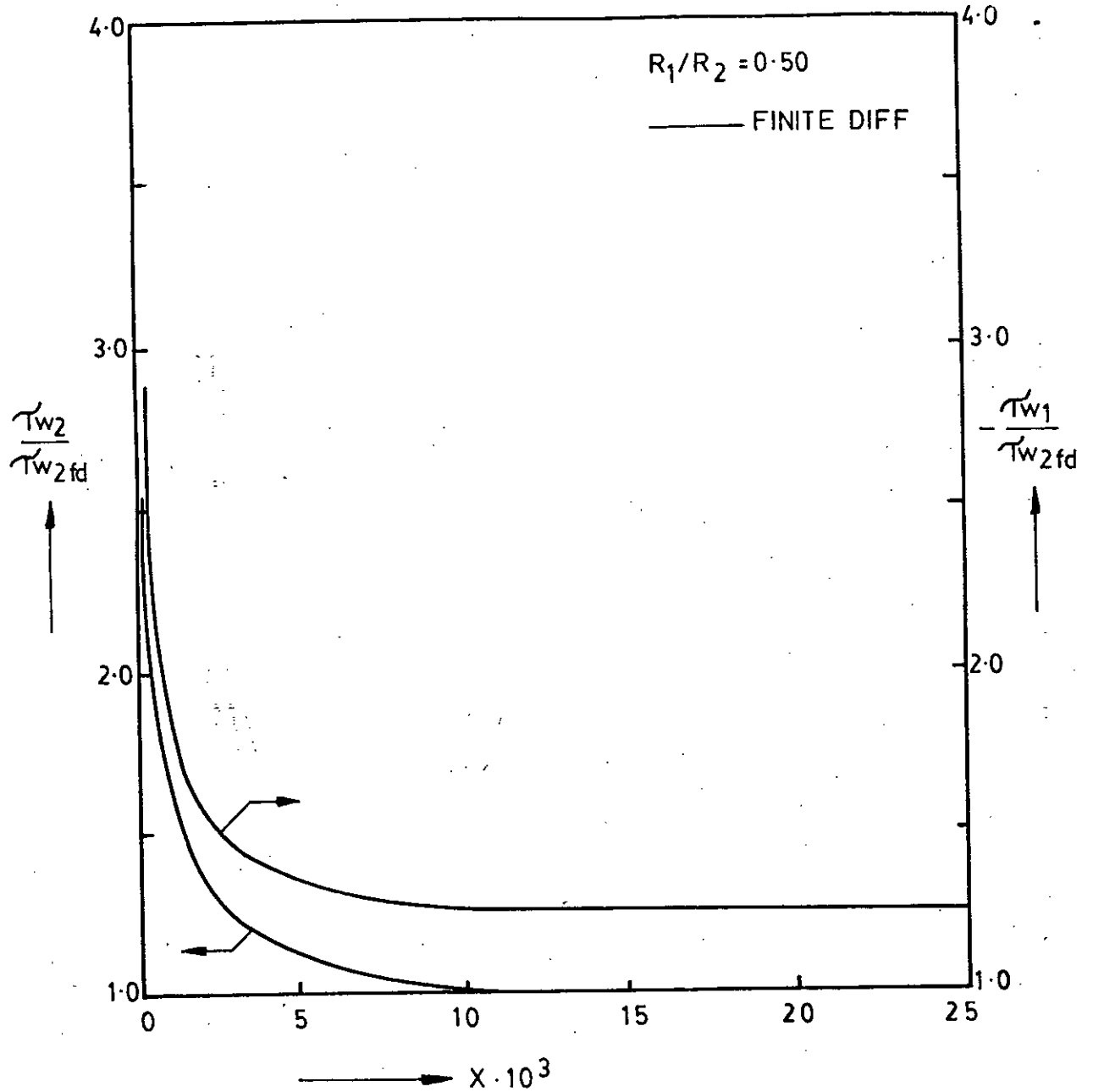


FIG. 11 (e) WALL SHEAR STRESSES VARIATION ALONG AXIAL DISTANCE FOR $R_1/R_2=0.50$

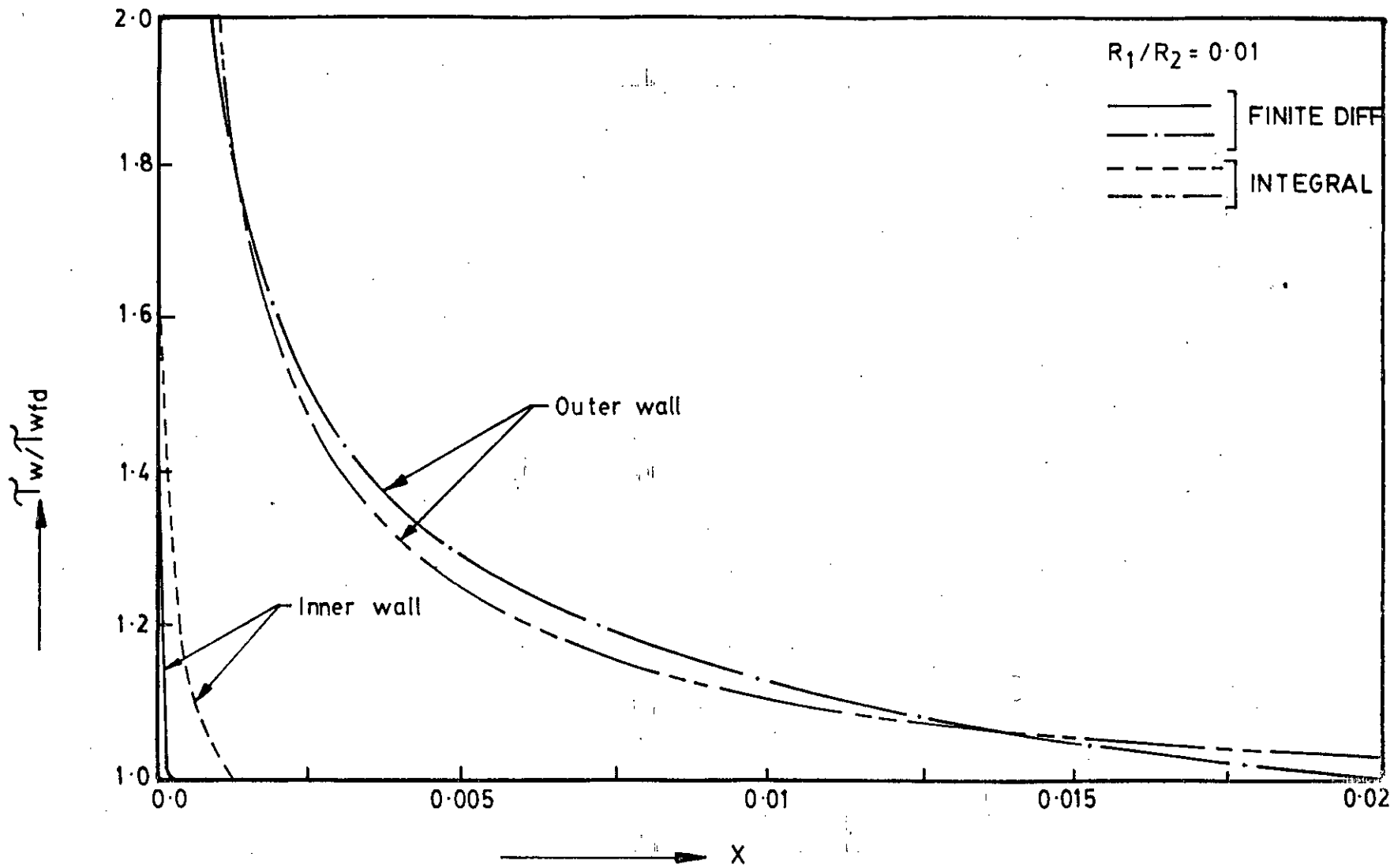


FIG. 11 (f) WALL SHEAR STRESSES VARIATION ALONG AXIAL DISTANCE FOR $R_1/R_2 = 0.01$

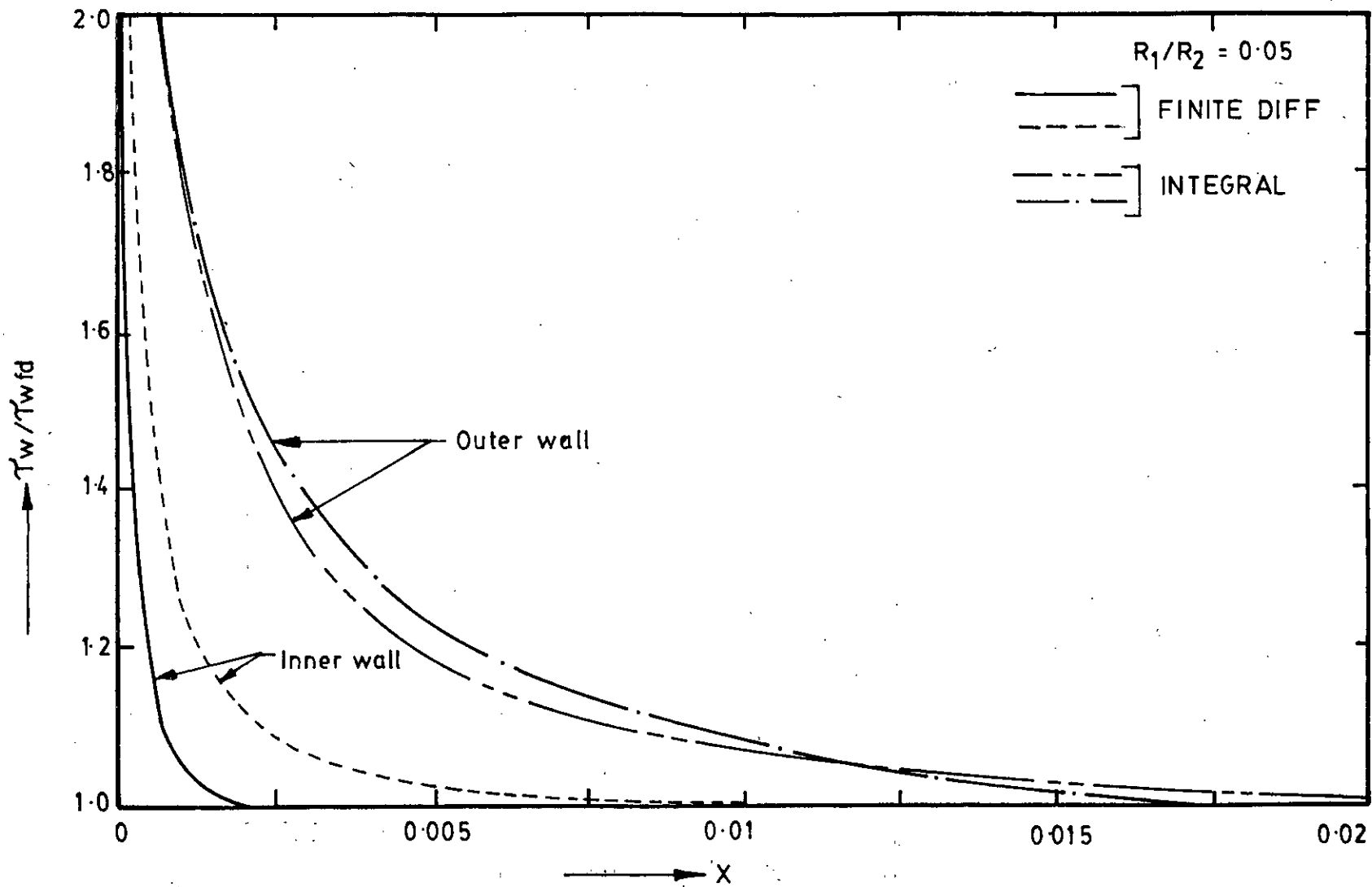


FIG. 11(g) WALL SHEAR STRESSES VARIATION ALONG AXIAL DISTANCE FOR $R_1/R_2 = 0.05$

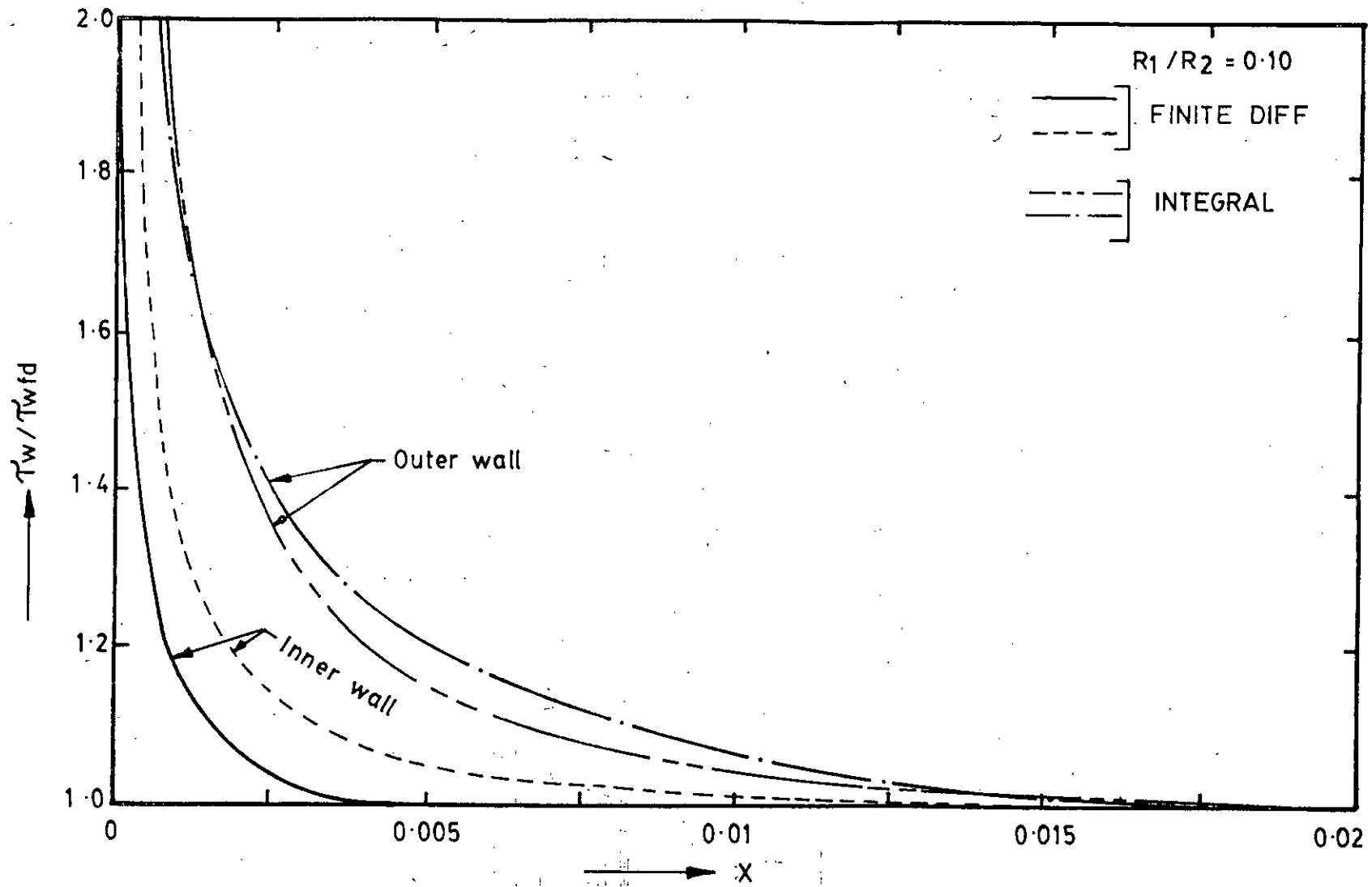


FIG. 11(h) WALL SHEAR STRESSES VARIATION ALONG AXIAL DISTANCE FOR $R_1/R_2 = 0.10$

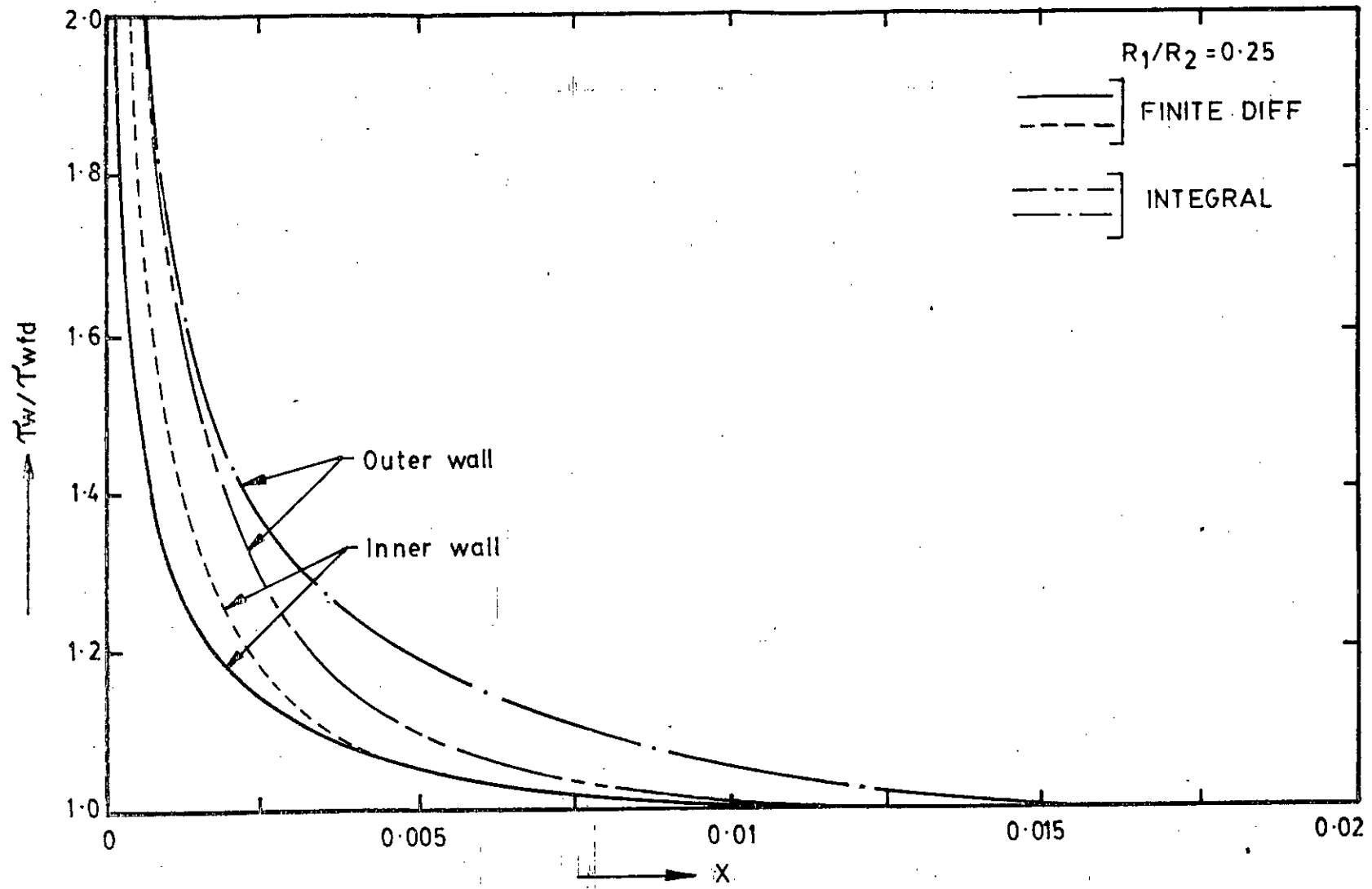


FIG-11 (i) WALL SHEAR STRESSES VARIATION ALONG AXIAL DISTANCE FOR $R_1/R_2 = 0.25$

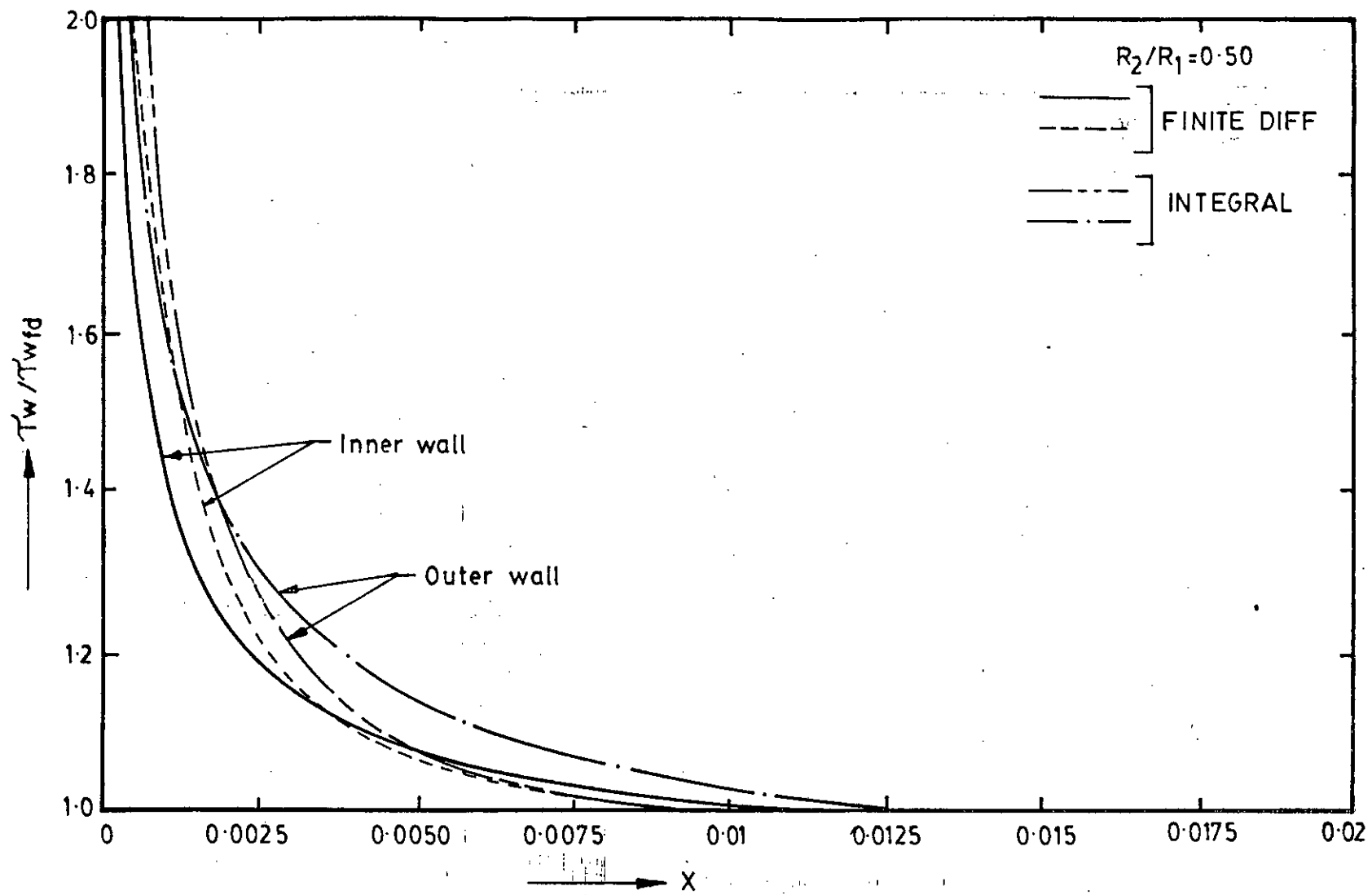


FIG.11(j) WALL SHEAR STRESSES VARIATION ALONG AXIAL DISTANCE FOR $R_1/R_2 = 0.50$

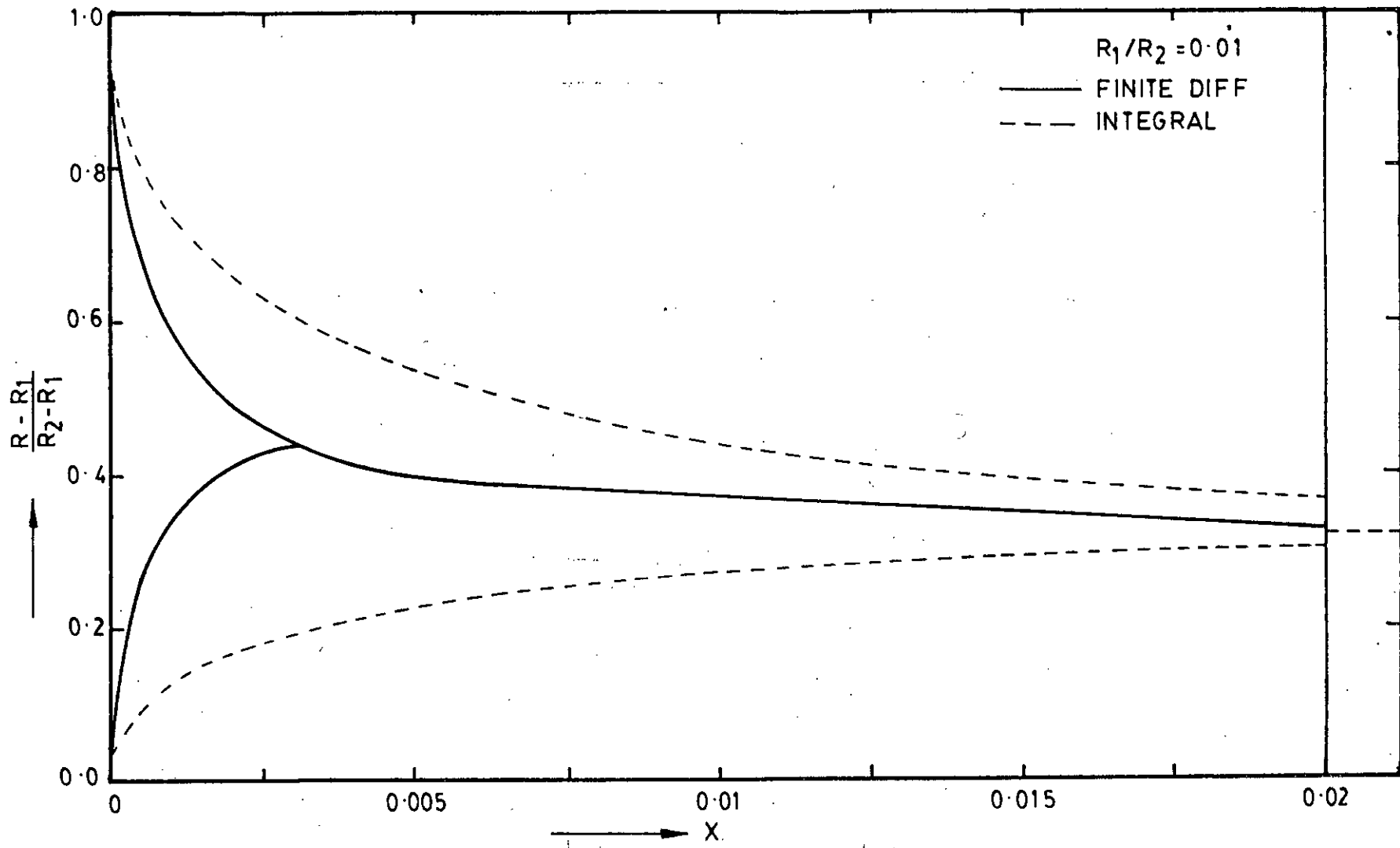


FIG. 12 (a) BOUNDARY LAYER DEVELOPMENT ALONG AXIAL DISTANCE FOR $R_1/R_2 = 0.01$

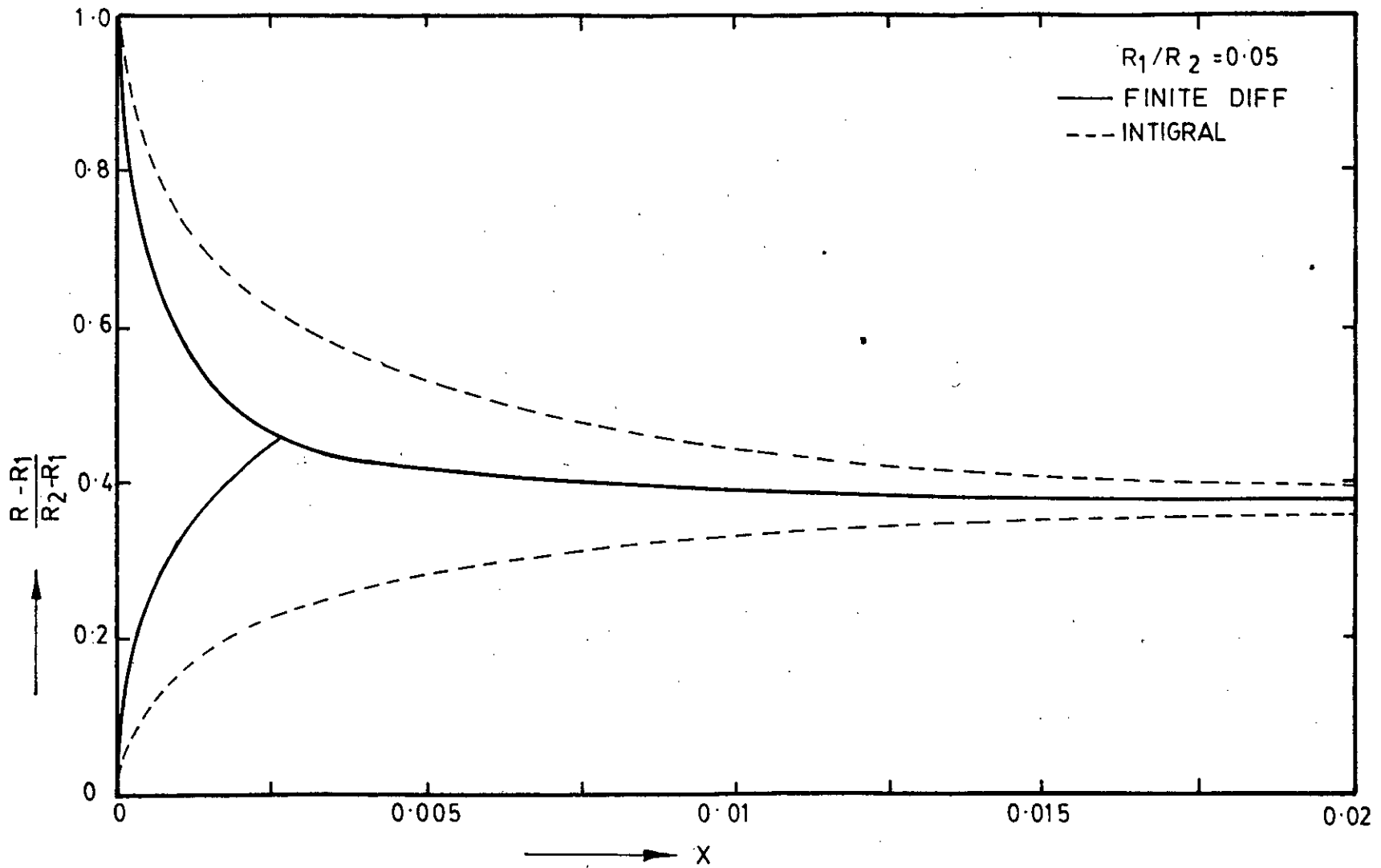


FIG. 12 (b) BOUNDARY LAYER DEVELOPMENT ALONG AXIAL DISTANCE FOR $R_1/R_2 = 0.05$

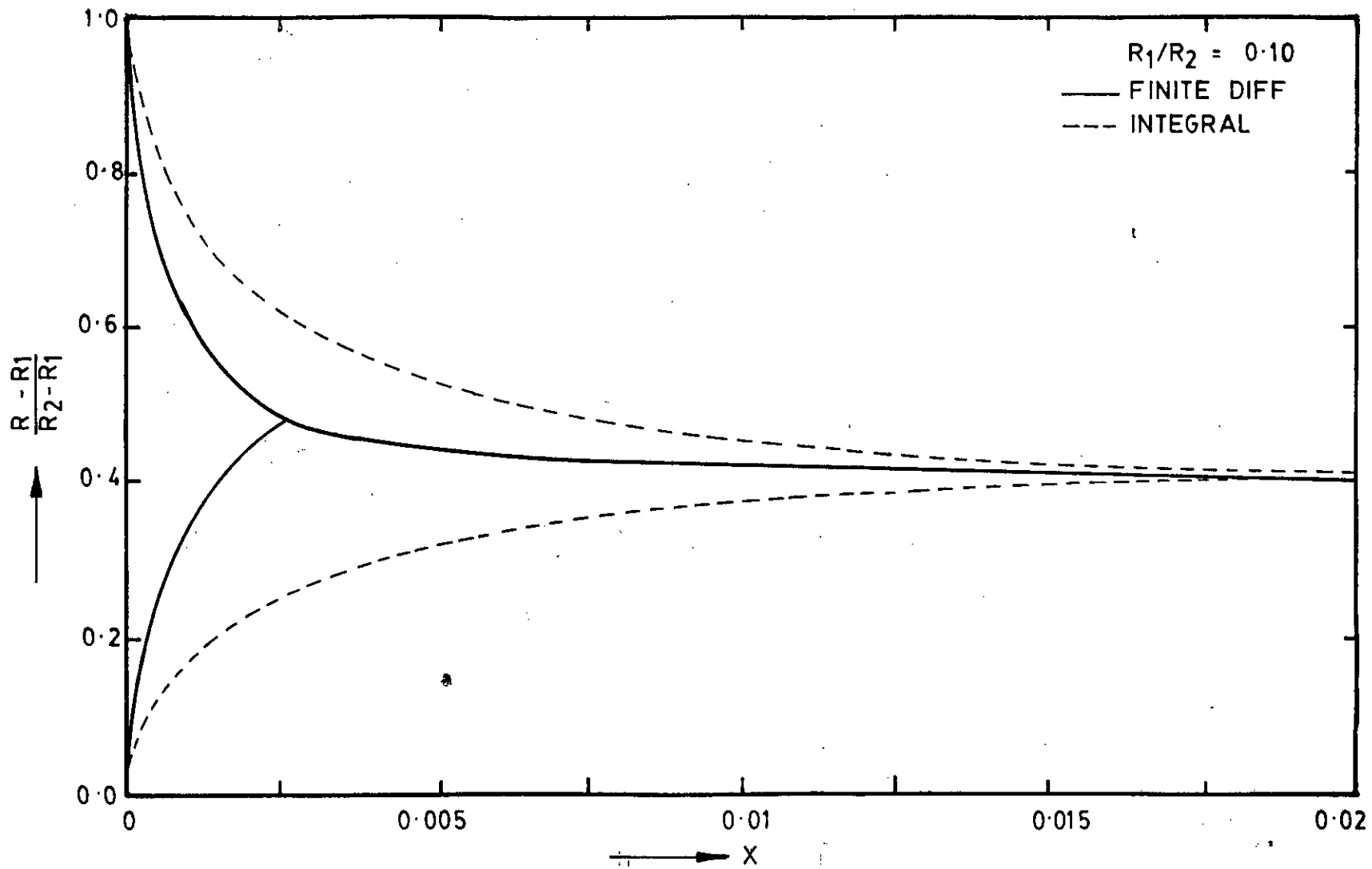


FIG-12 (c) BOUNDARY LAYER DEVELOPMENT ALONG AXIAL DISTANCE FOR $R_1/R_2 = 0.10$

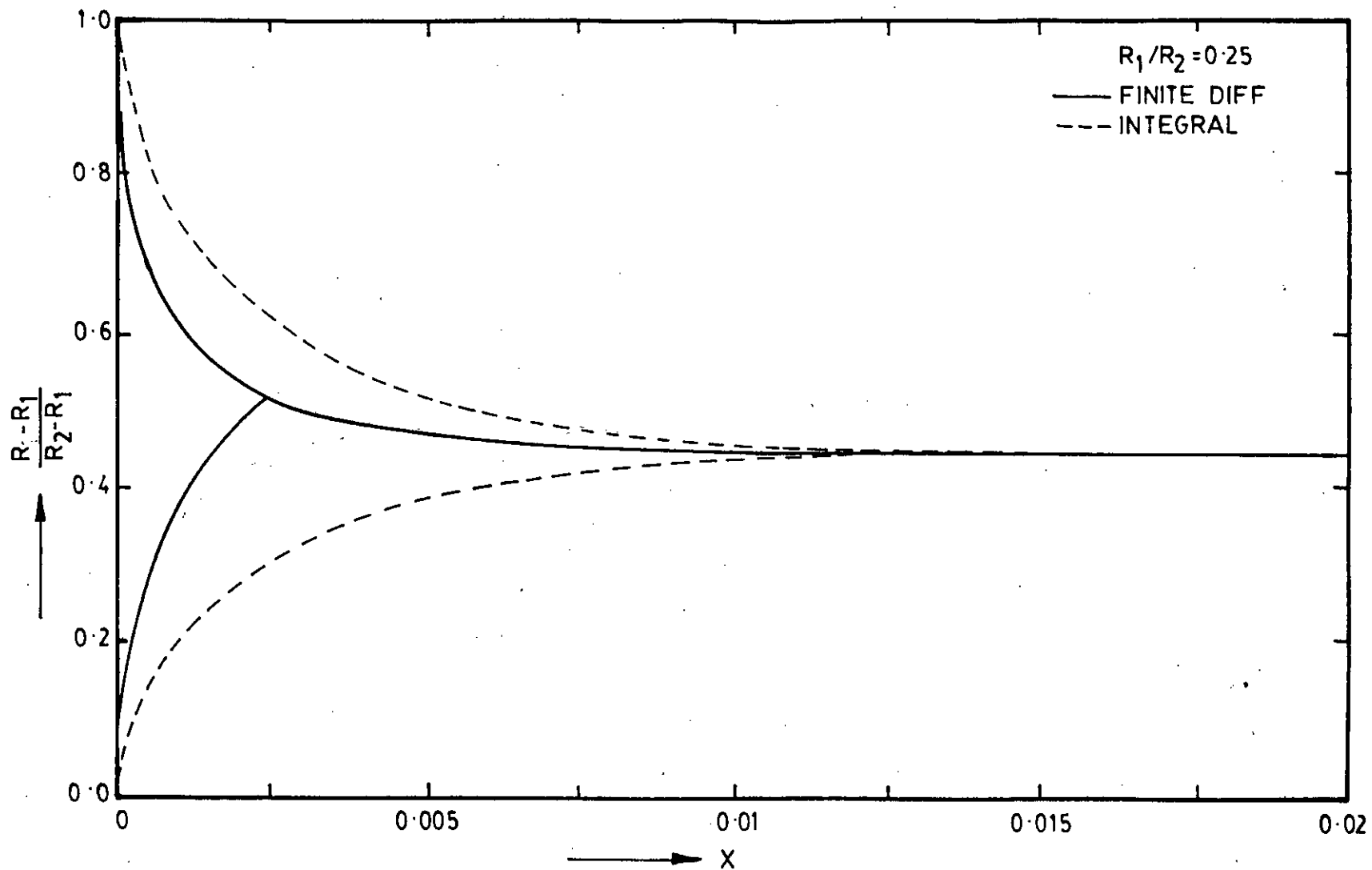


FIG. 12 (d) BOUNDARY LAYER DEVELOPMENT ALONG AXIAL DISTANCE, FOR $R_1/R_2 = 0.25$

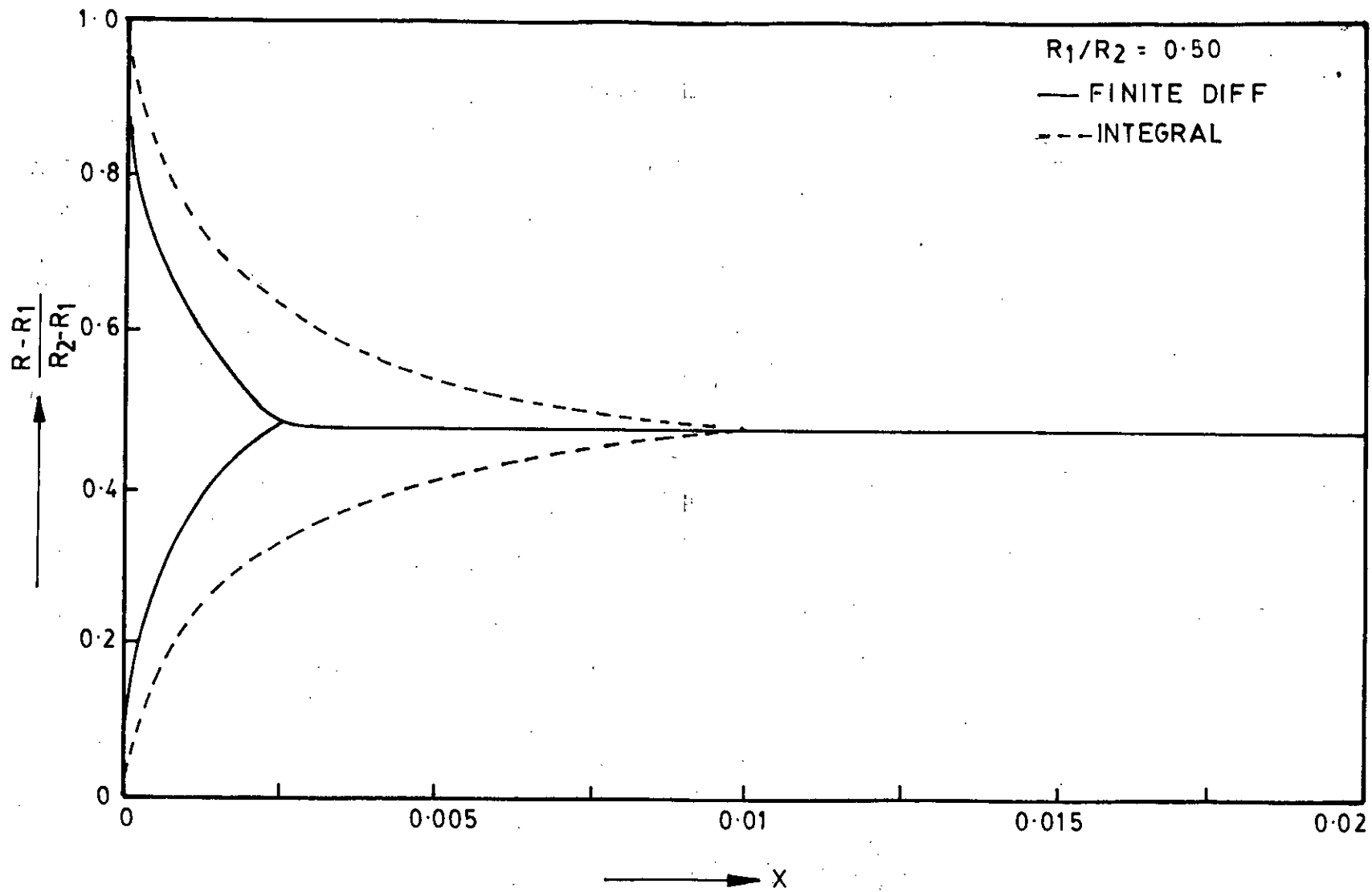


FIG. 12 (e) BOUNDARY LAYER DEVELOPMENT ALONG AXIAL DISTANCE FOR $R_1/R_2 = 0.50$

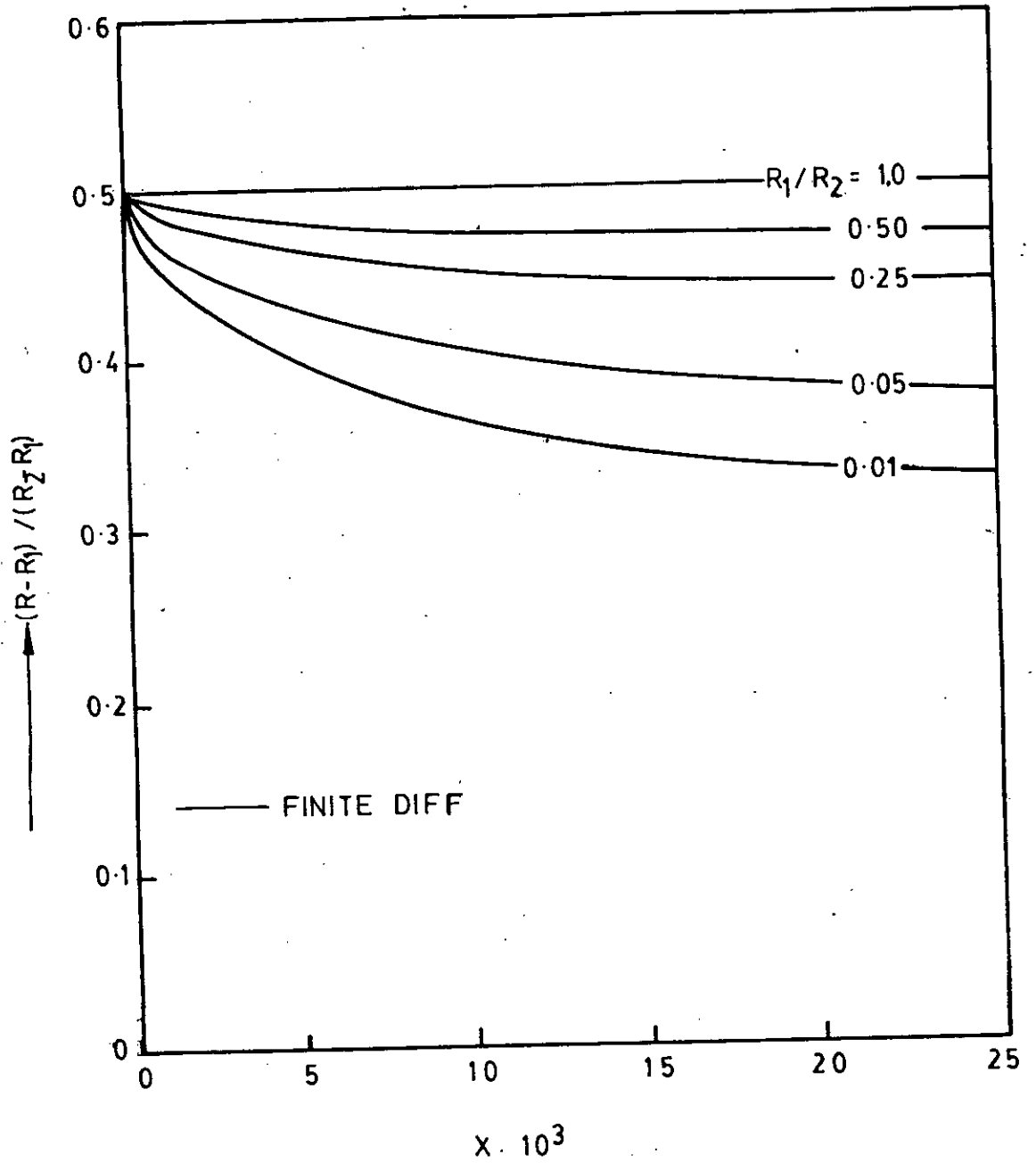
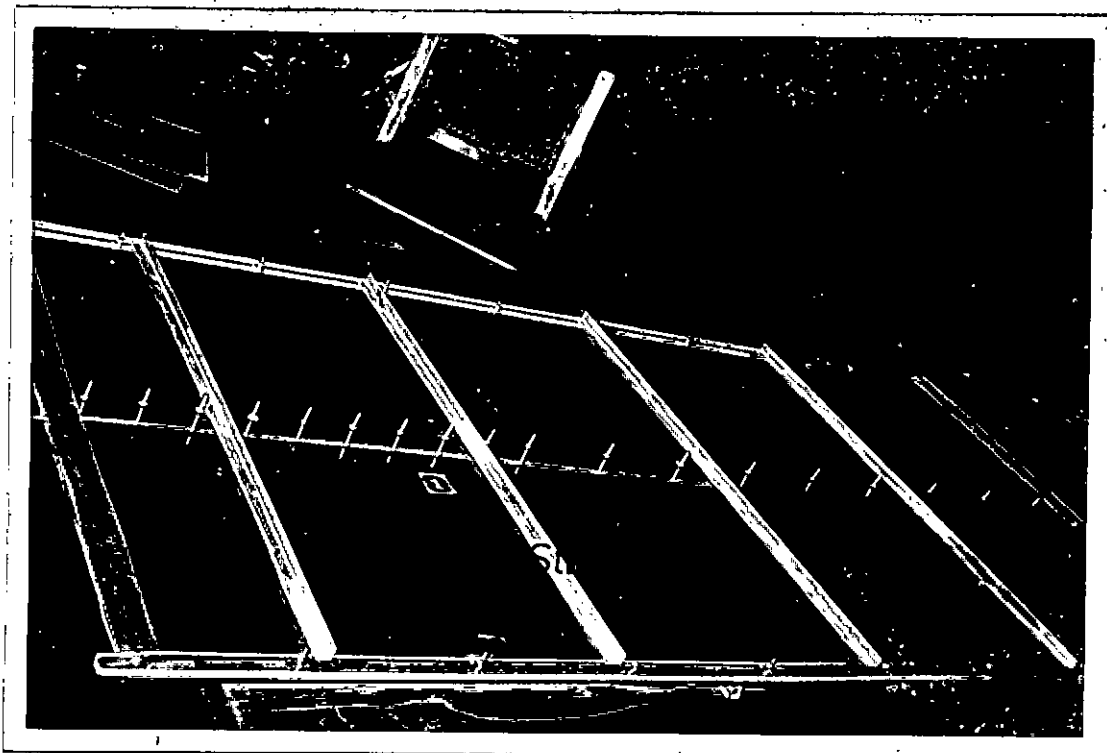
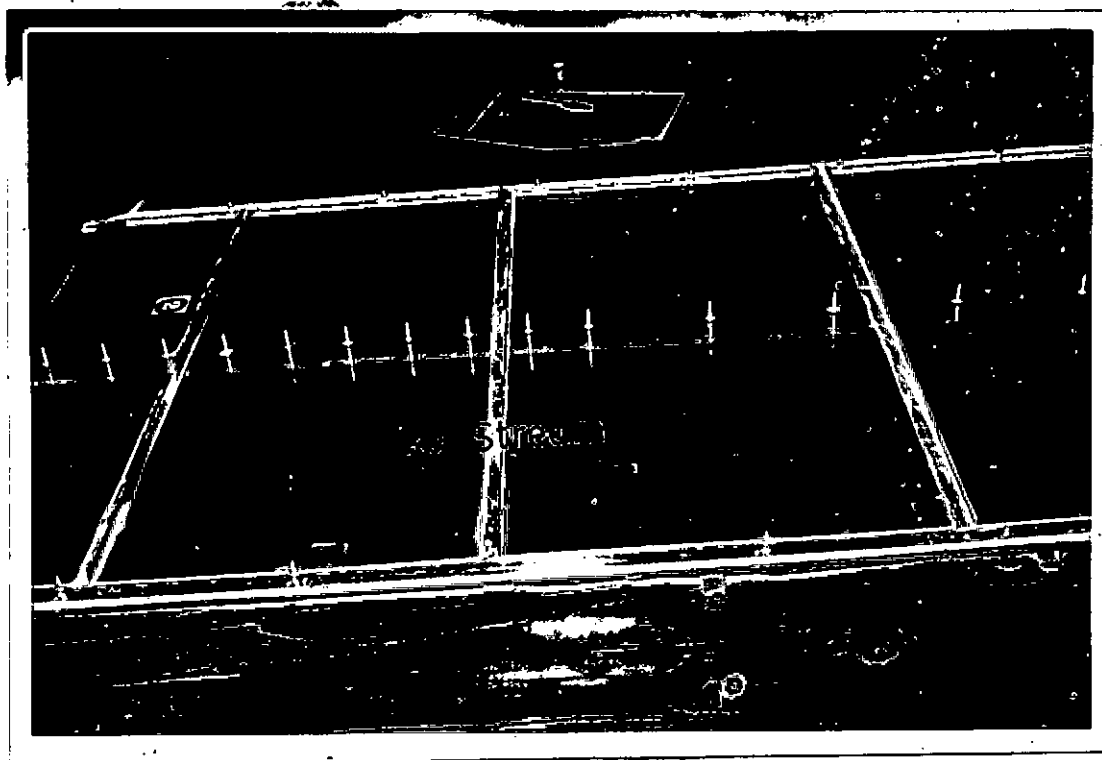


FIG. 13 CORE RADIUS VARIATION ALONG AXIAL DISTANCE FOR RADIUS-RATIO $\alpha = 0.01, 0.05, 0.25, \& 0.50$

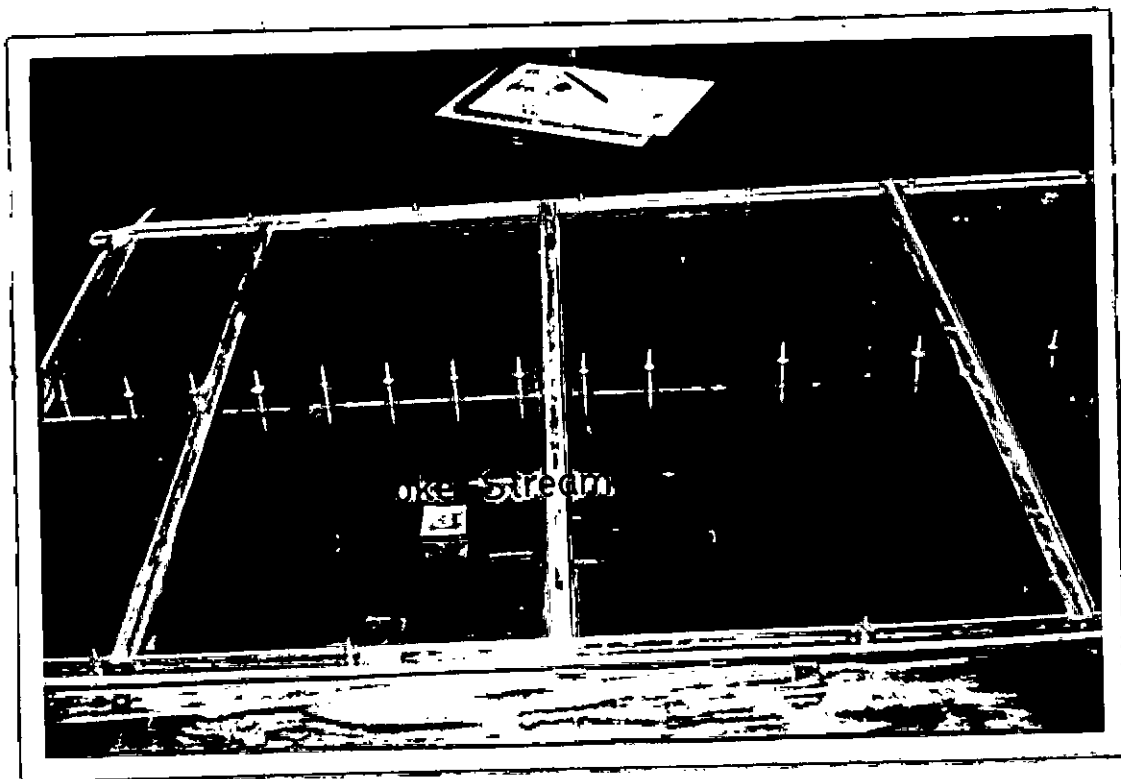


(a) $Re = 609$



(b) $Re = 1066$

Fig. 14 Photograph for Smoke Stream Through Parallel Plate Channel at Reynolds Number, (a) $Re = 609$, (b) $Re = 1066$.



(c) $Re = 1599$

Fig. 14 Photograph for Smoke Stream Through Parallel Plate Channel at Reynolds Number (c) $Re = 1599$.

APPENDICES

APPENDIX-A

EQUATIONS FOR FULLY-DEVELOPED FLOWA.1. Velocity Equation

Laminar flow is governed by the Navier-Stokes equations and the continuity equation. In cylindrical coordinate the Navier-Stokes equation for an incompressible Newtonian fluid for the developed region is:

$$\frac{1}{r} \frac{\partial}{\partial r} \left(r \frac{\partial u}{\partial r} \right) = \frac{1}{\mu} \frac{\partial p}{\partial x} = k = \text{constant} \quad (\text{A.1})$$

After integrating the equation (A.1) w.r.t. r ,

$$u = \frac{k}{4} r^2 + G_1 \ln r + G_2 \quad (\text{A.2})$$

Where G_1 and G_2 are constants to be evaluated with the boundary conditions:

$$u = 0 \text{ at } r = r_j; \quad j = 1, 2 \text{ refers to the inner and outer walls respectively.}$$

$$\left. \begin{array}{l} \frac{\partial u}{\partial r} = 0 \\ u = U_c \end{array} \right\} \text{ at } r = r_\delta$$

Then equation (A.1) becomes after substituting the values of G_1 and G_2

$$u_j = \frac{k}{4} (r^2 - r_j^2 - 2r_\delta^2 \ln r/r_j) \quad (\text{A.3})$$

at $r = r_\delta$

$$U_c = \frac{k}{4} (r_\delta^2 - r_j^2 - 2r_\delta^2 \ln r_\delta/r_j) \quad (\text{A.4})$$

Dividing equation (A.3) by equation (A.4)

$$u_j / U_c = \frac{r^2 - r_j^2 - 2r_\delta^2 \ln r/r_j}{r_\delta^2 - r_j^2 - 2r_\delta^2 \ln r_\delta/r_j} \quad (\text{A.5})$$

A.2. Radius of Maximum Velocity, r_δ

To evaluate G_1 and G_2 in equation (A.2) the following boundary conditions are assumed:

$$u = 0, \text{ at } r = r_1 \text{ and at } r = r_2$$

Then

$$0 = \frac{k}{4} (r_1^2 + G_1 \ln r_1 + G_2) \quad (\text{A.6})$$

$$\text{and } 0 = \frac{k}{4} (r_2^2 + G_1 \ln r_2 + G_2) \quad (\text{A.7})$$

Equating the R.H.S terms of eqns. (A.6) & (A.7),

$$G_1 = -\frac{k}{4} \left(\frac{r_1^2 - r_2^2}{\ln r_1/r_2} \right)$$

$$\text{and } G_2 = \frac{k}{4} \left(\frac{r_1^2 \ln r_2 - r_2^2 \ln r_1}{\ln r_1/r_2} \right)$$

Substituting these values in eqn. (A.2).

$$u = \frac{k}{4} \left(r^2 - \frac{r_1^2 - r_2^2}{\ln r_1/r_2} \ln r + \frac{r_1^2 \ln r_2 - r_2^2 \ln r_1}{\ln r_1/r_2} \right)$$

$$\text{or, } u = \frac{k}{4} \left\{ r^2 - \frac{r_2^2}{\ln \alpha} (\alpha^2 - 1) \ln r + \frac{r_2^2}{\ln \alpha} (\alpha^2 \ln r_2 - \ln r_1) \right\} \quad (\text{A.8})$$

At $r = r_\delta$, $\partial u / \partial r = 0$

$$\therefore \frac{\partial u}{\partial r} = \frac{k}{4} \left(2r_\delta - \frac{r_2^2}{r_\delta} \frac{\alpha^2 - 1}{\ln \alpha} \right) = 0$$

$$\text{or, } r_\delta = r_2 \left(\frac{\alpha^2 - 1}{\ln \alpha} \right)^{\frac{1}{2}} \quad (\text{A.9})$$

A.3. Maximum Velocity, U_c

At $r = r_\delta$, $u = U_c$

Then from equation (A.8)

$$U_c = \frac{k}{4} \left\{ r_\delta^2 - \frac{r_2^2}{\ln \alpha} (\alpha^2 - 1) \ln r_\delta + \frac{r_2^2}{\ln \alpha} (\alpha^2 \ln r_2 - \ln r_1) \right\}$$

Putting $r_\delta = r_2 \left(\frac{\alpha^2 - 1}{\ln \alpha} \right)^{\frac{1}{2}}$

$$U_c = \frac{k}{4} \left[\frac{r_2^2}{2 \ln \alpha} \left\{ (\alpha^2 - 1) - \ln \alpha^2 - (\alpha^2 - 1) \ln \frac{\alpha^2 - 1}{\ln \alpha} \right\} \right] \quad (\text{A.10})$$

The flow rate, $Q = 2\pi \int_{r_1}^{r_2} u r dr$

where u is given in equation (A.8)

After integrating,

$$Q = \frac{\pi k}{8} (r_2^2 - r_1^2) r_2^2 \left[\frac{\alpha^2 - 1}{\ln \alpha} - (1 + \alpha^2) \right]$$

Then the average velocity, U_o

$$U_o = \frac{Q}{\pi(r_2^2 - r_1^2)} = \frac{k}{8} r_2^2 \left\{ \frac{\alpha^2 - 1}{\ln \alpha} - (1 + \alpha^2) \right\} \quad (\text{A.11})$$

Dividing eqn. (A.10) by eqn. (A.11), and after simplification,

$$U_c/U_o = \frac{(\alpha^2 - 1) \left\{ 1 - \ln\left(\frac{\alpha^2 - 1}{2}\right) - \ln \alpha^2 \right\}}{(\alpha^2 - 1) - (1 + \alpha^2) \ln \alpha} \quad (\text{A.12})$$

A.4. Pressure Drop

From eqn. (A.11)

$$\frac{1}{\mu} \frac{dp}{dx} = k = \frac{8 U_o}{r_2^2 \left(\frac{\alpha^2 - 1}{\ln \alpha} - 1 - \alpha^2 \right)}$$

$$\text{or, } \int_{p_o}^p dp = \int_0^x \frac{8 U_o \mu}{r_2^2 \left(\frac{\alpha^2 - 1}{\ln \alpha} - 1 - \alpha^2 \right)} dx$$

$$\text{Putting } r_2 = \frac{D_h}{2(1-\alpha)} \quad \text{and } Re = \frac{\rho D_h U_o}{\mu}$$

$$\therefore \frac{p - p_o}{\frac{1}{2} \rho U_o^2} = \frac{64 (1-\alpha)^2 \frac{x}{Re D_h}}{\frac{\alpha^2 - 1}{\ln \alpha} - (1 + \alpha^2)} \quad (\text{A.13})$$

APPENDIX-B
INTEGRAL TECHNIQUE

B.2. Mattai's equation

The functions of A's, C₁ & C₂ defined by Mattai [21] are:

$$A_1 = 1 - B_1 + \ln B_1$$

$$A_2 = 1 - B_2 + \ln B_2$$

$$A_3 = \frac{5}{6} - B_1 + \frac{B_1}{2} - \frac{B_1^2}{3} + B_1 (B_1 - \ln B_1) \ln B_1$$

$$A_4 = \frac{5}{6} - B_2 + \frac{B_2^2}{2} - \frac{B_2^3}{3} + B_2 (B_2 - \ln B_2) \ln B_2$$

$$A_5 = \frac{7}{3} - 2B_1 - \frac{3}{4}B_1^2 + \frac{2}{3}B_1^3 - \frac{B_1^4}{4} + B_1(3 - \frac{3}{2}B_1 + B_1^2)\ln B_1 + B_1$$

$$(-\frac{3}{2}B_1 + \ln B_1)\ln^2 B_1$$

$$A_6 = \frac{7}{3} - 2B_2 - \frac{3}{4}B_2^2 + \frac{2}{3}B_2^3 - \frac{B_2^4}{4} + B_2(3 - \frac{3}{2}B_2 + B_2^2)\ln B_2 + B_2$$

$$(-\frac{3}{2}B_2 + \ln B_2)\ln^2 B_2$$

$$A_7 = \frac{11}{6} - 3B_1 + \frac{3}{2}B_1^2 - \frac{B_1^3}{3} + \ln B_1$$

$$A_8 = \frac{11}{6} - 3B_2 + \frac{3}{2}B_2^2 - \frac{B_2^3}{3} + \ln B_2$$

$$A_9 = (-1 + 1/B_1)/A_1$$

$$A_{10} = (-1 + \frac{1}{B_2})/A_2$$

$$A_{11} = \frac{1}{2}(1 - B_1^2) + B_1 \ln B_1$$

$$A_{12} = \frac{1}{2}(1 - B_2^2) + B_2 \ln B_2$$

$$A_{13} = -3 + 3B_1 - B_1^2 + 1/B_1$$

$$A_{14} = -3 + 3B_2 - B_2^2 + 1/B_2$$

$$A_{15} = \alpha^2(1 - B_1)^2 B_2 A_2 - (1 - B_2)^2 B_1 A_1$$

$$A_{16} = -(1 - B_1)^2 + 2(B_1 - 1)\ln B_1 - \ln^2 B_1$$

$$A_{17} = -(1 - B_2)^2 + 2(B_2 - 1)\ln B_2 - \ln^2 B_2$$

$$A_{18} = (1 - B_1)^3 + 3 \left[(1 - B_1)^2 - B_1 \ln B_1 \right] \ln B_1 + (3 + \ln B_1) \ln^2 B_1$$

$$A_{19} = (1 - B_2)^3 + 3 \left[(1 - B_2)^2 - B_2 \ln B_2 \right] \ln B_2 - (3 + \ln B_2) \ln^2 B_2$$

$$A_{20} = (-B_1 + 3A_{11}/A_1 + 3A_3/A_1^2 + A_5/A_1^3)/B_1$$

$$A_{21} = (-B_2 + 3A_{12}/A_2 + 3A_4/A_2^2 + A_6/A_2^3)/B_2$$

$$A_{22} = A_7/(B_1 A_1^2)$$

$$A_{23} = A_8/(B_2 A_2^2)$$

$$A_{24} = 2(1 - \alpha^2)B_1 B_2 A_1 A_2 / A_{15}$$

$$A_{25} = \frac{-\alpha^2}{2} A_{24} A_{20} + \frac{1}{2} A_{24} A_{21} + \alpha^2 A_{22} - A_{23}$$

$$A_{26} = -(1 - B_1^2) + 4(B_1 - 1) - 2 \ln B_1$$

$$A_{27} = (1 - B_2^2) + 4(B_2 - 1) - 2 \ln B_2$$

$$A_{28} = \left[-2(B_1 - 1) + (A_{24} A_{26}/A_1) \right] / A_1$$

$$A_{29} = \left[2(B_2 - 1) - A_{24} A_{27}/A_2 \right] / A_2$$

$$A_{30} = 3A_{11} \left[A_1/A_{11} - A_9 \right] / A_1$$

$$A_{31} = 3A_{12} \left[A_2/A_{12} - A_{10} \right] / A_2$$

$$A_{32} = 3A_3 (A_{16}/A_3 - 2A_9) / A_1^2$$

$$A_{33} = 3A_4 (A_{17}/A_4 - 2A_{10}) / A_2^2$$

$$A_{34} = A_5 (A_{18}/A_5 - 3A_9)/A_1^3$$

$$A_{35} = A_6 (A_{19}/A_6 - 3A_{10})/A_2^3$$

$$A_{36} = (-1 + A_{30} + A_{32} + A_{34})/A_{20}B_1 - 1/B_1$$

$$A_{37} = (-1 + A_{31} + A_{33} + A_{35})/(A_{21}B_2) - 1/B_2$$

$$A_{38} = 1/B_1 + A_9 + \{2\alpha^2(1 - B_1)^2 B_2 A_2\} / \{A_{15}(1 - B_1)\} +$$

$$\{B_1(1 - B_2)^2 A_1\} \{1/B_1 + A_9\} / A_{15}$$

$$A_{39} = 1/B_2 + A_{10} - \{2B_1(1 - B_2)^2 A_1\} / \{A_{15}(1 - B_2)\} - \{\alpha^2(1 - B_1)^2 B_2 A_2\}$$

$$\{1/B_2 + A_{10}\} / A_{15}$$

$$A_{40} = A_{13}/A_7 - 1/B_1 - 2A_9$$

$$A_{41} = A_{14}/A_8 - 1/B_2 - 2A_{10}$$

$$A_{42} = -(\alpha^2/2)A_{20}A_{24}(A_{36} + A_{38}) + \frac{1}{2}A_{21}A_{24}A_{38} + \alpha^2 A_{40} A_{22}$$

$$A_{43} = -(\alpha^2/2)A_{20}A_{24}A_{39} + (A_{24}/2)A_{21}A_{37} + (A_{24}/2)A_{21}A_{39} - A_{41}A_{23}$$

$$C_1 = A_{24} (A_{42} + 2A_{25} A_{38}) / (A_{28} + A_{29})$$

$$C_2 = A_{24} (A_{43} + 2A_{25} A_{39}) / (A_{28} + A_{29})$$

B.3. Modified Mattai's equation

Near the entrance, it can be assumed that in the core region the Bernoulli's equation holds good,

i.e. $U_c \frac{\partial U_c}{\partial x} = \frac{1}{\rho} \frac{dp}{dx}$ and using Mattai's [21] derivation for U_c

$$-\frac{dp}{dx} = \rho U_o^2 A_{24} \frac{dA_{24}}{dx} \quad (B.1)$$

The momentum balance equation is:

$$2 \left[-\tau_{w_1} r_1 + \tau_{w_2} r_2 \right] - (r_2^2 - r_1^2) \frac{dp}{dx} = \frac{d}{dx} \left[2\rho \int_{r_1}^{r_2} u^2 r dr \right]$$

Shear force term (SF)

Pressure force term (PF)

Change of momentum term (MF)

Now, from Mattai [21]

The Shear force term, (SF)

$$2 \left[-\tau_{w_1} r_1 + \tau_{w_2} r_2 \right] = 2 \left[-\frac{2\mu U_c (B_1 - 1)}{A_1} + \frac{2\mu U_c (B_2 - 1)}{A_2} \right]$$

$$\text{or, } 2 \left[-\tau_{w_1} r_1 + \tau_{w_2} r_2 \right] = 4\mu U_o A_{24} \left[-\frac{B_1 - 1}{A_1} + \frac{B_2 - 1}{A_2} \right] \quad (B.2)$$

The Pressure force term (PF):

Substituting eqn. (B.1) and using Mattai derivation for $\frac{dA_{24}}{dx}$, the pressure force term in the momentum balance equation becomes,

$$\rho U_o^2 A_{24} (r_2^2 - r_1^2) \frac{dA_{24}}{dx} = \rho U_o^2 r_2^2 (1 - \alpha^2) \left[A_{38} \frac{dB_1}{dx} + A_{39} \frac{dB_2}{dx} \right]$$

$$\text{and since } dB_1/dx = -(\gamma/\alpha)(B_1/B_2)^{3/2} \frac{dB_2}{dx}$$

$$\therefore \text{Pressure force term (PF)} = \rho U_0^2 r_2^2 A_{24}^2 (1-\alpha^2) \left[-\frac{\gamma}{\alpha} (B_1/B_2)^{3/2} \right. \\ \left. A_{38} + A_{39} \right] \frac{dB_2}{dx} \quad (\text{B.3})$$

Change of momentum term (MF):

$$2\rho \frac{d}{dx} \int_{r_1}^{r_2} u^2 r dr = \rho \frac{d}{dx} U_c^2 r_1^2 A_{22} - r_2^2 A_{23} \quad ; \text{ then from [21]}$$

$$MF = \rho U_0^2 r_2^2 \frac{d}{dx} A_{24}^2 (\alpha^2 A_{22} - A_{23})$$

$$\text{But } \frac{d}{dx} \left[A_{24}^2 (\alpha^2 A_{22} - A_{23}) \right]$$

$$= A_{24}^2 \left(\alpha^2 \frac{d}{dx} A_{22} - \frac{d}{dx} A_{23} \right) + 2A_{24} (\alpha^2 A_{22} - A_{23}) \frac{d}{dx} A_{24}$$

$$= A_{24}^2 \left(\alpha^2 A_{40} A_{22} \frac{dB_1}{dx} - A_{41} A_{23} \frac{dB_2}{dx} \right) + 2A_{24}^2 (\alpha^2 A_{22} - A_{23})$$

$$\left\{ A_{38} \frac{dB_1}{dx} + A_{39} \frac{dB_2}{dx} \right\}$$

$$= A_{24}^2 \left[\alpha^2 A_{40} A_{22} - \frac{\gamma}{\alpha} (B_1/B_2)^{3/2} - A_{41} A_{23} + 2(\alpha^2 A_{22} - A_{23}) \right]$$

$$\left\{ -\frac{\gamma}{\alpha} (B_1/B_2)^{3/2} A_{38} + A_{39} \right\} \frac{dB_2}{dx}$$

$$= A_{24}^2 \left[-\gamma \alpha (B_1/B_2)^{3/2} A_{40} A_{22} - A_{41} A_{23} + 2(\alpha^2 A_{22} - A_{23}) \right]$$

$$\left\{ -\frac{\gamma}{\alpha} (B_1/B_2)^{3/2} A_{38} + A_{39} \right\} \frac{dB_2}{dx}$$

∴ The change of momentum term,

$$= \rho U_0^2 r_2^2 A_{24}^2 \left[-\gamma \alpha (B_1/B_2)^{3/2} A_{40} A_{22} - A_{41} A_{23} + 2(\alpha^2 A_{22} - A_{23}) \left\{ -\gamma/\alpha (B_1/B_2)^{3/2} A_{38} + A_{39} \right\} \right] \frac{dB_2}{dx} \quad (B.4)$$

Now dividing all the three terms by $\rho U_0^2 r_2^2 A_{24}$, one gets

$$1) \quad SF = \frac{4\mu}{\rho U_0 r_2^2} \left\{ -\frac{B_1-1}{A_1} + \frac{B_2-1}{A_2} \right\} = \frac{16(1-\alpha)^2}{ReD_h} \left\{ -\frac{B_1-1}{A_1} + \frac{B_2-1}{A_2} \right\}$$

$$\text{Since } \frac{2\mu}{U_0 r_2^2} = \frac{8(1-\alpha)^2}{ReD_h}$$

$$2) \quad PF \cdot \frac{dB_2}{dx} = A_{24} (1-\alpha^2) \left\{ -\gamma/\alpha (B_1/B_2)^{3/2} A_{38} + A_{39} \right\} \frac{dB_2}{dx}$$

$$3) \quad MF \cdot \frac{dB_2}{dx} = A_{24} \left[-\gamma \alpha (B_1/B_2)^{3/2} A_{40} A_{22} - A_{41} A_{23} + 2(\alpha^2 A_{22} - A_{23}) \left\{ -\frac{\gamma}{\alpha} (B_1/B_2)^{3/2} A_{38} + A_{39} \right\} \right] \frac{dB_2}{dx}$$

Then the momentum balance equation is :

Shear force term + Pressure force term = Change of momentum term

$$\therefore SF + PF \cdot \frac{dB_2}{dx} = MF \cdot \frac{dB_2}{dx}$$

$$\text{or, } \frac{dx}{dB_2} = \frac{MF - PF}{SF} \quad (B.5)$$

APPENDIX-C

FINITE-DIFFERENCE TECHNIQUEC.1. General

A standard explicit finite-difference technique requires very small streamwise steps to satisfy the stability criterion. The DuFort-Frankel method [9] was found to be stable and was used here. The standard explicit scheme was used as a starting method for the DuFort-Frankel procedure which requires information from the two previous streamwise stations.

The finite-difference problem domain is usually established by letting ΔX and ΔR be small increments of the coordinates X and R and considering all the variables as existing on the finite set of points $X = i\Delta X$, $R = j\Delta R$ where i and j are integers. The dependent variables are expanded in Taylor series.

The basic variables are made non-dimensional by using the following transformation:

$$X = x/ReD_h, \quad U = u/U_0, \quad P = p/\frac{1}{2}\rho U_0^2,$$

$$R = r/D_h, \quad V = v.Re/U_0, \quad Re = D_h U_0/\nu.$$

Introducing the above transformations in equations (3.1) and (3.2):

the continuity equation becomes:

$$\frac{\partial(U R)}{\partial X} + \frac{\partial(V R)}{\partial R} = 0 \quad (C.1)$$

and the momentum equation becomes:

$$U \frac{\partial U}{\partial X} + V \frac{\partial U}{\partial R} = -\frac{1}{2} \frac{\partial P}{\partial X} + \frac{1}{R} \frac{\partial}{\partial R} \left(R \frac{\partial U}{\partial R} \right) + \frac{1}{Re} \frac{\partial^2 U}{\partial X^2}$$

Since the axial transport of momentum was assumed to be negligible the momentum equation can be written as:

$$U \frac{\partial U}{\partial X} + V \frac{\partial U}{\partial R} = - \frac{1}{2} \frac{\partial P}{\partial X} + \frac{1}{R} \frac{\partial}{\partial R} (R \frac{\partial U}{\partial R}) \quad (C.2)$$

C.2. Finite Difference Equations for the DuFort-Frankel Scheme

C.2.1. The Continuity Equation

Taylor's expansion about half a grid in the r-direction and one grid in the x-direction leads to:

$$U(i+1, j+1) = U(i, j+\frac{1}{2}) + \Delta X U_x + \frac{\Delta R}{2} U_r + \frac{1}{2} \{ (\Delta X)^2 U_{xx} + \Delta X R U_{xr} + (\frac{\Delta R}{2})^2 U_{rr} \} + O(\Delta^3) \quad (C.3)$$

$$U(i-1, j+1) = U(i, j+\frac{1}{2}) - \Delta X U_x + \frac{\Delta R}{2} U_r + \frac{1}{2} \{ (\Delta X)^2 U_{xx} - \Delta X \Delta R U_{xr} + (\frac{\Delta R}{2})^2 U_{rr} \} + O(\Delta^3) \quad (C.4)$$

$$U(i+1, j) = U(i, j+\frac{1}{2}) + \Delta X U_x - \frac{\Delta R}{2} U_r + \frac{1}{2} \{ (\Delta X)^2 U_{xx} - \Delta X \Delta R U_{xr} + (\frac{\Delta R}{2})^2 U_{rr} \} + O(\Delta^3) \quad (C.5)$$

$$U(i-1, j) = U(i, j+\frac{1}{2}) - \Delta X U_x - \frac{\Delta R}{2} U_r + \frac{1}{2} \{ (\Delta X)^2 U_{xx} + \Delta X \Delta R U_{xr} + (\frac{\Delta R}{2})^2 U_{rr} \} + O(\Delta^3) \quad (C.6)$$

Subtracting equations (C.6) from (C.4) and (C.5) from (C.3), and then adding the differences

$$\left(\frac{\partial U}{\partial X} \right)_{i, j+\frac{1}{2}} = \frac{U(i+1, j+1) + U(i+1, j) - U(i-1, j+1) - U(i-1, j)}{4\Delta X} + O(\Delta) \quad (C.7)$$

Subtracting expansions for V as in equations (C.3) and (C.5)

$$\left(\frac{\partial V}{\partial R} \right)_{i, j+\frac{1}{2}} = \frac{V(i+1, j+1) - V(i+1, j)}{\Delta R} \quad (C.8)$$

Using approximations (C.7) and (C.8) in the continuity equation (C.1), the finite difference equation becomes:

$$\begin{aligned} & \frac{R(j) + R(j+1)}{2} \frac{U(i+1, j+1) + U(i+1, j) - U(i-1, j+1) - U(i-1, j)}{4\Delta X} \\ & + \frac{R(j+1) U(i+1, j+1) - R(j) U(i+1, j)}{\Delta R} = 0 \end{aligned} \quad (C.9)$$

C.2.2. The Momentum Equation

Taylor's expansion of U about one grid in the r -direction leads to:

$$U(i, j+1) = U(i, j) + \Delta R U_{,r} + (\frac{1}{2}\Delta R)^2 U_{,rr} + O(\Delta^3) \quad (C.10)$$

$$U(i, j-1) = U(i, j) - \Delta R U_{,r} + (\frac{1}{2}\Delta R)^2 U_{,rr} + O(\Delta^3) \quad (C.11)$$

Subtracting eqns. (C.11) from (C.10)

$$\left(\frac{\partial U}{\partial R} \right)_{i, j} = \frac{U(i, j+1) - U(i, j-1)}{2\Delta R} + O(\Delta^2) \quad (C.12)$$

Similarly, expansion of U about one grid in the direction yields:

$$\left(\frac{\partial U}{\partial X}\right)_{i,j} = \frac{U(i+1,j) - U(i-1,j)}{2\Delta X} + O(\Delta^2) \quad (C.13)$$

Taylor's expansion of U about half a grid spacing in the r -direction yields:

$$U(i, j+\frac{1}{2}) = U(i, j) + \frac{1}{2}\Delta R U_r + \frac{1}{2}(\frac{1}{2}\Delta R)^2 U_{rr} + O(\Delta^3) \quad (C.14)$$

$$U(i, j-\frac{1}{2}) = U(i, j) - \frac{1}{2}\Delta R U_r + \frac{1}{2}(\frac{1}{2}\Delta R)^2 U_{rr} + O(\Delta^3) \quad (C.15)$$

$$\left(\frac{\partial U}{\partial R}\right)_{i,j} = \frac{1}{\Delta R} \{ U(i, j+\frac{1}{2}) - U(i, j-\frac{1}{2}) \} \quad (C.16)$$

Similarly,

$$\left\{ \frac{\partial}{\partial R} \left(R \frac{\partial U}{\partial R} \right) \right\}_{i,j} = \frac{1}{\Delta R} \left\{ \left(R \frac{\partial U}{\partial R} \right)_{i, j+\frac{1}{2}} - \left(R \frac{\partial U}{\partial R} \right)_{i, j-\frac{1}{2}} \right\}$$

or,

$$\left\{ \frac{\partial}{\partial R} \left(R \frac{\partial U}{\partial R} \right) \right\}_{i,j} = \frac{1}{\Delta R} \left\{ \frac{R(j)+R(j+1)}{2} \left(\frac{\partial U}{\partial R} \right)_{i, j+\frac{1}{2}} - \frac{R(j)+R(j-1)}{2} \left(\frac{\partial U}{\partial R} \right)_{i, j-\frac{1}{2}} \right\} \quad (C.17)$$

Using expansions similar to equations (C.14) and (C.15) one may write:

$$\left(\frac{\partial U}{\partial R}\right)_{i,j+\frac{1}{2}} = \frac{U(i,j+1) - U(i,j)}{\Delta R} + O(\Delta^2) \quad (C.18)$$

$$\left(\frac{\partial U}{\partial R}\right)_{i,j-\frac{1}{2}} = \frac{U(i,j) - U(i,j-1)}{\Delta R} + O(\Delta^2) \quad (C.18)$$

Writing the following expansions for U:

$$U(i+1, j) = U(i, j) + \Delta X U_x + \frac{1}{2}(\Delta X)^2 U_{xx} + O(\Delta^3) \quad (C.19)$$

$$U(i-1, j) = U(i, j) - \Delta X U_x + \frac{1}{2}(\Delta X)^2 U_{xx} + O(\Delta^3) \quad (C.20)$$

Adding eqns. (C.19) and (C.20):

$$U(i, j) = \frac{1}{2} U(i+1, j) + U(i-1, j) - \frac{1}{2}(\Delta X)^2 U_{xx} + O(\Delta^4) \quad (C.21)$$

Assuming U_{xx} to be negligibly small compared to U_{rr} , and using eqns. (C.21) and (C.18) in eqn. (C.17):

$$\left[\frac{\partial}{\partial R} \left(R \frac{\partial U}{\partial R}\right)\right]_{i,j} = \frac{1}{\Delta R} \left[\frac{R(j)+R(j+1)}{2} \frac{U(i,j+1) - 0.5 \{U(i+1,j) + U(i-1,j)\}}{\Delta R} - \frac{R(j)+R(j-1)}{2} \frac{0.5 \{U(i+1,j) + U(i-1,j)\} - U(i,j-1)}{\Delta R} \right] + O(\Delta) \quad (C.22)$$

Using equations (C.22), (C.13) and (C.12) in equation (C.2)

$$\begin{aligned}
 U(i,j) \frac{U(i+1,j)-U(i-1,j)}{2\Delta X} + v(i,j) \frac{U(i,j+1)-U(i,j-1)}{2\Delta R} = -\frac{1}{2} \frac{dP}{dX} \\
 + \frac{1}{R(j)\Delta R} \left[\frac{R(j)+R(j+1)}{2} \frac{U(i,j+1)-0.5\{U(i+1,j)+U(i-1,j)\}}{\Delta R} \right. \\
 \left. - \frac{R(j)+R(j-1)}{2} \frac{0.5\{U(i+1,j)+U(i-1,j)\}-U(i,j-1)}{\Delta R} \right] \quad (C.23)
 \end{aligned}$$

C.3 Direct Explicit Scheme

The finite-difference equations for this scheme were used to start the DuFort-Frankel method. These equations can be derived by the standard method:

The continuity equation is:

$$\begin{aligned}
 \frac{R(i)+R(j+1)}{2} \frac{U(i+1,j+1)+U(i+1,j)-U(i,j+1)-U(i,j-1)}{2\Delta X} \\
 + \frac{R(j+1)U(i+1,j+1)-R(j)U(i+1,j)}{\Delta R} = 0 \quad (C.24)
 \end{aligned}$$

The momentum equation is:

$$\begin{aligned}
 U(i,j) \frac{U(i+1,j)-U(i,j)}{\Delta X} + v(i,j) \frac{U(i,j)-U(i,j-1)}{\Delta R} = -\frac{1}{2} \frac{dP}{dX} \\
 + \frac{1}{R(j)\Delta R} \left[\frac{R(j+1)+R(j)}{2} \frac{U(i,j+1)-U(i,j)}{\Delta R} \right. \\
 \left. - \frac{R(j)+R(j-1)}{2} \frac{U(i,j)-U(i,j-1)}{\Delta R} \right] \quad (C.25)
 \end{aligned}$$

APPENDIX-D

STABILITY ANALYSIS OF THE MOMENTUM EQUATION

The finite-difference solution should ensure that:

- i) the finite difference representation is consistent.
- ii) due to the particular method of solution, round-off errors or errors from any source are not amplified or allowed to grow in subsequent steps in the solution.

The first point is called the consistency condition [11] which can be studied by expanding the dependent variables in Taylor's series expansions in a manner such that the difference between the partial differential equations and the finite difference representation can be observed [11]. This difference is known as truncation error of the equations; and if it vanishes in the limit as the mesh size is shrunk, the finite difference representation is said to be consistent.

The second point is called the stability condition. In dealing with the stability and convergence, the ideas of von Neumann [23] were used.

Let the error growth in U be δ and according to Numann it was expressed in the first harmonic by:

$$\delta = Ae^{\beta_1 R} e^{i\beta_2 X} \quad (D.1)$$

With the error, the velocities cahnged to:

$$\left. \begin{aligned} U(i, j+1) &\sim U(i, j+1) + \delta(i, j+1) \\ U(i, j-1) &\sim U(i, j-1) - \delta(i, j-1) \\ U(i+1, j) &\sim U(i+1, j) + \delta(i+1, j) \end{aligned} \right\} \quad (D.2)$$

and

$$\left. \begin{aligned} \delta(i, j+1) &= Ae^{\beta_1(R+R)} e^{i\beta_2 X} \\ \delta(i, j-1) &= Ae^{\beta_1(R-R)} e^{i\beta_2 X} \end{aligned} \right\} \quad (D.3)$$

et cetera.

Substituting eqns. (D.2) in equation (C.23) and then subtracting eqn. (2.23),

$$\begin{aligned} & \frac{U(i, j)}{2\Delta X} \{ \delta(i+1, j) + \delta(i-1, j) \} + \frac{V(i, j)}{2\Delta R} \{ \delta(i, j+1) + \delta(i, j-1) \} \\ &= \frac{1}{(\Delta R)^2} \left[\left(1 + \frac{\Delta R}{2R(j)} \right) \left\{ -\frac{\delta(i+1, j) - \delta(i-1, j)}{2} + \delta(i, j+1) \right\} \right. \\ & \quad \left. - \left(1 - \frac{\Delta R}{2R(j)} \right) \left\{ \frac{\delta(i+1, j) - \delta(i-1, j)}{2} + \delta(i, j-1) \right\} \right] \quad (D.4) \end{aligned}$$

Substituting eqn. (D.3) in eqn. (D.4), using $\xi = e^{\beta_1 \Delta R}$ and rearranging,

$$\xi^2 + A_0 \xi + B_0 = 0 \quad (D.5)$$

where

$$A_0 = \frac{U(i, j)/\Delta X}{\frac{V(i, j)}{\Delta R} - \frac{1}{(\Delta R)^2} - \frac{1}{2R(j)\Delta R}}$$

and

$$B_0 = \frac{V(i, j)/\Delta R + 1/(\Delta R)^2 - 1/\{2R(j)\Delta R\}}{U(i, j)/\Delta R - 1/(\Delta R)^2 - 1/\{2R(j)\Delta R\}}$$

The roots of eqn. (D.5) are:

$$\xi = -A_0/2 \pm \sqrt{(A_0/2)^2 - B_0} \quad (D.6)$$

According to von Neumann the stability condition,

$$|\xi| \leq 1 \quad (D.7)$$

For real roots, inequality (D.7) are:

$$-\frac{A_0}{2} + \left(\frac{A_0}{2}\right)^2 - B_0 \leq 1 \quad \text{where } A_0 < 0 \quad (D.8)$$

$$-\frac{A_0}{2} - \left(\frac{A_0}{2}\right)^2 - B_0 \geq -1 \quad \text{where } A_0 > 0 \quad (D.9)$$

Rearranging the eqn. (D.8)

$$\sqrt{\left(\frac{A_0}{2}\right)^2 - B_0} \leq 1 + \frac{A_0}{2}$$

$$\text{or, } \left(\frac{A_0}{2}\right)^2 - B_0 \leq 1 + A_0 + \left(\frac{A_0}{2}\right)^2$$

$$\text{or, } (-A_0 - B_0) \leq 1 \quad (D.10)$$

Using expressions of A_0 and B_0 in eqn.(D.10) and rearranging,

$$-\frac{\Delta R}{\Delta X} \leq \frac{2V(i,j) - 1/R(j)}{U(i,j)}$$

$$\text{or, } \left(\frac{\Delta R}{\Delta X}\right) \geq \frac{-2V(i,j) + 1/R(j)}{U(i,j)}$$

Since $U(i,j)$ is always positive,

$$\frac{\Delta R}{\Delta X} \geq \left| \frac{-2V(i,j) + 1/R(j)}{U(i,j)} \right| \quad (D.11)$$

The stability constraint given by the equation (D.11) determines the grid spacing in the x and r directions.

APPENDIX-E
UNCERTAINTY ANALYSIS

The uncertainty of the measurements of the pressure drop is influenced by the variations of the ambient temperature and pressure, the sp.gr. of the manometric liquid and the accuracy of the manometric readings.

E.1. Uncertainty of Measurement of Sp.Gr. of the Manometric Liquid

The sp.gr. of the manometric liquid was measured by the using the Archimedes principle at 20°C. The sensitivity of the balance scale was 0.0001 gm and the volume of the plumate was 2 ml ± 0.0001 ml.

Since density $D = \frac{\text{Mass}}{\text{volume}} = \frac{m}{v}$

$$\therefore \frac{\partial D}{\partial m} = \frac{1}{v} = \frac{D}{m}$$

$$\text{and } \frac{\partial D}{\partial v} = -\frac{m}{v^2} = -\frac{D}{v}$$

$$\therefore \text{Uncertainty, } \omega_Y = \left\{ \left(\frac{\partial D}{\partial m} \omega_m \right)^2 + \left(\frac{\partial D}{\partial v} \omega_v \right)^2 \right\}^{\frac{1}{2}}$$

where ω_m and ω_v are the uncertainties of mass and volume measurements respectively. Then, after evaluating,

$$\frac{\omega_Y}{D} = 0.013\%$$

E.2. Uncertainty of Pressure Drop Measurements

The non-dimensional pressure drop $P = \frac{\Delta p}{\frac{1}{2}\rho U_0^2} = h_{ma} \frac{\gamma_{ma}}{\gamma_{air}}$

where h_{ma} is the manometric reading in head of manometric liquid

and γ_{ma} and γ_{air} are the densities of the manometric liquid and air respectively.

But $\gamma_{air} = \frac{P_{at}}{R T_{at}}$, where P_{at} and T_{at} are the pressure and temperature of the ambient air.

$$\text{Then, } P = h_{ma} \gamma_{ma} R T_{at} / P_{at}$$

Differentiating,

$$\frac{\partial P}{\partial h_{ma}} = \gamma_{ma} \frac{R T_{at}}{P_{at}} = P / h_{ma}$$

$$\frac{\partial P}{\partial \gamma_{ma}} = h_{ma} \frac{R T_{at}}{P_{at}} = P / \gamma_{ma}$$

$$\frac{\partial P}{\partial T_{at}} = h_{ma} \gamma_{ma} R / P_{at} = P / T_{at}$$

$$\frac{\partial P}{\partial P_{at}} = - h_{ma} \gamma_{ma} R T_{at} / P_{at}^2 = - P / P_{at}$$

$$\therefore \text{Uncertainty, } \omega_P = \left\{ \left(\frac{\partial P}{\partial h_{ma}} \omega_{h_{ma}} \right)^2 + \left(\frac{\partial P}{\partial \gamma_{ma}} \omega_{\gamma_{ma}} \right)^2 + \left(\frac{\partial P}{\partial T_{at}} \omega_{T_{at}} \right)^2 + \left(\frac{\partial P}{\partial P_{at}} \omega_{P_{at}} \right)^2 \right\}^{\frac{1}{2}}$$

$$\text{or, } \frac{\omega_P}{P} = \left\{ \left(\frac{\omega_{h_{ma}}}{h_{ma}} \right)^2 + \left(\frac{\omega_{\gamma_{ma}}}{\gamma_{ma}} \right)^2 + \left(\frac{\omega_{T_{at}}}{T_{at}} \right)^2 + \left(\frac{\omega_{P_{at}}}{P_{at}} \right)^2 \right\}^{\frac{1}{2}}$$

where $\omega_{h_{ma}}$, $\omega_{\gamma_{ma}}$, $\omega_{T_{at}}$ and $\omega_{P_{at}}$ are the uncertainties of the manometric reading, the sp.gr. of manometric liquid, the atmospheric temperature and the atmospheric pressure respectively.

The values for ω_P/P were computed and they did not exceed $\pm 2.5\%$.

APPENDIX F
COMPUTER PROGRAMME

Two computer programmes, INMETH and FIMETH, written in the FORTRAN-IV language, were developed based on the Integral method and the Finite Difference method respectively. Lists of the programmes along with the definition of the variables used in the programmes are listed below.

F.1. Programme Documentation of INMETH

<u>Variable</u>	<u>Definition</u>
BB	B_2 for fully developed flow
BBB	B_1 for fully developed flow
BT	Value of B_2 at which eqns. (3.12) and (3.13) should be patched
DPRE	ΔP
H	ΔB_2
PRES	Pressure, P
Q	Radius ratio
RD1	$R_{\delta 1}$
RD2	$R_{\delta 2}$
SHEAR1	τ_{w1} / τ_{w1fd}
SHEAR2	τ_{w2} / τ_{w2fd}
UU	U_{cfd}
X	Axial distance, X

F.2 Programme Listing of INMETH

```

0001
0002 C
0003 C
0004 C
0005 C INTEGRAL SOLUTION FOR BOUNDARY LAYER THICKNESS IN THE DEVELOPING REGION
0006 C F=RADIUS RATIO, R1/R2
0007 C D1=DELTA1/R1
0008 C D2=DELTA2/R2
0009 C X=AXIAL DISTANCE/HYDRAULIC DIAMETER/FOUR'S NUMBER BASED ON HYDRAULIC DIA.
0010 C *****
0011     IMPLICIT REAL*8(A-H,O-Z)
0012     DIMENSION Q( 8),BB(8),UU(8),BBB(8),BT(8)
0013     COMMON Y(1000),XX(1000)
0014     READ(1,3) (R(J), J=1,6)
0015     3   FORMAT( 6D5.3)
0016     READ(1,13) (UU(J), J=1,6)
0017     READ(1,13) (BB(J), J=1,6)
0018     READ(1,13) (BBB(J), J=1,6)
0019     READ(1,13) (BT(J), J=1,6)
0020     13  FORMAT( 6D10.8)
0021     DO 600 K=1,2
0022     F=Q(K)
0023     WRITE(3,4)F
0024     4   FORMAT(/5X,'RADIUS RATIO =',D14.7)
0025     WRITE(3,333)
0026     333  FORMAT(/6X,'R2',9X,'X',9X,'PRES',9X,'YF',10X,'U/V',7X,'RD1',
0027     .8X,'RD2',9X,'SHEAR1',7X,'SHEAR2',9X,'ALFA',9X,'BETA')
0028 C
0029     I=1
0029     A2FD=UU(K)
0030     B2FD=BB(K)
0031     B1FD=BBB(K)
0032     A2FD=1.0-B2FD+DLOG(B2FD)
0033     B2ST=BT(K)
0034     SSUM=0.0
0035     KOUNT=0
0036     A1FD=1.0-B1FD+DLOG(B1FD)
0037     DPRE=0.0
0038     X=0.0
0039     H=0.010
0040     K2 =1.00001
0041     DO 500 N=1,2000
0042     L=0
0043     LM=0
0044     GAMMA =(((1.0-F**2)/(-2.0*DLOG(P)))*0.5-F)/(1.0-((1.-F**2)/(-2.0
0045     *DLOG(P)))*0.5)
0046     10  B1 =(1.0+(1.0-1.0/DSQRT(B2))*GAMMA/P)**(-2)
0047     LL=N
0048 C     L=0
0049 C
0050 C
0051 C     B1=B5(N)

```



```

0101      A40= A13/07-1.7/01-0.1*09          INMETH
0102      A41= A14/08-1.7/02-0.1*010         INMETH
0103      A42= -0.5*(1**2)*A20*A24*(A34+A38)+A21*A24*A38/2.0+P**2*A40*A22    INMETH
0104      A43= -0.5*(1**1)*A20*A24*A39+0.5*A24*A21*A37+0.5*A24*A21*A39-A41*A4    INMETH
0105      .23                                  INMETH
0106      C1= A24*(A32+2.0*A25*A38)/(A20+A29)   INMETH
0107      C2= A24*(A31+2.0*A25*A39)/(A20+A29)   INMETH
0108 C    WRITE(3,20) A1,A2,A3,A4,A5,A6,A7,A8,A9,A10,A11,A12,A13,A14,A15,    INMETH
0109 C      A16,A17,A18,A19,A20,A21,A22,A23,A24,A25,A26,A27,A28,A29,A30,A31,    INMETH
0110 C      A32,A33,A34,A35,A36,A37,A38,A39,A40,A41,A42,A43,C1,C2,B1,B2      INMETH
0111      IF(B2.GT.(B28)+H/2.0)GO TO 999       INMETH
0112 555  SF=16.0*(1.0-P)**2)*(-(R1-1.0)/41+(B2-1.0)/A2)    INMETH
0113      FF=A24*(1.0-P)*(-GAMA*(R1/B2)**1.5)*A38/P+A39)    INMETH
0114      FM=A24*(-GAMA*(R1/B2)**1.5)*A40*A22-A41*A23+2.0*(P**A22-A23)*    INMETH
0115      PF/A24/(1.0-P**P))                    INMETH
0116 C    EK1=-GAMA*(R1/B2)**1.5)*A20*A34-A21*A27          INMETH
0117 C    EK2=3.0*(P**A20-A21)*(-GAMA*(R1/B2)**1.5)*A38/P+A39)    INMETH
0118 C    VD=8.0*(1.0-P)**2)*(A26/(A1**2)-A27/(A2**2))    INMETH
0119 C    FK=A24*(EK1+EK2)/2.0                    INMETH
0120 C    WRITE(3,20)B2,SF,FF,FM,VD,EK        INMETH
0121      IF(FM .)222,223,223                    INMETH
0122 222  FN=0.0                                  INMETH
0123 223  F=(FM-PF)/SF                            INMETH
0124 C    WRITE(3,1111)B2,F                      INMETH
0125 C1111 FORMAT(5X,D14.7,5X,D14.7)           INMETH
0126 C    GO TO 500                                INMETH
0127      IF(LM.EQ.2)GO TO 224                    INMETH
0128      LM=LM+1                                  INMETH
0129      IF(LM.GT.4)GO TO 225                    INMETH
0130      XK1=F                                    INMETH
0131      R2=B2+H/2.0                              INMETH
0132      GO TO 10                                 INMETH
0133 225  XK2=F                                    INMETH
0134      XK3=F                                    INMETH
0135      R2=B2+H/2.0                              INMETH
0136      GO TO 10                                 INMETH
0137 224  XK4=F                                    INMETH
0138      XK=(XK1+2.0*XK2+2.0*XK3+XK4)/6.0      INMETH
0139      DX=XK*H                                  INMETH
0140      X=X+DX                                    INMETH
0141      PRES=2.0*A24*PF/(1.0-P**P)/XF          INMETH
0142 C    DP=PRES*DX                              INMETH
0143 C    DPRE=DPRE+DP                            INMETH
0144 C    WRITE(3,20)B2,X,PRES,DPRE,A24,DX,GAMA    INMETH
0145 C    YP=DPRE/4.0/Y                          INMETH
0146 C    XX(N)=X                                  INMETH
0147 C    Y(N)=YP                                  INMETH
0148 C    BETA=A24*A24*(P**A22-A23)/(1.0-P**P)    INMETH
0149 C    ALFA=A24*A23*(P**A20-A21)/(1.0-P**P)    INMETH
0150 C    WRITE(3,700)BETA,ALFA                  INMETH
0151      D1=1.0/DSQRT(B1)-1.0                    INMETH

```

```

0152          D2=1.0-1.0/0.001(B2)                                INMETH
0153 C        CALL LEAS1(N)                                       INMETH
0154          GO TO 510                                             INMETH
0155 C        GO TO 500                                             INMETH
0156 C        XK4=F                                               INMETH
0157 999      COP=1.0/1.0*(C2**0.5+(GAMA/P)*(B2**0.5-1.0)**3)    INMETH
0158          F=(-C1*GAMA/P*COP+C2 )/R.*(1.0-P**2)              INMETH
0159 C        FINV=1.0/F                                           INMETH
0160 C        WRITE(3,333)B2,FINV,F                                INMETH
0161 C333     FORMAT(5X,D14.7,5X,D14.7,5X,D14.7)                 INMETH
0162 C        GO TO 500                                             INMETH
0163          IF (L.EQ.2) GO TO 29                                  INMETH
0164          L=L+1                                                 INMETH
0165          IF (L.GT.1) GO TO 15                                  INMETH
0166          XK1=F                                               INMETH
0167          B2=B2+H/2.0                                          INMETH
0168          GO TO 10                                              INMETH
0169 15       XK2=F                                               INMETH
0170          XK3=F                                               INMETH
0171          B2=B2+H/2.0                                          INMETH
0172          GO TO 10                                              INMETH
0173 29      XK4=F                                               INMETH
0174          DX=H*(XK1+4.0*XK2+XK4)/6.0                          INMETH
0175 C        IF(LL.EQ.1)GO TO 800                                 INMETH
0176 C        GO TO 801                                             INMETH
0177 C800     DX=XK1*(R2-H-1.0)*(1.0-P**0.75)                    INMETH
0178 C        DPRE=DPRE+(A24**2-1.0)                              INMETH
0179 C        X=X+DX                                              INMETH
0180 C 30      FORMAT(/5X,'U/V=',D14.7)                            INMETH
0181 C        B5(N+1)=(1.0+1.0/P/E*(1.0-1.0/DSQRT(B5(N+1))))**(-2) INMETH
0182 301     X=X+H*(XK1+XK2*2.+XK3*2.+XK4)/6.                    INMETH
0183          D1=1.0/DSQRT(B1)-1.0                                  INMETH
0184          D2= 1.-1.0/DSQRT(B2)                                  INMETH
0185 C        WRITE (3,7) X,B1,B2,D1,D2,A24                        INMETH
0186 7        FORMAT (/5 X,'X=',D14.7,2X,'B1=',D14.7,2X,'B2=',D14.7,2X,'D1=',D1 INMETH
0187          ,4.7,2X,'D2=',D14.7,2X,'U/V=',D14.7)              INMETH
0188          S1=16.0*((1.0-P)**2)+((B1-1.0)/A1-(B2-1.0)/A2)    INMETH
0189          S2=2.0*((P**2)*A22-A23)*(-A38*GAMA*COP/P+A39)     INMETH
0190          S3=P*A40*A22*GAMA*COP+A41*A23                       INMETH
0191          PRES=(S1*A24+(S2-S3)*(A24**2)/XK4)*2.0/(1.0-P**2) INMETH
0192 510     RD1=(1.0+D1)*0.5/(1.0/P-1.0)                        INMETH
0193          RD2=(1.0+D2)*0.5/(1.0-P)                            INMETH
0194 C        WRITE(3,33) PRES,RD1,RD2                             INMETH
0195 C        IF(LL.EQ.1)GO TO 510                                  INMETH
0196          DP=PRES*DX                                           INMETH
0197          DPRE=DPRE+DP                                          INMETH
0198          SHEAR1=A24*(B1-1.0)/A24FD/(B1FD-1.0)*A1FD/A1      INMETH
0199          SHEAR2=A24*(B2-1.0)/A24FD/(B2FD-1.0)*A2FD/A2      INMETH
0200 C        WRITE(3,505)SHEAR1,SHEAR2                           INMETH

```


F.3. Programme Documentation of FIMETH

<u>Variable</u>	<u>Definitation</u>
A,B	Constants of eqn. (5.1)
DPRES	(dP/dX)
DX	Increment of X
DY	Increment of R
RD	R_δ
P	Radius ratio
PRESFD	$(dP/dX)_{fd}$
SHEAR	$\tau_w / \tau_{w_{fd}}$
T1FD	$\tau_{w1_{fd}}$
T2FD	$\tau_{w2_{fd}}$
U	Axial velocity, -U-
V	Radial velocity, -V-
UAVE	U_o
UFD	$(U_c / U_o)_{fd}$
X	Axial distance, -X-
Y	radial distance, -R-

F.4 Programme Listing of FIMETH

```

0001 C
0002 C
0003 C
0004 C
0005 C      IMPLICIT REAL*8(A-H,O-Z)
0006 C      DIMENSION V(5,202)
0007 C      COMMON Y(202),U( 11,202)
0008 C
0009 C      *****DEVELOPING LAMINAR FLOW THROUGH CONCENTRIC ANNULI*****
0010 C      A SOLUTION BY FINITE DIFFERENCE TECHNIQUE
0011 C
0012 C
0013 C
0014 C      SINH(X)=(DEXP(A*X**2*(B+X))-DEXP(-A*X**2*(B+X)))/2.0
0015 C      COSH(X)=(DEXP(A*X**2*(B+X))+DEXP(-A*X**2*(B+X)))/2.0
0016 C      DPRES(X)=4.0*COSH(X)/SINH(X)-4.0*A*X**2*(B+X+1.0)*(DLOG(X)+(B+X)/X)
0017 C      /(SINH(X))**2
0018 C      DATA P,A,B/0.01,0.18584,0.42928/
0019 C      DATA X,DX,M/0.00000,0.00001,50/
0020 C      DATA DX1,DX2,DX3,DX4/0.000010,0.000010,0.000010,0.000010/
0021 C      DATA DX5,DX6/0.00005,0.00010/
0022 C      DATA PRESFD /80.113/
0023 C      WRITE(3,100)P
0024 C
0025 C      YM=M
0026 C      DY=0.5/YM
0027 C      MP1=M+1
0028 C      R1=0.5/(1.0/P-1.0)
0029 C      R2=0.5/(1.0-P)
0030 C      RD=R2*((P*P-1.0)/DLOG(P*P))**0.5
0031 C      UFD=((P*P-1.0)*(1.0-DLOG((P*P-1.0)/DLOG(P*P)))-DLOG(P*P))/(P*P-1.
0032 C      0)-(1.0+P*P)*DLOG(P)
0033 C      RI=R1+DY
0034 C      RO=R2-DY
0035 C      UI=(RI*RI-R1*R1-2.0*RD*RD*DLOG(RI/R1))/(RD*RD-R1*P1-2.0*RD*RD*
0036 C      .DLOG(RD/R1))*UFD
0037 C      UO=(RO*RO-R2*R2-2.0*RD*RD*DLOG(RO/R2))/(RD*RD-R2*P2-2.0*RD*RD*
0038 C      .DLOG(RD/R2))*UFD
0039 C      T1FD=2.0*(R1-RD*RD/R1)*UFD/(RD*RD-R1*P1-2.0*RD*RD*DLOG(RD/R1))
0040 C      T2FD=2.0*(R2-RD*RD/R2)*UFD/(RD*RD-R2*P2-2.0*RD*RD*DLOG(RD/R2))
0041 C      WRITE(3,103)UFD,UI,UO,T1FD,T2FD,RD
0042 C
0043 C      Y(1)=R1
0044 C      Y(MP1)=R2
0045 C      DO 1 KY=2,M
0046 C      1 Y(KY)=Y(1)+DY*(KY-1)
0047 C
0048 C      DO 2 JX=2,M
0049 C      U(1,JX)=1.001
0050 C      2 V(1,JX)=0.0
0051 C      DO 3 KX=1,3
0052 C      U(KX,1)=0.0
0053 C      V(KX,1)=0.0

```

```

0054      U(KX,MP1)=0.0
0055      V(KX,MP1)=0.0
0056      KOUNT=1
0057      CONST=RD*(RD-R1)*R1-2.0*(RD)*RD*DL0G(RD/R1)
0058      CONSD=RD*(RD-R2)*R2-2.0*(RD)*RD*DL0G(RD/R2)
0059      WRITE(3,104)R,RD,UD
0060      WRITE(3,105)
0061      DO 800 ID=1,N1
0062      R=Y(ID)
0063      IF(R=RD)GO 1,801,802
0064      B01  U(10, ID)=(R*(R-R1)*R1-2.0*(RD)*RD*DL0G(R/R1))/CONST*UED
0065      GO TO 800
0066      B02  U(10, ID)=(R*(R-R2)*R2-2.0*(RD)*RD*DL0G(R/R2))/CONSD*UED
0067      B00  WRITE(3,103)R,U(10, ID)
0068      CALL STRES(KOUNT, U1, U0, T1, D, 12, D, 10, M, DY)
0069      CALL SIMSON(KOUNT, DY, M, MP1, R1, R2, 10)
0070      CALL VISECS(R1, DY, M, 10, V)
0071      C   KOUNT=1
0072      DO 4 KE=1, 1
0073      KOUNT=KOUNT+1
0074      KE1=KE+1
0075      XX=X+DX/2.
0076      IF(KOUNT.GT.2) XX=X
0077      PRES=DPRES(XX)
0078      X=X+DX
0079      C   WRITE(3,101) KOUNT, X, PRES
0080      DO 5 MA=2, M
0081      MA1=MA+1
0082      MA2=MA-1
0083      UE1=DX*PRES*0.5/U(KE, MA)+U(KE, MA)
0084      UE2=V(KE, MA)*(U(KE, MA)-U(KE, MA2))*DX/U(KE, MA)/DY
0085      UE3=(Y(MA1)+Y(MA))*(U(KE, MA1)-U(KE, MA))
0086      UE4=(Y(MA)+Y(MA2))*(U(KE, MA)-U(KE, MA2))
0087      UE5=DX/U(KE, MA)/Y(MA)/2.0/DY/DY
0088      5   U(KE1, MA)=UE1-UE2+UE5*(UE3-UE4)
0089      C   KK=0
0090      SUM=0.0
0091      CALL AVE(M, KE1, SUM, DY, R1, R2, KOUNT, RMS, RMSU, 10)
0092      WRITE(3,101)KOUNT, X, PRES, RMS, RMSU
0093      DO 6 MV=2, M
0094      MV1=MV-1
0095      V1=Y(MV1)*V(KE1, MV1)/Y(MV)
0096      V2=(Y(MV)+Y(MV1))*DY/4.0/Y(MV)/DX
0097      V3=U(KE1, MV)+U(KE1, MV1)-U(KE, MV)-U(KE, MV1)
0098      V(KE1, MV)=V1-V2*V3
0099      IF(V(KE1, MV).LT.0.0)V(KE1, MV)=0.0
0100      IF(Y(MV)=RD)6, 6, 7

```

```

0101 6 CONTINUE
0102 7 MK=MP1-MV
0103 DO 8 KK=1,MK
0104 MV2=MP1-KK
0105 MV3=MV2+1
0106 V01=Y(MV3)*V(KE1,MV3)/Y(MV2)
0107 V02=(Y(MV3)+Y(MV2))*DY/4,0/Y(MV2)/DX
0108 V03=U(KE1,MV3)+U(KE1,MV2)-U(KE1,MV3)-U(KE1,MV2)
0109 V(KE1,MV2)=V01+V02*V03
0110 C WRITE(3,103)MV2,MV3,V01,V02,V03,V(KE1,MV3),V(KE1,MV2),U(KE1,MV2),
0111 C U(KE1,MV3),U(KE1,MV2),U(KE1,MV3)
0112 C IF(V(KE1,MV2).GT.0.0) V(KE1,MV2)=0.0
0113 8 CONTINUE
0114 WRITE(3,102)
0115 DO 9 KV=1,MP1
0116 KY=(Y(KV)-Y(1))/0.5
0117 UGRAF=U(KE1,KV)/0.025
0118 9 WRITE(3,103) Y(KV),U(KE1,KV),V(KE1,KV),UGRAF,KY
0119 CALL STRESS(KOUNT,UI,U0,T1FD,T2FD,KE1,M,DY)
0120 CALL SIMSON(KOUNT,DY,M,MP1,R1,R2,KE1)
0121 C
0122 4 CONTINUE
0123 C
0124 KL=KOUNT-1
0125 DO 10 MM=2,M
0126 U(1,MM)=U(KL,MM)
0127 V(1,MM)=V(KL,MM)
0128 U(2,MM)=U(KOUNT,MM)
0129 10 V(2,MM)=V(KOUNT,MM)
0130 N=1
0131 999 NP=2
0132 DXX=DX
0133 IF(KOUNT.EQ.11) GO TO 20
0134 IF(KOUNT.GT.11.AND.KOUNT.LT.21)GO TO 21
0135 IF(KOUNT.EQ.21) GO TO 22
0136 IF(KOUNT.GT.21.AND.KOUNT.LT.35)GO TO 23
0137 IF(KOUNT.EQ.35) GO TO 24
0138 IF(KOUNT.GT.35.AND.KOUNT.LT.45) GO TO 25
0139 IF(KOUNT.EQ.45) GO TO 26
0140 IF(KOUNT.GT.45.AND.KOUNT.LT.2501)GO TO 27
0141 IF(KOUNT.EQ.2501)GO TO 28
0142 IF(KOUNT.GT.2501.AND.KOUNT.LT.2601)GO TO 29
0143 IF(KOUNT.EQ.2601)GO TO 40
0144 IF(KOUNT.GT.2601)GO TO 41
0145 GO TO 19
0146 20 DX=(DX+DX1)/2.0
0147 DXX=DX1
0148 GO TO 19
0149 21 DX=DX1
0150 DXX=DX1
0151 GO TO 19

```

```

0152 22 DX=(DX1+DX2)/2.0
0153 DXX=DX2
0154 GO TO 19
0155 23 DX=DX2
0156 DXX=DX2
0157 GO TO 19
0158 24 DX=(DX2+DX3)/2.0
0159 DXX=DX3
0160 GO TO 19
0161 25 DX=DX3
0162 DXX=DX3
0163 GO TO 19
0164 26 DX=(DX3+DX4)/2.0
0165 DXX=DX4
0166 GO TO 19
0167 27 DX=DX4
0168 DXX=DX4
0169 GO TO 19
0170 28 DX=(DX4+DX5)/2.0
0171 DXX=DX5
0172 GO TO 19
0173 29 DX=DX5
0174 DXX=DX5
0175 GO TO 19
0176 40 DX=(DX5+DX6)/2.0
0177 DXX=DX6
0178 GO TO 19
0179 41 DX=DX6
0180 DXX=DX6
0181 19 DO 11 I=2,NP
0182 KOUNT=KOUNT+1
0183 II=I-1
0184 III=I+1
0185 PRES=DPRES(X)
0186 IF (PRES.LT.PRESFD) PRES=PRESFD
0187 X=X+DXX
0188 C WRITE (3,101)KOUNT,X,PRES
0189 DO 12 J=2,m
0190 JJ=J-1
0191 JJJ=J+1
0192 UD1=0.5*PRES+U(I,J)*U(II,J)/2.0/DX
0193 UD2=V(I,J)*U(I,JJJ)-U(I,JJ)/2.0/DY
0194 UD3=(Y(JJJ)+Y(J))*U(I,JJJ)-0.5*U(II,J)
0195 UD4=(Y(J)+Y(JJ))*U(I,JJJ)-0.5*U(II,J)
0196 UD5=(UD3-UD4)/Y(J)/2.0/DY/DY
0197 UD6=U(I,J)/2.0/DX+1.0/DY/DY
0198 U(III,J)=(UD1-UD2+UD5)/UD6
0199 IF(U(III,2).LT.U1) U(III,2)=U1
0200 C IF(U(III,2).EQ.U1) U(III,3)=U(I,3)
0201 12 CONTINUE

```

```

0202 CALL AVE(M, I11, SUB, DY, R1, R2, KOUNT, RMS, RMSU, 10)
0203 DO 13 JD=2, M
0204 JD1=JD-1
0205 VD1=V(I11, JD1)*Y(JD1)/Y(JD)
0206 VD2=U(I11, JD)+U(I11, JD1)-U(I11, JD)-U(I11, JD1)
0207 V(I11, JD)=VD1+VD2*(Y(JD)+Y(JD1))*DY/Y(JD)/8.0/DX
0208 IF (V(I11, JD).LT.0.0) V(I11, JD)=0.0
0209 IF (Y(JD)-RD) 13, 13, 14
0210 13 CONTINUE
0211 14 NK=MP1-JD
0212 DO 17 NN=1, NK
0213 J2=MP1-NN
0214 J3=J2+1
0215 VD01=V(I11, J3)*Y(J3)/Y(J2)
0216 VD02=U(I11, J3)+U(I11, J2)-U(I11, J3)-U(I11, J2)
0217 V(I11, J2)=VD01+VD02*(Y(J3)+Y(J2))*DY/Y(J2)/8.0/DX
0218 IF (V(I11, J2).LT.0.0) V(I11, J2)=0.0
0219 17 CONTINUE
0220 11 CONTINUE
0221 C WRITE(3, 101) KOUNT, X, PRES
0222 C WRITE(3, 102)
0223 DO 16 JM=1, MP1
0224 U(1, JM)=U(NF, JM)
0225 U(2, JM)=U(I11, JM)
0226 V(1, JM)=V(NF, JM)
0227 16 V(2, JM)=V(I11, JM)
0228 C
0229 IKOUNT= N
0230 IF (KOUNT.LE.301) IKOUNT=5*N
0231 IF (KOUNT.GT.301) IKOUNT=50*N-2650
0232 C IF (KOUNT.GE.35.AND.KOUNT.LT.67) IKOUNT=10*N-6
0233 C IF (KOUNT.EQ.67) IKOUNT=10*N-14
0234 C IF (KOUNT.GT.67) IKOUNT=20*N-94
0235 IF (KOUNT.LE.IKOUNT) GO TO 999
0236 WRITE(3, 101) KOUNT, X, PRES, RMS, RMSU
0237 C WRITE(3, 102)
0238 C DO 18 KM=1, MP1
0239 C UGRAF=U(I11, KM)/0.025
0240 C UDEVI=U(10, KM)-U(I11, KM)
0241 C RY=(Y(KM)-Y(1))/0.5
0242 C18 WRITE(3, 103) Y(KM), U(I11, KM), V(I11, KM), UGRAF, RY, UDEVI
0243 CALL STRES(KOUNT, UJ, UO, T1FD, T2FD, I11, M, DY)
0244 CALL SIMSON(KOUNT, DY, M, MP1, R1, R2, I11)
0245 CALL VISCOS(R1, DY, M, I11, V)
0246 N=N+1
0247 C
0248 IF (X.GT.0.001) GO TO 555
0249 GO TO 999

```

```

( 0250 555 CONST=RD*RD-R1*R1-2.0*RD*RD*DLOG(RD/R1)
0251 CONSO=(R2-R1)*R1-2.0*RD*RD*DLOG(RD/R2)
0252 WRITE(3,104)I, RD, UFD
( 0253 WRITE(3,105)
0254 DO 30 IC=1, MP1
0255 R=Y(IC)
( 0256 RY=(Y(IC)-R1)/0.5
0257 IF(R-RD)31,31,32
0258 31 U(1,IC)=(R2-R1*(R1-2.0*RD*RD*DLOG(R/R1))/CONST*UFD
( 0259 GO TO 30
0260 32 U(1,IC)=(R2-R1*(R2-2.0*RD*RD*DLOG(R/R2))/CONSO*UFD
0261 30 WRITE(3,103)R,U(1,IC),RY
( 0262 CALL STRES(KOUNT,UI,UO,T1FD,T2FD,I,M,DY)
0263 CALL SIMSON(KOUNT,DY,M,MP1,R1,R2,I)
0264 C
( 0265 104 FORMAT(//,2X,'FULLY DEVELOPED VELOCITY PROFILE FOR R1/R2=',D14.7,
0266 ,2X,'RD=',D14.7,2X,'UFD=',D14.7,/)
0267 105 FORMAT(/,10X,'Y/DH',15X,'U/VAVE',10X,'(R-R1)/(R2-R1)')
( 0268 100 FORMAT(/.5X,'RADIUS RATIO=',D14.7)
0269 101 FORMAT(//2X,'STATION=',I5,2X,'X=',D14.7,2X,'DF/DX=',D14.7,
0270 ,2X,'RMS DEVIATION OF UAVE=',D14.7,2X,'RMS FROM U DEVD=',D14.7)
( 0271 102 FORMAT(/,10X,'Y/DH',10X,'U/VAVE',12X,'V.RE/VAVE',10X,'UGRAF',
0272 ,12X,'(R-R1)/(R2-R1)',10X,'U DEVD-U')
0273 103 FORMAT(2X,7(4X,D14.7))
( 0274 STOP
0275 END
0276 SUBROUTINE STRES(KOUNT,UI,UO,T1FD,T2FD,I11,M,DY)
0277 IMPLICIT REAL*8(A-H,U-Z)
0278 COMMON Y(202),U(11,202)
0279 SHEAR1=(4.0*U(I11,2)-U(I11,3))/2.0/DY/T1FD
( 0280 L=M-1
0281 SHEAR2=(U(I11,L)-4.0*U(I11,M))/2.0/DY/T2FD
0282 TAU1=U(I11,2)/UI
( 0283 TAU2=U(I11,M)/UO
0284 WRITE(3,200)KOUNT,SHEAR1,SHEAR2,TAU1,TAU2
0285 200 FORMAT(/,2X,'STATION=',I5,'SHEAR1=',D14.7,'SHEAR2=',D14.7,'TAU1=',
( 0286 ,D14.7,'TAU2=',D14.7)
0287 RETURN
0288 END

```



```

0289      SUBROUTINE SIMSON(KOUNT,DY,M,MP1,R1,R2,IIT)
0290      IMPLICIT REAL*8(A-H,O-Z)
0291      COMMON      Y(202),U(11,202)
0292      S1=0.0
0293      S2=0.0
0294      S3=0.0
0295      MA=M/2
0296      DO 500 I=1,MA
0297      J=2*I-1
0298      K=2*I
0299      S1=S1+2.0*Y(J)*DY*U(IIT,J)**2
0300      S1=S1+4.0*Y(K)*DY*U(IIT,K)**2
0301      S2=S2+2.0*Y(J)*DY*U(IIT,J)**3
0302      S2=S2+4.0*Y(K)*DY*U(IIT,K)**3
0303      S3=S3+2.0*Y(J)*DY*U(IIT,J)
0304      S3=S3+4.0*Y(K)*DY*U(IIT,K)
0305      B=2.0*S1/(R2*R2-R1*R1)/3.0
0306      A=2.0*S2/(R2*R2-R1*R1)/3.0
0307      UAVE=2.0*S3/(R2*R2-R1*R1)/3.0
0308      WRITE(3,550)KOUNT,B,A,UAVE
0309      550 FORMAT(2X,'STATION=',I5,2X,'ALFA=',D14.7,2X,'BETA=',D14.7,2X,
0310      'UAVE=',D14.7)
0311      RETURN
0312      END
0313      SUBROUTINE AVE(M,IIT,SUM,DY,R1,R2,KOUNT,RMS,RMSU,KK)

0314      IMPLICIT REAL*8(A-H,O-Z)
0315      COMMON Y(202),U(11,202)
0316      103 S=0.0
0317      MA=M/2
0318      DO 100 J=1,MA
0319      K=2*J-1
0320      L=2*J
0321      S=S+2.0*Y(K)*U(IIT,K)
0322      100 S=S+4.0*Y(L)*U(IIT,L)
0323      UAVE=2.0*S*DY/3.0/(R2*R2-R1*R1)
0324      MP1=M+1
0325      SU=0.0
0326      DO 551 K=1,MP1
0327      DEVI=U(KK,K)-U(IIT,K)
0328      551 SU=SU+DEVI*DEVI
0329      RMSU=DSQRT(SU)/MP1
0330      104 SUM=SUM+(1.0-UAVE)*(1.0-UAVE)
0331      RMS=DSQRT(SUM)/(KOUNT-1)
0332      C WRITE(3,101)KOUNT,UAVE,RMS,RMSU
0333      C101 FORMAT(2X,'STATION=',I5,2X,'UAVE=',D14.7,5X,'CUMULATIVE RMS OF
0334      C UAVE=',D14.7,2X,D14.7)
0335      RETURN
0336      END

```

```

0337 SUBROUTINE VISCOS(R1,DY,M,I,V)
0338 IMPLICIT REAL*8(A-H,O-Z)
0339 COMMON Y(202),U(11,202)
0340 DIMENSION VC(5,202),DV(100)
0341 WRITE(3,5)
0342 DD=0.0
0343 DO 10 J=2,M
0344 J1=J-1
0345 J2=J+1
0346 DU1=(U(I,J2)-U(I,J1))/DY/2.0
0347 DU2=(U(I,J2)+U(I,J1)-2.0*U(I,J))/DY/DY
0348 DU3=DU1/Y(J)+DU2
0349 DD=DD+DU3
0350 DV(J)=DU3
0351 R=(Y(J)-R1)/0.15
0352 WRITE(3,15)R,U(I,J),DU1,DU2,DU3,V(I,J)
0353 10 CONTINUE
0354 DDAVE=DD/FLUAT(M-1)
0355 WRITE(3,25)DD,DDAVE
0356 S1=0.0
0357 S2=0.0
0358 LH=H/2-1
0359 DO 35 L=2,LH
0360 LL=2*L-1
0361 KK=2*L
0362 S1=S1+4.0*DV(LL)
0363 35 S2=S2+2.0*DV(KK)
0364 ST=DY*(DV(2)+DV(50)+4.0*DV(49)+S1+S2)/3.0
0365 SAVE=ST/(DY*(M-2))
0366 WRITE(3,45)ST,SAVE
0367 45 FORMAT(/5X,'ST=',D14.7,5X,'SAVE=',D14.7)
0368 25 FORMAT(/5X,'SUM DU3=',D14.7,5X,'DDAVE=',D14.7)
0369 5 FORMAT(/7X,'(R-R1)/(R2-R1)',10X,'U/DAVE',10X,'DU/DY',10X,'D/DY(D
0370 U/DY)',6 X,'1/DY(YDU/DY)/Y',6X,'V/DAVE',/)
0371 15 FORMAT(2X,7(4X,D14.7))
0372 RETURN
0373 END
*END PRINT
*READY

```

